Dissertation for the attainment of the academic title Dr. rer. nat.

Functional role of the immunoproteasome in (glomerular) endothelial cells

Prepared by

Lukas Blume

born in Göttingen

Department of Chemistry

Faculty for Mathematics, Computer studies and Science

Hamburg University

Hamburg, February 2025

The work described in this thesis was carried out between March 2020 and December 2024 externally in the Institute of Cellular and Integrative Physiology at the University Medical Centre Eppendorf under the supervision of Catherine Meyer-Schwesinger.

1. Reviewer: Prof. Dr. rer. nat. Hartmut Schlüter

2. Reviewer: Prof. Dr. med. Catherine Meyer-Schwesinger

Date of the disputation: 23.05.2025

Table of Contents

Zusammenfassung

Das Proteasom spielt als katalytischer Komplex im Ubiquitin-Proteasom-System (UPS) eine zentrale Rolle für die zelluläre Proteostase. Das Immunoproteasom als spezielle Form des Proteasoms wurde bisher vor allem im Kontext des Immunsystems und zellulärem Stress beschrieben. Es wird jedoch zunehmend deutlich, dass Endothelzellen immunoproteasomale Untereinheiten auch unter homöostatischen Bedingungen exprimieren. Die funktionale Relevanz dieser Expression ist bisher jedoch kaum erforscht. Daher wurde in der vorliegenden Arbeit eine neue Mauslinie etabliert, die den endothelzellspezifischen Knockout der immunoproteasomalen Untereinheit LMP7 erlaubt (LMP7$^{\Delta EnC}$). Isolierte glomeruläre, peritubuläre, Herz-, Leber- und Lungenendothelzellen zeigten einen vollständigen Verlust an LMP7 sowie deutlich höhere Level der korrespondierenden konstitutiven Untereinheit β5c und einen Verlust von MHC Klasse I - Molekülen auf der Zelloberfläche. Interessanterweise schienen Nierenendothelzellen empfindlicher auf den Verlust der LMP7-Expression zu reagieren als Endothelzellen anderer Organe. So zeigten nur Endothelzellen der Niere eine Zunahme der Zellgröße und – granularität und peritubuläre Endothelzellen wiesen verringerte Oberflächenlevel an MHC Klasse II-Molekülen auf, während in glomerulären Endothelzellen Immunglobulin G (IgG) akkumulierte. Weiterhin wies die glomeruläre Filtrationsbarriere (GFB) eine deutlich veränderte Ultrastruktur auf. Neben einem Verlust der glomerulären Fenestrierung, zeigte sich auch eine deutliche Fußfortsatzverschmelzung der Podozyten. Diese Beobachtungen standen in starkem Kontrast dazu, dass die Tiere keine erhöhte Albuminurie aufwiesen, einem klassischen Marker für eine beeinträchtigte GFB. Die erhöhte Granularität zusammen mit den veränderten Oberflächenlevel mehrerer Proteine und einer Veränderung im IgG-Handling deuten eine Beeinträchtigung des endozytischen Systems durch den Verlust von LMP7 an. Die Analyse des globalen Transkriptoms und Proteoms erlaubte die Identifikation möglicher Mechanismen für die beobachteten phänotypischen zellulären Veränderungen. MORF4L2 wurde dabei als mögliches Immunoproteasom-spezifisches Substrat identifiziert.

Eine mögliche Rolle des endothelialen Immunoproteasoms in Krankheitsbildern wurde mithilfe des BTBR *ob/ob*-Modells der diabetischen Nephropathie (DN) und des NTN-Modells einer rasch progressiven Glomerulonephritis untersucht. Dabei zeigte sich, dass das (Immuno)Proteasom in der DN vor allem in Endothelzellen und Podozyten induziert war. Erhöhte Proteinlevel der katalytischen Untereinheiten spiegelten sich jedoch nicht in einer gesteigerten proteasomalen Aktivität wider, die im Gegenteil leicht reduziert war. Überraschenderweise konnte keine Akkumulation proteasomaler Substrate wie K48-polyubiquitinierter Proteine beobachtet werden.

Mechanistische Untersuchungen im NTN-Modell in der LMP7$^{\Delta EnC}$ – Mauslinie deuteten einen protektiven Effekt endothelialer LMP7-Expression in immunvermittelten glomerulären Erkrankungen an. So zeigten Knockout-Tiere einen aggravierten klinischen und morphologischen Krankheitsverlauf mit höherer Albuminurie, schlechteren Serumwerten und stärkerer Halbmondbildung in den Glomeruli. Sowohl glomeruläre Endothelzellen als auch Podozyten wiesen in der Abwesenheit von LMP7 stärkeren Schaden auf.

Die vorliegende Arbeit betont die funktionale Relevanz der endothelialen Expression des Immunoproteasoms unter homöostatischen Bedingungen, nicht nur für die Endothelzellen selbst. Diese Daten zur organspezifischen Rolle und zur Involvierung des endothelialen Immunoproteasoms in pathologische Prozesse liefern vielversprechende Anhaltspunkte zur weiteren Untersuchung der für die beobachteten Veränderungen verantwortlichen Mechanismen.

Abstract

The proteasome as the catalytic complex of the ubiquitin proteasome system (UPS) plays a central role in cellular proteostasis. The immunoproteasome as a specialised form of the proteasome was originally described in the context of immune cells and cellular stress. However, it is increasingly recognised that endothelial cells (EnCs) express immuno-proteasomal subunits even under homeostatic conditions. Nevertheless, the functional relevance of this expression is so far hardly described. Therefore, a new mouse line allowing the endothelial specific knockout of the immunoproteasomal subunit LMP7 (LMP7$^{\Delta EnC}$) was established. EnCs isolated from glomerular, peritubular, heart, liver and lung tissue exhibited a robust loss of LMP7 as well as an upregulation of the corresponding constitutive subunit β5c and a loss of cell surface MHC class I. Interestingly, kidney EnCs appeared to be more strongly affected by the loss of LMP7 than EnCs from other organs. As such, kidney EnCs increased both in cell size and granularity and peritubular EnCs (PtEnCs) also exhibited reduced MHC class II levels, whereas immunoglobulin G (IgG) accumulated in glomerular endothelial cells. Additionally, the glomerular filtration barrier (GFB) showed a strongly altered ultrastructure with loss of endothelial fenestrations and podocyte foot process effacement. This was in stark contrast to the lack of albuminuria observed in these mice under basal conditions, a classical marker of GFB impairment. The higher granularity of EnCs together with the altered cell surface levels of several proteins and differences in msIgG handling indicate an impairment of the endocytic pathway by the loss of endothelial immunoproteasome. Untargeted analyses of both mRNA and protein levels in endothelial cells isolated from LMP7$^{\Delta EnC}$ mice and control littermates allowed the identification of possible mechanisms behind the observed phenotypic cellular alterations. MORF4L2 was identified as a potential immunoproteasome specific substrate.

Potential involvement of the endothelial immunoproteasome in disease conditions was analysed using the BTBR *ob/ob* mouse model of diabetic nephropathy (DN) and the nephrotoxic nephritis (NTN) model of crescentic glomerulonephritis (cGN). In BTBR *ob/ob* mice, alterations in (immuno)proteasomal subunit expression could be observed, most strongly in EnCs and podocytes of the glomerulus. Increased levels of immunoproteasomal catalytic subunits did not relate to a higher proteasomal activity, which in contrast was rather impaired. Surprisingly, no accumulation of proteasomal substrates like K48-polyubiquitinated proteins could be observed.

Mechanistic studies employing the NTN model of cGN in LMP7$^{\Delta EnC}$ mice indicated a protective effect of the endothelial immunoproteasome in immune-mediated glomerular disease. As such, knockout animals exhibited an exacerbated clinical and morphologic disease course with

higher albuminuria, worse serum parameters and increased crescent formation. Both glomerular endothelial cells and podocytes showed a higher susceptibility to stress in the absence of LMP7.

The data presented here highlight the functional relevance of endothelial immunoproteasome expression under homeostatic conditions and offer interesting insights into the mechanisms. The observed organotypic reactions and the involvement of endothelial LMP7 in disease provide promising starting points for further study.

1 Introduction

1.1 Proteostasis

Proteostasis describes the maintenance of a cell's proteome adapted to its current function and external environmental cues. A cell's proteome is constantly changing as proteins get damaged, their function is no longer needed or the cells internal or external status changes. As such, proteostasis is a highly dynamic process and therefore regulated in multiple ways. The basic levels at which this regulation takes place are the transcription of mRNAs from genomic DNA, mRNA processing and transport, protein translation, posttranslational modifications, protein localisation and, finally, targeted protein degradation. A disturbance at any of these stages can greatly affect the cellular proteome and therefore impair cellular function with potentially severe implications (1). Targeted protein degradation alone is a highly adaptive and regulated process and the focus of this work. Most intracellular proteins are degraded either via the ubiquitin proteasome system (UPS) or via the autophagosomal-lysosomal pathway (ALP), the two most important cellular pathways for the removal of proteins. This work mainly focuses on the degradation via the UPS, although the ALP is also briefly described and especially relevant, when crosstalk mechanisms between the UPS and the ALP come into play.

1.2 The UPS and the proteasome

The UPS is one of the two main proteolytic systems and consists of three basic regulatory layers: The labelling of proteins with ubiquitin to target them for degradation, the degradation of these proteins by the proteasome and the rescue of already tagged proteins by deubiquitinating enzymes (DUBs). Ubiquitin is a small, 7.6 kDa large protein that can be attached to lysine residues of other proteins and thus influence their function, localisation and degradation. Ubiquitin conjugation to lysine residues on the target proteins relies on E1, E2 and E3 enzymes (reviewed in (2)). The ubiquitin-activating enzyme (E1) activates the ubiquitin under ATP consumption, forming a thioester bond between the ubiquitin and the E1 enzyme. After activation, the ubiquitin is transferred to a ubiquitin-conjugating E2 enzyme, which transfers the ubiquitin to the target protein. Several E2 enzymes have been discovered in mammals. Often, an E3 ubiquitin ligase assists in or even directly catalyses the transfer of the ubiquitin from an E2 enzyme to the target protein. Hundreds of E3 ligases are known, enabling highly selective ligation of ubiquitin to their respective target proteins (reviewed in (3)). Therefore, E3 ligases are a major regulator of degradation specificity. Figure 1-1 shows the principle of protein degradation after ubiquitin tagging, either via the UPS or the ALP. The UPS mostly degrades short-lived and damaged cytosolic, but also nuclear proteins. As such, it is involved in the degradation of many regulatory proteins responsible, among other processes,

for cell cycle control and apoptosis (reviewed in (4) and (5), respectively). Proteasomal impairment can therefore have profound implications for cellular function and differentiation pathways.

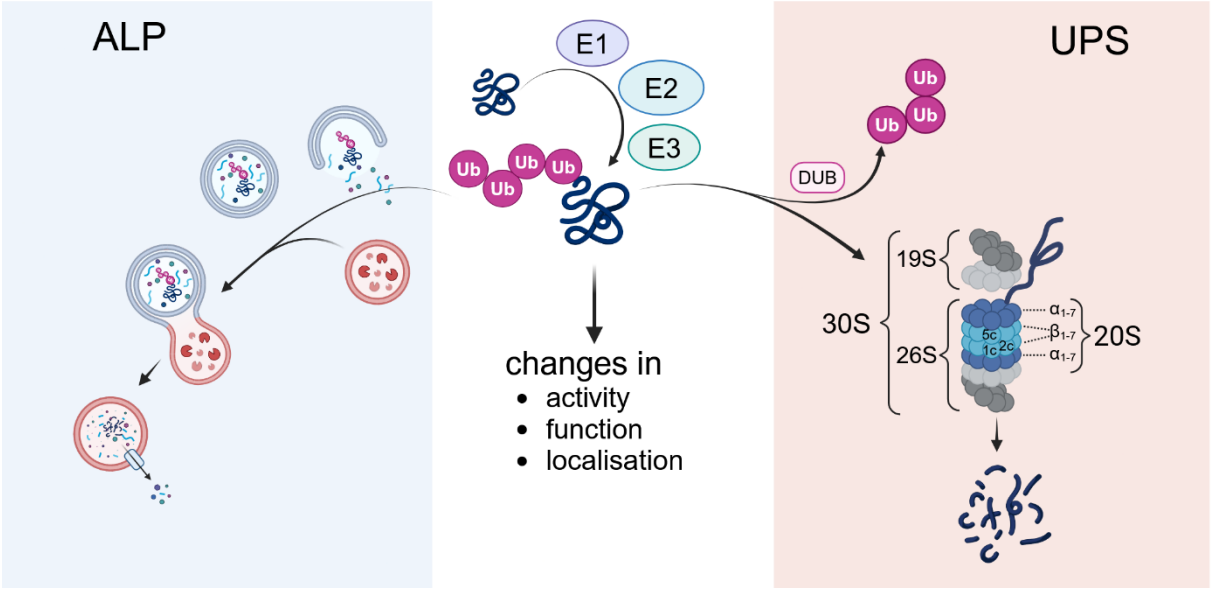

Figure 1-1: The attachment of ubiquitin to proteins can mediate their degradation both via the UPS and the ALP. An enzymatic cascade of E1, E2 and E3 enzymes mediates the attachment of ubiquitin to target proteins. Based on the type of ubiquitin attachment and the corresponding ubiquitin receptors, this can lead to degradation via both the UPS and ALP or have non-degradative effects such as changes in subcellular localisation or interaction partners of the target protein (6). Figure created with BioRender.

1.2.1 The ubiquitin code

The attachment of a single ubiquitin to a target protein only marks the first step of protein ubiquitination. Once a single ubiquitin has been attached to a lysine residue of a target protein, it can be elongated into a ubiquitin chain – or even be removed again by deubiquitinating enzymes. Ubiquitin contains seven lysine (K) residues, providing seven different possibilities to build homotypic chains. Depending on the residue used, these are termed K6, K11, K27, K29, K33, K48, K63 polyubiquitin chains (7). Additionally, the formation of a linear ubiquitin chain has recently gained attention, forming linkages between methionine-1 and glycine-76 of two adjacent ubiquitins (8). Historically, K48 ubiquitin chains have been considered to target proteins for proteasomal degradation, while K63 chains were thought to target proteins for autophagosomal-lysosomal degradation. Some very clear evidence still supports this hypothesis. For example, proteasome impairment results in the rapid accumulation of K48-linked poly-ubiquitinated proteins (9). On the other hand, it has been shown that proteasomal ubiquitin receptors bind both K48 and K63- linked polyubiquitin chains with similar affinity and that K48-pUb-tagged proteins can be degraded by the ALP in situations of UPS impairment (10). The reason behind these conflicting results is not yet fully elucidated. One hypothesis is that ALP ubiquitin receptors are more rapidly degraded upon receptor bundling and that the more linear conformation of K63-linked chains promote this bundling in comparison to the

sterically more hindering K48-linked chains (11). Complicating things further, it is becoming increasingly evident that both mixed linkage and branched ubiquitin chains play a role in many processes, expanding the functional effects of the ubiquitin code even further. Additionally, ubiquitin like modifiers can also be incorporated into ubiquitin chains (reviewed in (12)). The semantics behind this complex tagging patterns are still the topic of intense research efforts.

1.2.2 The proteasome

The proteasome is the catalytic unit within the UPS, being ultimately responsible for proteolytic degradation of proteins. It is a large protein complex that is itself regulated at different levels. The 20S core particle (CP) consists of 28 subunits that are arranged in four rings, two outer α- and two inner β-rings. Each ring consists of seven subunits $\alpha_{1\text{-}7}$ and $\beta_{1\text{-}7}$, respectively. Importantly, three of the β-subunits, namely β1, β2 and β5, harbour the catalytically active centres of the proteasome. Therefore, each proteasome contains several proteolytically active sites (13). Once delivered to the proteasome, target proteins are cleaved into peptides, but not into single amino acids, which can subsequently be achieved by cytosolic peptidases (14).

The proteasome can be present in many different subforms and subtypes. The discrimination between these two terms is not completely consistent throughout the literature. In the present work, the term “subform” refers to various combinations of the 20S core particle with different regulatory caps. The 20S, 26S and PA28 proteasomes are some of the possible subforms (see Figure 1-2 on page 11). The term “subtypes” on the other hand describes the fact that different (catalytical) subunits can be present in the 20S core particle, altering (catalytic) properties of the proteasomal complex.

1.2.3 Proteasome Subtypes

Depending on the catalytic subunits incorporated into the 20S CP during its assembly, different proteasome subtypes have been described: The constitutive proteasome (cP), the immunoproteasome (iP), intermediate proteasomes (intP), the thymoproteasome (tP) and a testes-specific proteasome (15-17). The thymoproteasome has recently been described as a proteasome specific to cortical thymic epithelial cells relevant for positive T cell selection (16, 18). The testes-specific proteasome is distinct from the other subtypes by the incorporation of the α4s subunit (19). For the immuno- and the intermediate proteasomes, increasing evidence for their expression and functional relevance in structural cells such as EnCs throughout the body, has been described in the recent past (20-22). The constitutive proteasome, on the other hand, is essential in all cells across the organism. Therefore, the constitutive and immunoproteasome were the focus of this work and will be described in more detail in the following paragraphs. The exact subunit composition of fully assembled proteasomal

complexes is difficult to determine in most samples and often unclear. Therefore, functional changes resulting from this are clearly understudied.

Table 1-1: Murine and human gene and protein names of proteasomal subunits as they are used throughout this thesis. Also given are the subunit names within the proteasomal complex and the proteasome subtype they constitute. cP: constitutive proteasome, iP: immunoproteasome

Mouse gene	Human gene	Protein	Subunit	Subtype
Psmb5	*PSMB5*	PSMB5	β5c	cP
Psmb6	*PSMB6*	PSMB6	β1c	cP
Psmb7	*PSMB7*	PSMB7	β2c	cP
Psmb8	*PSMB8*	LMP7	β5i	iP
Psmb9	*PSMB9*	LMP2	β1i	iP
Psmb10	*PSMB10*	MECL1	β2i	iP

1.2.3.1 Constitutive proteasome

The constitutive proteasome contains the standard subunits β1c (encoded by the gene *Psmb6*), β2c (*Psmb7*) and β5c (*Psmb5*). Based on structural analyses of their substrate binding pockets, it was proposed very early that these subunits harbour caspase like, trypsin like and chymotrypsin like (CTL) catalytic activities, respectively. These observations have since been substantiated using fluorescence labelled peptide substrates (reviewed in (23)). The constitutive proteasome is expressed in all cells of the murine and human organism and plays a central role for protein degradation. Loss of proteasomal genes essential for proteasome assembly is embryonically lethal, strongly highlighting the essential function proteasomal activity fulfils in all cells. Beyond its proteostatic function to degrade defective or unwanted proteins, the (constitutive) proteasome is also involved in many regulatory cellular processes. Two prominent examples of this proteasomal involvement are the NF-κb and the p53 pathway, both of which are regulated by proteasomal activity (24, 25).

Another central and well described cellular function of the proteasome is the generation of self-peptides for presentation on MHC class I molecules on the cell surface. As such, in some studies more than 30% of all newly synthesized proteins were described to be defective ribosomal products (DRiPs) that are immediately degraded by the proteasome to generate these peptides (26). They are then translocated into the ER, loaded onto MHC class I molecules and these complexes are transported to the cell surface (27). Importantly, one function prescribed very early to the immunoproteasome is the more efficient generation of these peptides (28), although this hypothesis has also repeatedly been challenged (29).

1.2.3.2 Immunoproteasome

In immunoproteasomes, the three catalytic subunits β1c, β2c and β5c of the constitutive proteasome are replaced by β1i (gene *Psmb9*, protein LMP2), β2i (gene *Psmb10*, protein MECL1) and β5i (gene *Psmb8*, protein LMP7), respectively. Expression of these genes has been mostly described in cells of hematopoietic origin, but their expression can be increased and in resident cells induced by external stimuli. While IFNγ is the most commonly described cytokine to induce immunoproteasome expression (30), this has also been described for type I interferons (31) and TNFα (32). Evolutionarily speaking, immunoproteasomal genes have only appeared fairly recently, only being present in jawed vertebrates and having seemingly developed in parallel to other components of the adaptive immune system (33).

Structural studies clearly showed that the catalytic immunosubunits feature different substrate binding pockets than their constitutive counterparts. It has been suggested that these have consequences for their preferences of cleavage sites regarding the amino acid residues neighbouring the scissile bond. The β5i subunit retains the CTL activity of β5c, but prefers even bulkier amino acids due to its larger binding pocket (34). β1i switches from the caspase like activity of β1c to a CTL activity, while β2i retains the trypsin like activity of β2c, but can also cleave after branched amino acids. The changes in substrate binding properties led to the hypothesis that peptides produced by the immunoproteasome have a higher affinity for MHC class I complex binding (15). The structural data also indicates that the β5i subunit might have a higher catalytic activity than β5c. This hypothesis has been supported by experimental evidence that the iP seems to maintain proteostasis under conditions of cellular stress (35). However, these findings have been challenged and it should be noted that relating (subunit) protein amounts to complex assembly or even activities is not straightforward due to the complex nature of the proteasome and the UPS in general (36).

The different binding specificities caused by their binding pockets result in a different peptide repertoire produced by the different proteasome subtypes. These differences in the generated peptide pool by the different proteasomes have implications for cellular processes, most importantly MHC class I- mediated peptide presentation (37). The bulkier hydrophobic amino acids at the end of peptides generated by the immunoproteasome and especially β5i are predicted to bind to the peptide binding groove of MHC class I molecules with higher affinity. Regarding the exact differences in peptide generation between the constitutive and the immunoproteasome, conflicting results have been published. While some studies report that certain epitopes are only generated by one of the two proteasome subforms, others have found that the two only differ in the quantity of certain amino acid cleavage motifs (38).

The immunoproteasome has been implicated in a number of different both physiologic (innate immune regulation, proteostasis) and especially pathological processes, among them cancer, infection and autoimmunity (reviewed in (39)). The complete mechanistic link between the proteasome and the pathologic situation is often unclear as the involvement of the proteasome in cellular processes is highly complex.

It has been described that incorporation of immunosubunits favours the incorporation of the other immunosubunits over constitutive subunits (40). This cooperative mechanism of iP assembly usually favours homogeneous iPs, where all three constitutive catalytic subunits are replaced by their immuno counterpart in both β-rings. Nevertheless, clear evidence also supports the existence of proteasomal complexes that contain both immuno and constitutive subunits, dubbed intermediate proteasomes (intPs) (41).

1.2.3.3 Intermediate proteasomes

Intermediate proteasomal complexes contain both constitutive and immuno catalytic subunits, e.g. β1c, β2c and β5i within the same proteasomal complex. Conflicting evidence has been reported about which combinations of constitutive and immuno subunits can be formed (42-44). How common these intermediate proteasomes really are, is not clear, just as their functional relevance in cells. However, their general presence has been demonstrated *in vivo* (45) and a unique processing of certain antigens by these intermediate proteasomes has been described (46) - a finding in line with the different cleavage properties described for constitutive and immunoproteasomal subunits. Importantly, even asymmetric intermediate proteasomes have been identified, in which the two β rings do not show the same subunit composition (47). The presence of intermediate proteasomes could both complement the peptide pool generated by constitutive and immunoproteasomes in the cell and change the way certain proteins are specifically processed by the proteasome.

In summary, the incorporation of different subunits into the 20S CP gives rise to different proteasomal subtypes. The different structures exhibited by these subunits both raise scientific questions and offer opportunities to (pharmaceutically) target the proteasome. Therefore, (structural) properties of the different subunits are the topic of intense research efforts, especially for future use in clinical applications. While pan-proteasomal inhibition via bortezomib (Velcade®) is already in clinical use for multiple myeloma and mantel cell lymphoma, both adverse side effects and resistance against this treatment greatly limit its efficacy (48). Therefore, inhibitors have been and still are being developed that more specifically target one or only some proteasomal subunit(s), promising better drug suitability (49). In preclinical settings, several potential benefits of selective inhibition of immunoproteasomal activity have been described, e.g. the attenuation of disease burden in an arthritis model (50).

1.2.4 Proteasome subforms

The 20S core particle defines the proteasome subtype, depending on the subunits incorporated during its assembly. After assembly, the 20S CP can associate to different regulatory caps that facilitate and regulate substrate binding and degradation. All subtypes of the 20S proteasome can principally associate with any of the proteasomal caps, although preferences for certain subtype – cap combinations might well exist. Binding to one or two 19 S caps forms a 26 S or 30 S proteasome, respectively. The proteasomal composition and the functional relevance of these subforms is not always clear, especially not in tissue or disease specific contexts (51, 52).

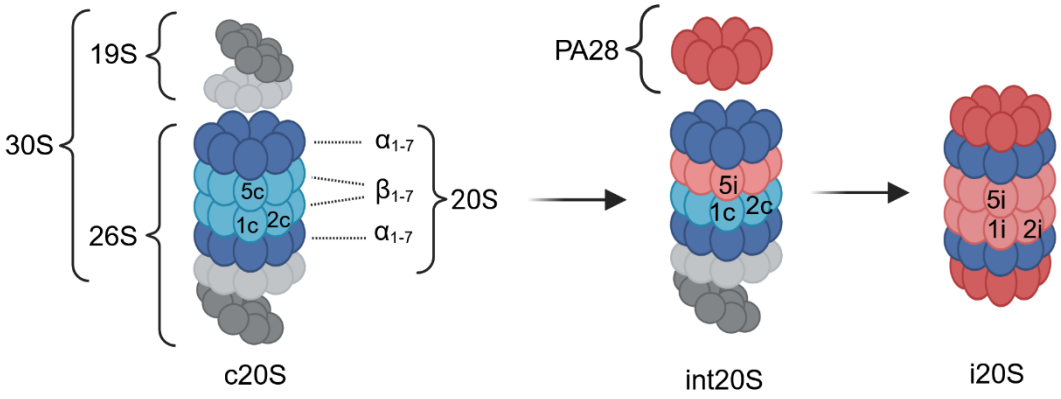

Figure 1-2: The proteasome can be present in different subtypes and subforms. Fundamentally, the 20S core particle consists of four rings, two outer α- and two inner β-rings, each ring containing seven subunits. Depending on the incorporated catalytical subunits, a constitutive (c20S), an intermediate (int20S) or an immunoproteasome (i20S) can be formed. When different regulatory caps attach to the 20S core particle, these different subtypes can assemble to different subforms like the 26S, 30S and PA28 proteasomes. Figure created with BioRender.

1.2.4.1 20S proteasome

The 20S core particle harbours the catalytic centres of the proteasome and forms the basis for all other proteasome subforms. The assembled complex forms a barrel like structure consisting of 28 subunits arranged in the four stacked rings. While the β ring harbours the catalytic chamber, the α ring mediates the docking to proteasomal caps and restricts access to the inner catalytic chamber. Depending on the type of subunit that is incorporated into the complex, the 20S core particle defines the proteasome subtype (e.g. standard/constitutive or immunoproteasome), irrespective of the subform (e.g. 20S or 26S proteasome). The 20S core particle can associate with different caps that regulate its function, forming the different subforms of the proteasome. Therefore, different subform and -type combinations can be present in cells.

The 20S proteasome is not merely the core building block of the other proteasomal subforms, only serving as a pool to quickly assemble functional complexes. Instead, it can function as a standalone protease, representing up to 75% of all proteasomes present in cells, depending

on the tissue and cell type analysed (53) and being proteolytically active even without any caps (54). More importantly, differences exist in the substrate repertoire between the 20S proteasome and other subforms. The 20S proteasome can degrade substrates independently of ATP and ubiquitin, contrasting the degradation mechanism of 26S and 30S proteasomes (reviewed in (55)). This is particularly important in the case of oxidative stress, as 20S proteasomes have been shown to be the most important proteasome sub-form that removes oxidatively damaged proteins. As such, the 20S proteasome has been shown to be much more resistant against oxidative damage than the 26S/30S proteasome (56). Recently, the substrate repertoire of the 20S proteasome has been systematically examined (57). This systematic analysis has strengthened earlier reports that the 20S proteasome mostly cleaves peptide bonds within structurally disordered regions. On the one hand, this allows the degradation of intrinsically disordered proteins and peptides. On the other hand, a targeted proteolytic cleavage within intrinsically disordered regions, in contrast to complete degradation, of specific substrate proteins by the 20S proteasome has been described. This latter phenomenon opens new potential mechanisms of how the (20S) proteasome might regulate cellular pathways beyond the degradation of involved proteins.

1.2.4.2 26S/30S proteasome

The best described regulatory cap binding to the 20S CP is the 19S regulatory cap, sometimes also referred to as PA700. When one or two 19S caps combines with a 20S CP, a 26S or 30S proteasome is formed, respectively. Like the 20S core particle, the 19S regulatory cap consists of numerous subunits, and can be subdivided into a base and a lid. The base mediates docking to the α-ring of the 20S CP, whereas the lid is responsible for substrate binding, unfolding and deubiquitylation (58). It therefore regulates substrate entry into the 20S proteolytic chamber, ensuring highly specific protein degradation and making the degradation both ubiquitin- and ATP-dependent. The 19S regulatory cap can recognize different types of ubiquitin chains for proteasomal degradation, mediated through its different ubiquitin receptors Rpn1, Rpn10 and Rpn13 (59).

Once proteins have been tagged for proteasomal degradation by the addition of ubiquitin, they loosely bind to the proteasome in a first, non-ATP-dependent binding step. At this stage, the tagged protein could still be deubiquitylated by DUBs, thereby “rescuing” the protein from proteasomal degradation. The second step, tightly binding the substrate to the proteasome and committing it for degradation, requires ATP (reviewed in (60)).

1.2.4.3 PA28αβ proteasome

The PA28αβ regulator is a heteroheptameric complex consisting of PA28α and PA28β subunits that assemble in an alternating manner to form a ring. Conflicting evidence has been found regarding the exact stoichiometry. While some studies described an $\alpha_4\beta_3$ organisation

(61), others claimed an $\alpha_3\beta_4$ to be the subunit composition (62). Like the immunoproteasomal subunits of the 20S CP, the expression of the PA28αβ cap genes (*Psme1* and *Psme2*) are inducible by interferon γ (IFNγ) (63). Of note, the PA28αβ cap increases the proteasomes catalytic capacity for peptides, but not for folded proteins, which are mainly degraded via the 26S or 30S proteasome. i20S-PA28 proteasomes were found to preferentially produce shorter peptides compared to both i20S and i26S proteasomes in an *in vitro* setting (64). At the same time, relative catalytic activities seemed to be altered by the PA28αβ cap, with the caspase-like activity being the most induced one. Additionally, peptides were more hydrophilic on average when generated by a PA28αβ proteasome.

1.2.4.4 PA28γ

The PA28γ cap is closely related to the PA28αβ cap but consists of seven γ subunits (encoded by *Psme3*) forming a homoheptameric ring. While PA28αβ is located both cytoplasmic and in the nucleus, PA28γ is almost exclusively found in the nucleus of cells (65). Molecularly, PA28γ has been shown to allosterically activate the trypsin like activity of bound proteasomal complexes without altering properties of the other active sites (66).

1.3 Crosstalk between the UPS and the ALP

As the two main systems responsible for the degradation of proteins in cells, both the ubiquitin-proteasomal system (UPS) and the autophagosomal-lysosomal pathway (ALP) are highly relevant for proteostasis. One important aspect is the fact that the two systems are not clearly separated but instead are closely interlinked and can influence one another. This connection is present at different levels.

For example, K48-pUb proteins, the most commonly described proteasomal substrate, are degraded by the ALP in situations of proteasomal impairment (67). Conversely, the proteasomal 19S cap has been shown to bind both K48- and K63-pUb with very similar affinities (68). In line with this, it has been reported that in case of lysosomal impairment, the UPS can, at least partially, compensate this loss of proteostatic capacity (69). Another link between the two degradative systems is proteaphagy – the removal of proteasomes via the ALP. Proteasomes, especially inactive/damaged/inhibited ones have been shown to be polyubiquitylated and be degraded via autophagy or sequestered into aggresomes (70). Interestingly, it has also been proposed that immunoproteasomal subunits can be specifically targeted for degradation via the ALP in macrophages in situations of FGFR inhibition (71). While in vivo evidence for this effect is still missing, it opens interesting possibilities for the regulation of immunoproteasome abundance.

While the ubiquitin receptor p62 is generally considered to mediate degradation of K63-polyubiquitinated proteins by the ALP, it has also been shown to mediate the proteasomal

degradation of certain proteins (72). Furthermore, it has been shown that p62 is an important mediator between the two degradative systems (73, 74).

1.4 Endothelial cells

Endothelial cells form the inner lining of all blood vessels in the body and for a long time were only regarded as a passive barrier forming channels for blood and everything it transports. The discrimination of endothelial cells into arterial, venous and microvascular EnCs has long been acknowledged. Additionally, morphological differences between microvascular vessels of different organs were also described a long time ago (reviewed in (75)). As such, some endothelia have been described to be fenestrated (e.g. liver, kidney), while others fulfil tight barrier functions (e.g. brain endothelium). However, the functional and molecular differences behind these observed organotypic features have only been described more recently, fuelled by the increasing use of transcriptomic, translatomic and proteomic approaches. For example, translatomic approaches showed strong differences in gene expression profiles between kidney, brain, liver and heart EnCs, both under homeostatic and LPS-challenged conditions (76, 77). In one bulk mRNAseq dataset, structural cells (i.e., epithelial cells, fibroblasts, endothelial cells) isolated from one organ were actually more similar to one another than the cell types isolated from different organs among themselves (22).

As a single cell layer, EnCs are the cells at direct contact between the blood stream and the underlying tissue. As such, they are involved in a multitude of both physiological and pathological processes. While the general involvement of EnCs in immune system processes is well acknowledged, potential differences between organotypic microvascular EnCs with regard to this EnC-immune interaction remain understudied (78).

1.5 The kidney and the glomerulus

Many waste substances can only be cleared from the body via the urine. To that end, human kidneys produce up to 180 liter primary urine per day. The importance of the kidney is also mirrored by the renal blood flow, which accounts for 20% of the cardiac output. The ultrafiltration of primary urine ultimately takes place at the glomeruli. Each glomerulus is mainly comprised of three different cell types: Glomerular endothelial cells (GEnCs), mesangial cells (MCs) and podocytes (PCs). GEnCs and PCs form the filtration barrier, together with the glomerular basement membrane which they synthesize in a coordinated fashion. In total, the filtration barrier consists of four layers: 1) The endothelial glycocalyx, 2) the endothelium itself with its characteristic fenestrations, 3) the glomerular basement membrane and 4) the slit diaphragm formed between podocyte foot processes (79). The filtration barrier possesses both size and charge selective properties ensuring that larger macromolecules like proteins do not pass, while smaller molecules and electrolytes are freely filtered into the primary urine. The primary urine therefore contains many solutes (e.g. electrolytes, glucose, urea) in the same

concentrations as the serum. The tubular system then reabsorbs many of the solutes of the primary urine, and regulates important physiologic processes like organismal volume, salt and pH balance. To fulfil these regulatory functions, the tubular system can also specifically excrete substances, like urea or hydrogen carbonate (80). Together, the glomerulus and the following tubular system form the nephron, the smallest functional unit of the kidney. Disturbances of this complex process of filtration and reabsorption at any stage can have severe consequences for the organism.

1.5.1 Podocytes

Podocytes, as the visceral epithelial cells of the glomerulus, are terminally differentiated, arborised and highly specialised cells within the kidney. With their foot processes, they tightly surround the glomerular capillaries and connect to the foot processes of neighbouring podocytes. The connection between the foot processes is formed by the slit diaphragm, a highly complex protein network that contributes to the glomerular filtration barrier (GFB) (80). The core components of the slit diaphragm are nephrin and neph1 which form heterodimers in a zipper like fashion (81). Additionally, podocytes synthesise components of the glomerular basement membrane to which they also attach with their foot processes (82). Together with the components produced by glomerular endothelial cells, they form the glomerular basement membrane (GBM). The complex morphological structure of podocytes is often lost in glomerular damage, leading to foot process effacement, podocyte hypertrophy and loss into the urine. The resulting impairment of the GFB results in albumin loss to the urine (albuminuria), a hallmark of proteinuric kidney disease (80).

1.5.2 GEnCs

Endothelial cells of the glomerular capillaries (glomerular endothelial cells (GEnCs)) are highly specialised. They form the innermost layer of the glomerular filtration barrier and therefore exhibit unique properties. They must provide high hydraulic conductivity while simultaneously contributing to the filter function of the GFB. To that end, they harbour a substantial glycocalyx and are highly fenestrated, but do not show diaphragms in the fenestrae (79). Together with podocytes, they synthesise components of the glomerular basement membrane (83). Therefore, GEnCs critically contribute to GFB function.

1.5.3 Mesangial cells

Mesangial cells comprise the central stalk of glomeruli and play an essential part in glomerular function. They are specialised pericytes and are located between glomerular capillaries. In contrast to most other pericytes, they are in direct contact with the glomerular endothelial cells, without a basement membrane separating the two cell types (80). One essential function carried out by MCs is the clearance of waste material from the glomerular space. To that end,

MCs are phagocytic cells capable of taking up large amounts of extracellular material for degradation, keeping the glomerular space clear of immunoglobulins and other macromolecules not able to pass the filtration barrier (reviewed in (84)). Additionally, MCs secrete growth factors and cytokines and likely regulate the glomerular filtration surface by exerting contractile forces on the glomerular capillaries (reviewed in (85)).

For the glomerulus to function properly, these three cell types form a functional syncytium. Numerous secreted signals have been shown to be essential for glomerular maintenance and function (reviewed in (86)). Extensive crosstalk between these cell types has been described in different circumstances to be relevant both in health and disease. As such, maintenance of the endothelial layer with its fenestrations and glycocalyx relies on VEGF-A expression and secretion by podocytes (87). Vice versa, endothelial cell senescence has been shown to lead to podocyte damage and kidney disease, mediated by PAI-1 (88). In an even more complex interplay, the sensitivity of podocytes towards the Shiga toxin has been shown to rely on podocyte VEGF-A production and endothelial complement activation (89).

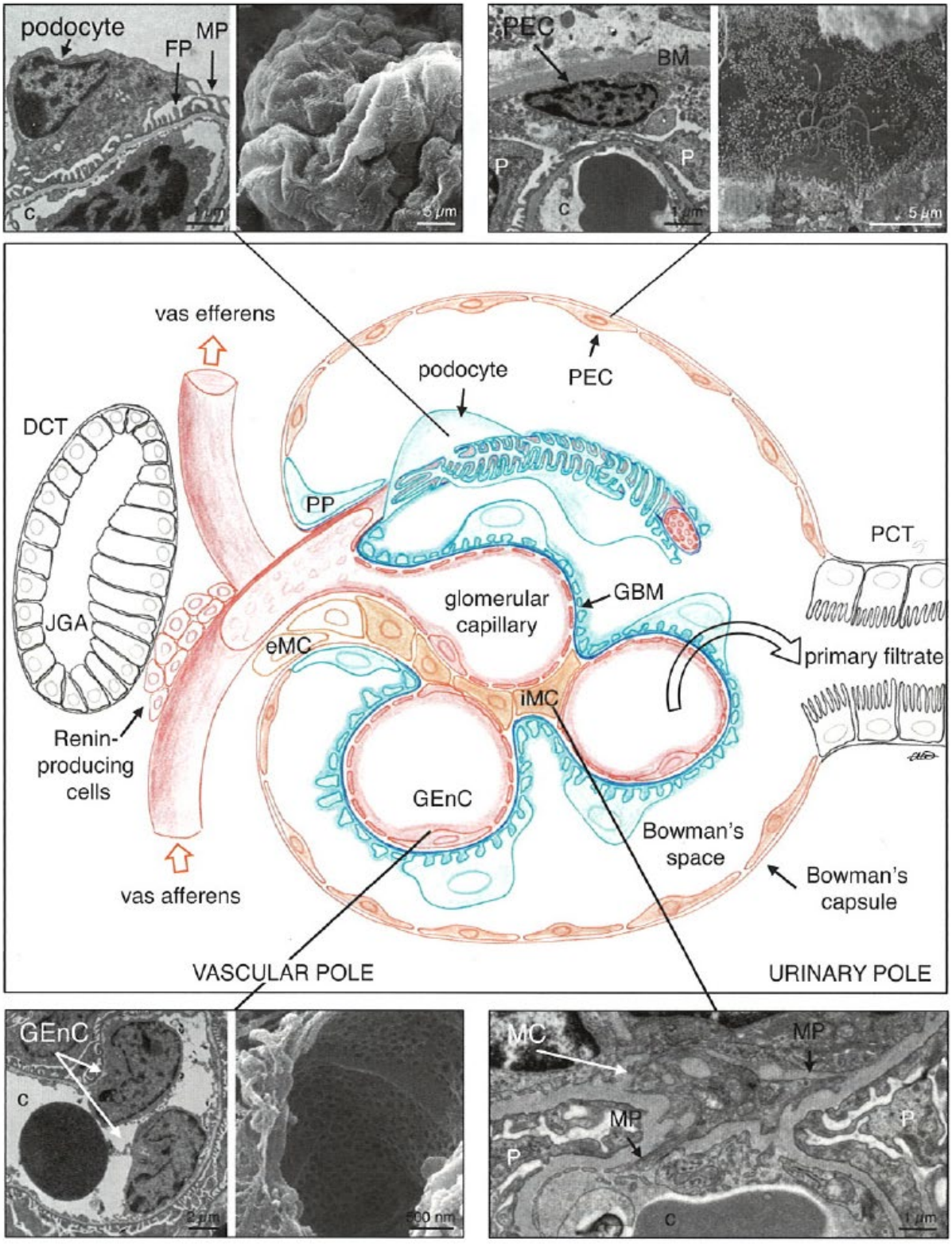

Figure 1-3: The intricate architecture of the glomerulus within the kidney. The glomerulus is mainly comprised of glomerular endothelial cells (GEnCs), podocytes (PCs) and mesangial cells (MCs). Together with the glomerular basement membrane (GBM), GEnCs and PCs form the glomerular filtration barrier (GFB). Over the GFB, the filtration of serum into primary urine takes place. Note the complex architecture of podocyte foot processes (top row, second panel) and of the fenestrated glomerular endothelium (bottom row, second panel). Figure taken from (80), chapter 4 figure 1.

1.6 Kidney disease

Chronic kidney disease has become one of the leading causes of death and morbidity during the first years of the 21st century. As many other lifestyle related health risks, patient numbers have also been increasing (90). The most prominent examples here are obesity and the increasing prevalence of diabetic nephropathy (DN) as a renal involvement in type 2 diabetes (T2D). Chronic kidney disease is characterised through a decline in glomerular filtration rate (GFR), often diagnosed using a filtration marker like serum creatinine or cystatin.

Diabetic kidney disease or DN is a common complication of diabetes in humans. Already today, DN is the leading cause of end-stage renal disease (ESRD) in western countries (91). The prevalence of diabetes will most likely continue to increase world-wide, which would also affect diabetic nephropathy (92). Therefore, gaining more insights into the underlying pathomechanisms and potential treatment strategies for diabetic nephropathy is of clinical interest. While some evidence on the involved mechanisms leading to glomerular damage in DN already exists, it is far from being fully understood, especially since not all aspects can be transferred from rodent models to human disease (91).

Acute glomerulonephritis describes a heterologous group of diseases that all feature immune-mediated glomerular damage. As such, glomerular inflammation results in impairment of the filtration barrier with subsequent loss of protein into the urine (proteinuria), kidney damage and decreased kidney function (93). Lymphocytes, especially cytotoxic T cells infiltrate kidney tissue and mediate glomerular damage (94). The antigenic targets of the immune reaction are diverse, often unknown and can even target different compartments of the glomerulus. While the involvement of different immune cell subsets and cytokines has gained some interest over the recent past, the role of resident kidney cells remains understudied. Especially the antigen presenting endothelial cells present a promising target for further research (reviewed in (95)).

1.7 Murine disease models

To gain more insight into the functional role of LMP7 in different kidney diseases, mouse models were employed in this study. As a model for human type 2 diabetes, the BTBR *ob/ob* mouse was used, whereas the model of nephrotoxic nephritis was used to study antibody- and immune mediated kidney disease in an endothelial specific LMP7 knockout mouse line.

1.7.1 BTBR *ob/ob* mice

The BTBR *ob/ob* mouse line has been well established and described as a model for human type 2 diabetes (T2D) (96). It features leptin deficiency (*ob/ob* genotype), leading to appetite dysregulation (hyperphagia) and subsequent obesity (97). At the same time, mice exhibit insulin resistance, resulting in high blood glucose levels. Importantly, it also shows relevant symptoms of diabetic nephropathy, which is not the case for other diabetic mouse models (98).

As such, albuminuria is observed very early and increases with age, indicating an impairment of the glomerular filtration barrier. While quite some studies have been conducted analysing the ALP in murine diabetes models and the BTBR *ob/ob* mouse itself (99), very little is known about the involvement of the UPS.

1.7.2 Nephrotoxic Nephritis

The model of nephrotoxic nephritis is a well-established model to study the pathomechanisms of antibody-mediated glomerulonephritis. To induce disease, sheep are immunized with glomerular extracts from mice. The sheep form antibodies against mouse glomerular antigens which are then purified and injected back into mice. The antibodies bind to their antigens in the glomerulus, leading to the initial glomerular damage in the early heterologous phase, which is at least partially mediated by the complement system (100). The following autologous phase is characterised by an adaptive immune reaction to the bound/deposited shIgG, perpetuating and exacerbating the damage (101). This phase has been shown to be dependent on Fcγ receptors (102) and, more recently, a critical involvement of TH_{17} cells has been described (103).

2 Aims

The aims of this study were

1. to characterise the expression of immunoproteasomal subunits among endothelial cells of different organs,
2. to gain insights into the functional role of the immunoproteasome in endothelial cells, especially in glomerular endothelial cells and
3. to elucidate possible connections between the endothelial immunoproteasome and human kidney diseases, potentially establishing the immunoproteasome as an additional therapeutic target.

3 Materials and Methods

3.1 Material

3.1.1 Lab instruments used

Table 3-1: Lab instruments used during the experiments of this study.

Type of instrument	Model	Manufacturer
Analytical scale	AC100	Mettler Toledo, Columbus, USA
Biochemical analyser	Cobas Integra 400	Roche Diagnostics, Indianapolis, USA
Biosafety cabinet	Maxisafe 2030i	ThermoFisher, Waltham, USA
Cell counter	LUNA-II™	Logos biosystems, South Korea
Cell incubator	BB-15	ThermoFisher, Waltham, USA
Cell sorters	FACSAria™ IIIu FACSAria™ Fusion	Becton, Dickinson and Company, Franklin Lakes, USA
Centrifuges	5427R 5417R 5804R	Eppendorf AG, Hamburg, Germany
Confocal Laser Scanning microscopes	LSM 800 LSM 980	Carl Zeiss AG, Oberkochen, Germany
Electron transmission microscope	TEM910	Carl Zeiss AG, Oberkochen, Germany
Electrophoresis chambers	MiniProtean Tetra System Criterion Cells	BioRad, Hercules, USA
ELISA plate reader	EL808 Ultra Microplate Reader	BioTek Instruments
Flow cytometers	LSRFortessa™ FACSymphony™ A3 LSR II	Becton, Dickinson and Company, Franklin Lakes, USA
Immunoblotting	Transblot Turbo Transfer system	BioRad, Hercules, USA

Type of instrument	**Model**	**Manufacturer**
Lab pipettes	Research plus	Eppendorf AG, Hamburg, Germany
Light Microscope	Axioskop with Axiocam Hrc	Carl Zeiss AG, Oberkochen, Germany
Magnetic Particle Collector	DynaMag™-2 octoMACS magnet	ThermoFisher, Waltham, USA Miltenyi Biotec, Bergisch-Gladbach, Germany
Magnetic stirrer	RCT digital	Ika-Werke GmbH und Co KG, Staufen, Germany
Pipette boys	Accu-jet (pro)	Brand GmbH + Co KG, Wertheim, Germany
Power Supply	PowerPac Universal	BioRad Laboratories Inc, Hercules, USA
qPCR Thermocycler	QuantStudio3 QuantSudio5	Applied Biosystems, Foster City, USA
Rocking incubators	Rocky VWR Rocking platform GFL-3013	Fröbel Labortechnik GmbH, Lindau, Germany VWR International GmbH, Darmstadt, Germany Gesellschaft für Labortechnik, Burgwedel, Germany
Spectrophotometer	DS11	Denovix Inc, Wilmington, USA
Scales	BP2100S Kern 510	Sartorius AG, Göttingen, Germany Kern & Sohn GmbH, Balingen-Frommern, Germany
Spin tissue processor	STP120	ThermoFisher, Waltham, USA

Type of instrument	Model	Manufacturer
Steam Cooker	FS10	Braun GmbH, Kronberg im Taunus, Germany
Thermocycler	Thermocycler	Biometra, Göttingen, Germany
Thermosphere's	Thermomixer C Thermomixer comfort	Eppendorf AG, Hamburg, Germany
Tissue dissociator	gentleMACS™ (octo) dissociator	Miltenyi Biotec, Bergisch-Gladbach, Germany
Ultramicrotome	UC6	Leica Biosystems, Nussloch, Germany
Vortexer	Vortex Genie2	Scientific Industries, Bohemia, USA
Water bath	-	Gesellschaft für Labortechnik, Burgwedel, Germany
Western Blot imager	Amersham Imager 600 Amersham ImageQuant 800 Fusion FX7	GE Healthcare, Chicago, USA Vilber Lourmat Deutschland GmbH

3.1.2 Lab Consumables

Table 3-2: Consumables used in the experiments. For consumables used in various sizes, not all order numbers are given.

Consumable	Manufacturer	Catalogue number
Reaction tubes 0.5, 1.5, 2 ml	Sarstedt	various
1.5 ml SafeLock tubes	Sarstedt	72.706.400
Pipette tips 10, 200, 1000 µl	Sarstedt	various
Filter pipette tips 10, 200, 1000 µl	Sarstedt	various
15 ml tube	Sarstedt	62.554.502
50 ml tube	Sarstedt	62.547.254
FACS tubes	Falcon	352052

Consumable	Manufacturer	Catalogue number
100 µm cell strainers	Sarstedt	833945100
40 µm cell strainers	Sarstedt	833945040
Cannulas 20, 24, 27, 30 G	B. Braun	various
96 well plates	Sarstedt	82.1581
96 well HighBind plates	Sarstedt	82.1581.200
10 cm petri dish	Sarstedt	821472
Aluminium foil	Roth	2596.1
Combi tips 10, 25 ml	Eppendorf AG, Hamburg	various
Cover slips	Leica	3800147G
Dako pen	ScienceServices	N71310-N
Gloves, nitrile	Dermagrip	SAP150995
Miltenyi C tubes	Miltenyi Biotec	130-093-237
Miltenyi MS columns	Miltenyi Biotec	130-042-201
MultiStix 10SG	Siemens	1526748
Parafilm	Amcor	PM-996
4-15% MiniProtean TGX	Biorad	various
SERVA Native Gel 3 - 12 %	Serva	43250.01
PVDF membrane	Merck Millipore Ltd	IPVH00010
Scalpels	Dahlhausen	11.000.00.723
Serological pipettes	Sarstedt	various
Surgical tape	Leukosilk	0956700
Syringes 2 – 50 ml	B. Braun	various
Lab tissues	Van Merhagen+Seeger GmbH	7730010
Whatman paper	Th-Geyer	3030-6189

3.1.3 Antibodies and dyes

Table 3-3: Antibodies used for the detection of proteins in immunoblot analyses. SB: Superblock

Antigen	host	Dilution	Diluent	Manufacturer	Order number
β-actin	mouse	1:10,000	SB	Sigma	A5441-100UL
β5	rabbit	1:5000	SB	Saskia Schlossarek, Hamburg	Self made
β5	rabbit	1:1000	SB	Invitrogen	PA1-977
Limp2	Rabbit	1:2000	SB	Paul Saftig, Kiel	Self made
LMP7	rabbit	1:5000	3% milk	Elke Krüger, Greifswald	Self made
K48-pUb	rabbit	1:1000	SB	Abcam	140601
K48-pUb	rabbit	1:1000	SB	Millipore	05-1307
K63-pUb	Rabbit	1:1000	SB	Millipore	05-1308
α2	rabbit	1:1000	SB	Cell Signalling	#2455
α3	mouse	1:1000	SB	Santa Cruz	sc-166205
α4	goat	1:1000	SB	Invitrogen	PA5-19368
FcRn	goat	1:1000	SB	R&D	AF6775
Rab5	goat	1:1000	SB	Biorbyt	orb11628-100
Rab7	rabbit	1:1000	SB	Abcam	ab137029
Rab11	mouse	1:500	SB	BD	610656
Rpt1	Mouse	1:5000	SB	Enzo	BML-PW8825
Rpt5	mouse	1:500	SB	Enzo	BML-PW8770

Table 3-4: Antibodies, lectins and dyes used for the detection of proteins in immunofluorescence microscopy. All antibodies were diluted in blocking buffer (5% horse serum in PBS + 0.05% Triton X-100). For FFPE sections, used antigen retrieval methods are also given.

Antigen	**host**	**Dilution**	**Antigen retrieval**	**Manufacturer**	**Order #**
CD31	rat	1:50	Proteinase K	BD	550274
cl. caspase 3	rabbit	1:100	Dako pH 6 (#2369), 40 minutes at 98°C	Cell Signalling	9661S
DNA - Hoechst	-	1:1000	-	Invitrogen	H3570
Kim1	goat	1:500	Dako pH 6 (#2369), 40 minutes at 98°C	R&D	AF1817
LMP7	rabbit	1:400	Dako pH9 (#2367) 40min 98°C	Elke Krüger, Greifswald	Self-made
LMP7	rabbit	1:400	Dako pH9 (#2367) 40min 98°C	Abcam	ab3329
MHCII	rat	1:100	Proteinase K	SantaCruz	59322
msIgG	donkey	1:100	Proteinase 24	Jackson	715-225-151
Nephrin	guinea pig	1:200	Dako pH9 (#2367) 40min 98°C; Dako pH 6 (#2369), 40 minutes at 98°C	Progene	GP-N2
SMA	rabbit	1:400	Dako pH 6 (#2369), 40 minutes at 98°C	Abcam	ab5694
Thsd7a	mouse	1:50	-	Nicola Tomas, Hamburg	Self-made
Tomato lectin	-	1:40	-	Vector	DL-1178
a-Tubulin	mouse	1:100	Dako pH 6 (#2369)	Sigma	T9026-2m
Cy3-WGA	-	1:400	pH9 (2367) 40min 98°C	Vector	RL-1022

All secondary antibodies for both immunoblot and immunohistochemistry experiments were bought from Jackson Immunoresearch, coupled either to HRP or fluorophore tags.

3.1.4 Chemicals

Table 3-5: Chemicals used in the experiments conducted during this project.

Chemical	Manufacturer	Order number	H and P statements
Ammonium chloride	Sigma	A9434-500g	H302, H319; P264, P280, P301+P312, P305+P351+P338, P337+P313, P501
BisTris	Applichem	A1025	-
BSA	Sigma Aldrich	A7906-100G	-
Buprenorphine	Indivior	00345928	H302, H361; P201, P301+P312+P330, P308+P313
Bromphenolblue	Th. Geyer	11844788	-
Calcium acetate	Sigma	402850-100G	-
Calyculin A	Abcr	AB348875	H301+H311+H331, H335; P261, P280, P310, P304+P340, P302+P352, P301+P330
Carbonate buffer	Sigma-Aldrich	C3041	H319; P264, P280, P305+P351+P338, P337+P313
Chloroform	J.T. Baker	7386	H302, H331, H315, H319, H351, H361d, H336, H372, H412; P201, P273, P301+P312+P330, P302+P352, P304+P340+P311, P308+P313
Protease inhibitor cocktail	Sigma	S8820	H314, H335; P260, P271, P280, P303+P361+P353, P304+P340+P310, P305+P351+P338
CD146 beads	Miltenyi Biotec	130-092-007	-
Citric acid	J.T. Baker	0088.1000	H319, H335; P261, P280, P264, P305+P351+P338, P337+P313
Creatinine	Sigma-Aldrich	C4255-10G	-
Dithiothreitol	Sigma-Aldrich	D9779-5G	H302, H315, H318; P264, P280, P301+P312, P302+P352, P305+P351+P338, P332+P313
DMSO	Roth	70291	-

Chemical	Manufacturer	Order number	H and P statements
dNTP set	Invitrogen	10297018	-
DPBS	Gibco	14190-169	-
Dynabeads	ThermoFisher	14013	-
Beads	Spherotech	PM-40-10	-
ECL reagent	ThermoFisher	34578	-
ECL reagent	ThermoFisher	34096	-
EDTA	Sigma Aldrich	E4884-500G	H332, H373; P260, P271, P304+P340+P312, P314, P501
Ethanol	Th.Geyer	2273.2500	H225, H319; P210, P233, P241, P243, P280, P337+P313, P403+P235
Ethanol, denatured	Th.Geyer	2209.5000	H225, H319; P210, P233, P241, P243, P280, P337+P313, P403+P235
Glycerol	Th.Geyer	12150418	-
Glycine	Roth	3908.2	-
HBSS	Gibco	14170-138	-
HCl, 37%	Roth	4625.1	H290, H314, H335; P280, P303+P361+P353, P304+P340, P305+P351+P338, P310
Heparin	Sintetica	EESA10.5PSO	-
HEPES buffer	Gibco	15630-056	-
Horse serum	Biozol	ENH9010-10	-
IMDM	ThermoFisher	12440-053	-
Isoflurane	Baxter	HDG9623	H336; P261, P271, P304+P340+P312, P403+P233, P405, P501
Isopropanol	Roth	9866.2	H225, H319, H336; P210, P233, P305+P351+P338
β-Mercaptoethanol	Gibco	31350-010	H317, H361, H402; P261, P201, P273, P280, P272, P202, P302+P352, P308+P313, P333+P313, P362+P364
MgCl2x6H2O	Merck	1.05832.1000	-
Milk powder	Roth	T145.2	-

Chemical	Manufacturer	Order number	H and P statements
Methanol	Chemsolute	1462.2511	H225, H301+H311+H331, H370; P210, P233, P280, P301+P310, P303+P361+P353, P304+P340+P311
2-Methylbutan	Roth	3926.1	H224, H304, H336, H411; P210, P240, P273, P301+P310, P403+P235
Milk powder	Roth	T145.2	-
Paraformaldehyde (PFA)	Electron microscopy science	15710	H301+H311+H331, H314, H317, H335, H341, H350, H370; P201, P280, P301+ P330+P331, P303+ P361+P353, P304+P340, P305+P351+P338, P308+P310
Periodic acid	Roth	3257.1	H271, H314, H372, H400; P220, P273, P280, P303+P361+P353, P305+P351+P338, P310
Phosphoric acid	Roth	6366.1	H290-H302-H314; P280, P301+P330+P331, P303+P361+P353, P305+P351+P338, P310
Ponceau S	Serva	33427.01	H315, H318, H335, H411; P273, P280, P302+P352, P304+P340, P305+P351+P338, P332+P313
KCl	Merck	1.04936.1000	-
SDS	Roth	2326.2	H228, H302+H332, H315, H318, H335, H412; P210, P261, P280, P302+P352, P305+P351+P338, P312
NaCl	Th.Geyer	1367.5000	-
NaF	Merck	1.06449.0250	H301, H315, H319; P264, P280, P301+310, P302+P352, P305+P351+P338, P332+P313
Na_2HPO_4	Merck	1.06580.1000	-
NaH_2PO_4	Merck	1.06346.1000	-
NaOH	Sigma	71687-500G	H290, H314; P234, P260, P280, P303+P361+P353,

Chemical	Manufacturer	Order number	H and P statements
			P304+P340+P310, P305+P351+P338
Sodium pyruvate	Gibco	11360-039	-
NaV_3O_4	Sigma	S6508-10G	H302+H312+H332, H315, H319; P261, P280, P301+P312, P302+P352+P312, P304+P340+P312, P305+P351+P338
PFA	Sigma Aldrich	441244	H228, H302, H332, H315, H317, H318, H335, H341, H350; P210, P280, P301+P312, P304+P340+P312, P305+P351+P338, P308+P313
Penicillin-streptomycin	Gibco	15140-122	H317, H361fd; P201, P202, P261, P272, P280, P302+P352, P308+P313, P333+P313, P362+P364, P501
PVDF membrane	Merck	IPVH00010	-
Schiff reagent	Sigma	1.09033	-
Suc-LLVY-Amc	Bachem	4011369	-
Sunflower seed oil	Sigma	S5007-250ml	-
Tamoxifen	Sigma	T5648-1G	H350, H360, H410; P202, P273, P280, P308+P313, P391, P405
TissueTek	Sakura	4583	H302+H312+H332, H335; P501
TMB Peroxidase substrate	Aviva	OORA01684	H315, H319, H335; P261, P305+P351+P338
p-toluene sulfonic acid	Merck	402885-100G	H290, H314, H335; P234, P260, P273, P280, P303+P361+P353, P305+P351+P338
TPER	Thermo Scientific	78510	-
Tris-HCl	Merck	1.08219.1000	-
Triton X-100	Sigma	T8787	H302, H315, H318, H410; P264, P273, P280,

Chemical	Manufacturer	Order number	H and P statements
			P301+P312, P302+P352, P305+P351+P338
Trizma base	Sigma	T1503-1KG	-
Tween20	Sigma	P1379-500ML	-
Xylol	J.T. Baker	8080.2500	H226, H304, H312+H332, H315, H319, H335, H373; P210, P260, P280, P301+P310, P331
Zinc acetate	Sigma	Z0625-500G	H302, H318, H411; P264, P273, P280, P301+P312, P305+P351+P338, P391
Zinc chloride	Sigma	793523-100G	H302, H314, H335, H410; P260, P273, P280, P301+P312, P303+P361+P353, P305+P351+P338

3.1.5 Enzymes

Table 3-6: Enzymes used in the experiments

Enzyme	Manufacturer	Order number	H and P statements
Collagenase 1A	Sigma	C9891-1G	H315, H319, H334, H335; P261
DNAse I	Roche	10104159001	H317, H334; P261, P280, P284, P304+P340, P333+P313, P342+P311
Liberase	Roche	5401020001	H315, H319, H334, H335; P261, P264, P280, P284, P304+P340+P312, P342+ P311
DreamTaq	ThermoFisher	EP0713	-
RevertAid RT	ThermoFisher	EP0442	-

3.1.6 Kits

The following kits were used during the work described in this thesis.

Kit	Manufacturer	Order number
Creatinine measurement kit	Hengler Analytik	114444
NucleoSpin RNA Plus XS	Macherey-Nagel	740990.250
RNeasy plus micro kit	Qiagen	74034

3.1.7 Software

The following software was used during the work described in this thesis to control instruments as well as record, analyse and visualise data.

Table 3-7: Software used for data recording, analysis and visualization.

Program	Version(s) used	Manufacturer
Adobe Illustrator	24 - 27.1	Adobe Inc., San Jose, USA
Adobe Photoshop	21 - 25	Adobe Inc., San Jose, USA
EndNote	21.4	Clarivate Analytics, London, UK
FACSDiva	-	Becton, Dickinson and Company, Franklin Lakes, USA
FlowJo	10.6.2 - 10.10	Becton, Dickinson and Company, Franklin Lakes, USA
Fiji	1.52u - 1.54f	-
KC Junior	1.41.6	BioTek Instruments
Office365	-	Microsoft
Perseus	2.0.11	Max Planck Institute of Biochemistry
Prism	9 - 10.3	GraphPad Software, Inc.
R	4.0.0 - 4.4.1	The R Statistical Foundation
RStudio	> 1.2.5042-1	Posit PBC, Boston, USA

For the analysis and visualization of more complex datasets, both published, and generated during this thesis, the R programming environment was used. The following table lists the packages used for data wrangling, analysis and visualisation.

Table 3-8: R packages used for the analysis of complex datasets.

Package	**Version(s) used**	**purpose**
Biomart	2.62.0	Converting gene names, retrieving GO symbols
clusterProfiler	4.14.3	Enrichment analyses
dplyr	0.8.5 -1.1.4	Data wrangling
ggplot2	3.3.0 - 3.5.1	Data visualization
ggprism	1.0.4 - 1.0.5	Data visualization
Readxl	1.3.1 - 1.4.3	Handling excel files
stats	4.2.3	Principal component analysis
stringr	1.5.0	String analysis
tidyr	1.3.0	Data wrangling
Seurat	4.2.0 - 5.1.0	Analysing scRNAseq data
writexl	1.2 - 1.4.2	Handling excel files

3.2 Methods

3.2.1 Mouse work

Mice were housed in a specific pathogen-free animal facility at the University Medical Centre Eppendorf, Hamburg. Mice were kept at ambient temperature (20-24°C) and humidity (45-65%) and were synchronized to a 12 hour light/12 hour dark cycle. Mice had free access to water and standard animal chow (Altromin 1328P). All animal experimental procedures were performed according to the institutional guidelines and approved by the local authorities (Behörde für Justiz und Verbraucherschutz, Hamburg; N038/2020, ORG970, ORG1111, N115/2020).

3.2.1.1 LMP7$^{\Delta EnC}$ mice

For the generation of mice carrying an inducible conditional LMP7 knockout in endothelial cells (LMP7$^{\Delta EnC}$ mice), *Psmb8*$^{fl/fl}$ mice carrying a floxed exon 3 of the *Psmb8* gene were crossed with *Cdh5*-(PAC)-CreERT^2 mice expressing an inducible Cre recombinase under the control of the *Cdh5* promoter (104, 105). Presence of the flox sites as well as of the Cre driver gene were confirmed via PCR based genotyping. Only homozygous floxed animals were used for experiments. Mice additionally carrying the Cre driver gene were used as knockout animals whereas Cre$^-$ littermates served as littermate controls. Induction of the knockout was carried out by injecting the mice intraperitoneally with 75 mg/kg bodyweight tamoxifen in sunflower seed oil per day on five consecutive days. Concentration of the tamoxifen solution was adapted so that only volumes between 70 µl and 110 µl had to be applied and a 30 G cannula was used for injections. Tamoxifen is a hazardous substance and has been shown to be excreted by mice after injections (106). Therefore, ventilation hoods were put on the cages from the day of first injection until three days after the last injection to avoid exposure of the staff handling the mice. Cages and bedding material were changed three days after the last injection. To allow for complete removal of the tamoxifen and degradation of the existing LMP7 protein, at least four weeks passed between the last injection and further experimental steps.

3.2.1.2 BTBR ob/ob mice

BTBR *ob/ob* mice were used as a murine model of type 2 diabetes. Mice displayed increased weight already at 8 weeks of age. When necessary, mice were held on softer bedding material to avoid skin irritation. Mice also received food and water on the cage floor as soon as they showed difficulties reaching food at the top of the cage.

3.2.1.3 Genotyping of animals

Tail biopsies were taken by animal housing staff. Tail biopsies were lysed using DirectPCR Lysis Reagent (Mouse Tail) (Viagen 102-T) according to the manufacturer's instruction. Briefly, tails were lysed in 100 µl lysis reagent containing 0.2 mg/ml Proteinase K overnight. Lysis was

stopped by incubation at 85°C for 45 minutes. 1 µl of DNA solution was used as the PCR template. PCR programmes and primer sequences used for amplification are given in the following tables.

Table 3-9: PCR programme used to verify the presence of the Cdh5-Cre transgene. The PCR was set up as a touch down PCR.

Step	**Temperature**	**duration**	
1.	94°C	2 min	
2.	94°C	20 sec	2-4: 10 cycles
3.	65°C; -0,5°C/cycle	15 sec	
4.	68°C	10 sec	
5.	94°C	15 sec	5-7: 28 cycles
6.	60°C	15 sec	
7.	72°C	10 sec	
8.	72°C	2 min	
9.	4°C	hold	

Table 3-10: PCR programme used to amplify the genomic region around exon 3 of the Psmb8 gene.

Step	**Temperature**	**Duration**	
1.	94°C	120 sec	
2.	94°C	30 sec	2-4: 35 cycles
3.	58°C	45 sec	
4.	72°C	60 sec	
5.	72°C	480 sec	
6.	10°C*	infinity	

After PCR, the amplicons were separated on a 2% agarose gel and the genotypes determined based on the band pattern. After being sacrificed in experiments, mice were genotyped again to verify the originally determined genotypes.

Table 3-11: Primer sequences used for the genotyping of LMP7$^{\Delta EnC}$ mice.

Primer	Sequence
LMP7 flox-fw	5' - GCT ATA ATG CCA GCT CTG TCT GAA CTT CG - 3'
LMP7 flox-rev	5' - TGC CTC TTG CAT CTC TTA GCC CAC C - 3'
Cre-fw	5' - GCG GTC TGG CAG TAA AAA CTA TC - 3'
Cre-rev	5' - GTG AAA CAG CAT TGC TGT CAC TT - 3'
Cre Control-fw	5' - CTA GGC CAC AGA ATT GAA AGA TCT - 3'
Cre Control-rev	5' - GTA GGT GGA AAT TCT AGC ATC ATC C - 3'

3.2.1.4 Induction of nephrotoxic nephritis

LMP7$^{\Delta EnC}$ mice received tamoxifen for knockout induction at least four weeks before the induction of nephrotoxic nephritis (NTN). Serum from sheep that were immunised against mouse glomerular basement membrane was used. Mice were intraperitoneally injected with the antibody containing serum as described (107). Control animals were injected with the same volume of pre-immune sheep serum. The amount of serum per injection differed between the lots of NTN serum and was determined via pre-experiments. These were performed by the group of Ulf Panzer, Hamburg, who also kindly provided the nephrotoxic serum.

3.2.1.5 Urine collection

For the collection of urine, mice were placed on a metabolic cage for two to five hours with free access to water. At the end of the collection period, urine was collected and stored at -20°C until the determination of urinary albumin and creatinine concentration required for the calculation of the albumin to creatinine ratio (uACR). Final urine was directly taken from the animal's bladder during terminal organ extraction.

3.2.2 Terminal organ extraction

Thirty minutes after subcutaneous buprenorphine injection (0.1 mg/kg body weight), mice were put under isoflurane anaesthesia. Sufficient analgetic coverage was verified via absent reflexes. Tail biopsies were taken for regenotyping. The abdomen was opened, and bladder urine was taken for uACR determination, aortic blood for the determination of serum parameters. Finally, kidney packages and other organs were taken and stored in cold HBSS on ice until further processing. Cervical dislocation was performed right after the mice were removed from isoflurane inhalation.

3.2.3 Glomeruli isolation

HBSS + BSA:	*0.05% BSA (w/v) in HBSS*
Collagenase digestive solution:	*1.2 mg/ml Collagenase 1D + 100 U/ml DNase I in HBSS*

Kidneys were perfused with 4.0-4.5 µm large magnetic beads (200 µl Spherotech PM-40-10 in 50 ml HBSS) through the kidney arteries and minced using a scalpel. Tissue was digested in collagenase digestive solution for 15 minutes at 37°C at 1300 rpm on a thermoshaker. The suspension was filtered through 100 µm cell strainers twice and pelleted for 5 minutes at 600 x g at 4°C. Glomeruli were resuspended in 6 ml HBSS and split into four 2 ml reaction tubes. The tubes were placed on a magnetic particle collector and the glomeruli collected at the magnet for five minutes. The supernatant containing non-glomerular tissue was discarded. Glomeruli were washed three times by the addition and removal of 1.5 ml HBSS + BSA in each step. Finally, glomeruli were counted, pelleted and the pellets frozen at -80°C.

3.2.4 Isolating glomerular cell populations

HBSS + BSA:	*0.05% BSA (w/v) in HBSS*
Collagenase digestive solution:	*1.2 mg/ml Collagenase 1D + 100 U/ml DNase I in HBSS*
Liberase digestive solution:	*1 mg/ml Liberase TL, 100 U/ml DNase I, 10% FBS, 1% P/S, 5.55 ml Na-Pyruvat, 8.5 ml HEPES 1M in RPMI 1640*
MACS buffer:	*0.5% BSA (w/v) and 2 mM EDTA in DPBS*

For the isolation of glomerular cell types, the glomeruli isolation protocol was slightly adapted. Instead of three washing steps with HBSS+BSA, the following multistep washing procedure was employed to reduce the loss of glomeruli. Glomeruli were resuspended in only 3 ml HBSS and split into two 2 ml reaction tubes.

1. Up to 16 tubes were processed in parallel:
    a. Tubes were inverted several times, put on MPC for 1 min
    b. 1 ml of the supernatant was removed
    c. 1 ml HBSS was added, 1 ml supernatant removed
    d. Step c was repeated 2 times (1 ml of HBSS was added 3x in total)
    e. 1 ml of HBSS + 0.05% BSA was added, tubes were removed from the MPC and the glomeruli resuspended by shaking.

2. Samples were vortexed.
3. Tubes were inverted several times, put on MPC for 1 min
    a. 1 ml of the supernatant was removed
    b. 1 ml HBSS added, 1 ml of supernatant was removed
    c. Step b was repeated 2 times (1 ml HBSS was added 3x in total)
    d. Entire supernatant was removed
    e. 1.5 ml of HBSS + BSA were added, tubes removed from the MPC and well shaken
4. Step 3 was repeated once

After the procedure described in steps 1-4, glomeruli were collected at the MPC for 5 minutes. The supernatant was removed and the glomeruli from each mouse were collected in 1 ml of HBSS. Optionally, glomeruli were counted and purity assessed under a microscope. If necessary, glomeruli were rewashed. Isolated glomeruli were digested for two hours in Liberase digestive solution at 1400 rpm on a thermoshaker and repeatedly mechanically stressed as detailed in the following table. For shearing, samples were passed through a 27 G cannula on a 2 ml syringe. At Pasteur pipette steps, samples were passed through a Pasteur pipette once.

Table 3-12: Time course of the generation of single cells from glomerular samples.

Time remaining in hours	**Type of mechanical stress**	**Incubation time after treatment**
2:00		30 min
1:30	**V**ortex, **S**hear, **V**ortex	20 min
1:10	V, S, V, **P**asteur **p**ipette, V	20 min
0:50	V, S, V, PP, V	10 min
0:40	V, S, V, PP, V	10 min
0:30	V, PP, V	10 min
0:20	V, S, V	5 min
0:15	V	5 min
0:10	V	5 min
0:05	V	5 min
0:00	3 x V	

After glomeruli were dissociated into single cells, beads were removed for 5 minutes at the magnetic particle collector. The supernatant containing the cells was transferred to a fresh tube. Cells were pelleted for 10 minutes at 1000 x *g* and were stained for isolation via cell sorting or flow cytometric analysis.

3.2.5 Generating single cell suspensions from mouse organs

HBSS + BSA:	*0.05% BSA (w/v) in HBSS*
MACS buffer:	*0.5% BSA (w/v) and 2 mM EDTA in DPBS*
Erythrocyte lysis buffer:	*144 mM NH_4Cl, 17 mM Tris-HCl pH7.6*

For non-glomerular tissue, experimental workups differed between organs. Mice were transcardially perfused with 20 ml PBS under isoflurane anaesthesia to reduce the number of erythrocytes and leukocytes for later steps of cell isolation. Organs were taken and stored in ice-cold HBSS on ice until further processing. Organs were shredded using a scalpel, digested in Liberase digestive solution and mechanically stressed. Exact treatment conditions were different for the organs and are detailed in the following table.

Table 3-13: Digestion times and mechanical stresses used to generate single cells from different organs.

Tissue	Digestion time	Mechanical stresses
Heart	45 minutes	gentleMACS
Lung	45 minutes	gentleMACS
Liver	45 minutes	gentleMACS
Kidney, non-glomerular	50 minutes	Shearing

For gentleMACS™ treatment, cells were transferred to gentleMACS™ C tubes with 3 ml HBSS+BSA and subjected to the program m_Spleen_01_01 once. For tubular samples, shearing was performed through a 27G cannula after 30 and 50 min of digestion. After dissociation, cell suspensions were filtered through 100 µm cell strainers to remove tissue debris. If necessary, erythrocyte lysis was performed for five minutes at room temperature in erythrocyte lysis buffer. Lysis was stopped by adding 10 ml DPBS and cells were pelleted for 5 minutes at 600 x *g* and 4°C. To prevent unspecific binding of antibodies to Fc receptors, Fc block was carried out using 5% normal mouse serum in MACS buffer for 15 minutes at 4°C. Cell suspensions isolated from heart, liver and the non-glomerular kidney fraction were then incubated for 15 minutes with 10% anti-CD146 beads at 4°C and pre-enriched using Miltenyi MS columns. The eluted $CD146^+$ fraction was then stained for cell sorting or flow cytometric analysis.

3.2.6 Staining of isolated cells

MACS buffer*:* 0.5% BSA and 2mM EDTA in DPBS

For staining, cell pellets were resuspended in staining solution (MACS buffer containing the antibodies at the concentrations given in the following tables). Staining was carried out at 4°C in the dark for 30 - 45 minutes. Staining was stopped by adding 1 ml DPBS. Cells were pelleted for 10 min at 1000 x *g* and resuspended in DPBS. Finally, cells were strained through a 40 µm cell strainer into FACS tubes.

Table 3-14: Antibodies used for the staining of murine glomerular cell types.

Antigen	**Fluorophore**	**Source**	**Cat No.**	**Final concentration µg/ml**
CD31	BV421	BD Biosciences	562939	0.25
MHCI (H2Kb)	AF488	BioLegend	116510	2.00
Podoplanin	PE	BioLegend	127408	1.00
MHCII	APC	BioLegend	107614	2.00
CD73	AF700	BioLegend	127230	0.25
CD45	APC-Cy7	BioLegend	103116	2.00
FcRn	APC	Biorbyt	1004685	10.00
Viability stain	APC-Cy7	Invitrogen	L10119	Dilution 1:1000

Table 3-15: Antibodies used for the staining of murine non-glomerular endothelial cells.

Antigen	**Fluorophore**	**Source**	**Cat No.**	**Final concentration µg/ml**
CD31	BV421	BD Biosciences	562939	0.25
MHCI (H2Kb)	AF488	BioLegend	116510	2.00
Podoplanin	PE	BioLegend	127408	1.00
MHCII	APC	BioLegend	107614	2.00
CD45	AF700	BioLegend	103128	5.00
FcRn	APC	Biorbyt	1004685	10.00
Viability stain	APC-Cy7	Invitrogen	L10119	Dilution 1:1000

3.2.7 Cell sorting

For cell isolation via sorting, cells were sorted at either the FACSAria™ Fusion or FACSAria™ IIIu cell sorter using a 100 µm nozzle. Cells were collected in SafeLock 1.5 ml tubes using the 4-way purity mode. If protein biochemical analyses were to be carried out, cells were resuspended and collected in DPBS to avoid BSA contamination from MACS buffer. The gating strategy slightly differed between the tissues. For isolation of glomerular cell types (podocytes, mesangial cells and endothelial cells), the gating strategy can be seen in Figure 3-1 (established in (108)). After debris and doublet exclusion, live/dead staining and the exclusion of CD45$^+$ cells, mesangial cells were separated from PCs and EnCs using CD73-AF700. To remove podocyte contamination, Podoplanin (Pdpn$^+$) cells were excluded from this gate. PCs and EnCs were separated from one another using CD31-BV421 as an endothelial cell marker. PCs, GEnCs and MCs were collected in individual tubes. Due to fewer isolated podocytes and mesangial cells, 400 µl DPBS were given into the PC and MC collection tubes prior to sorting.

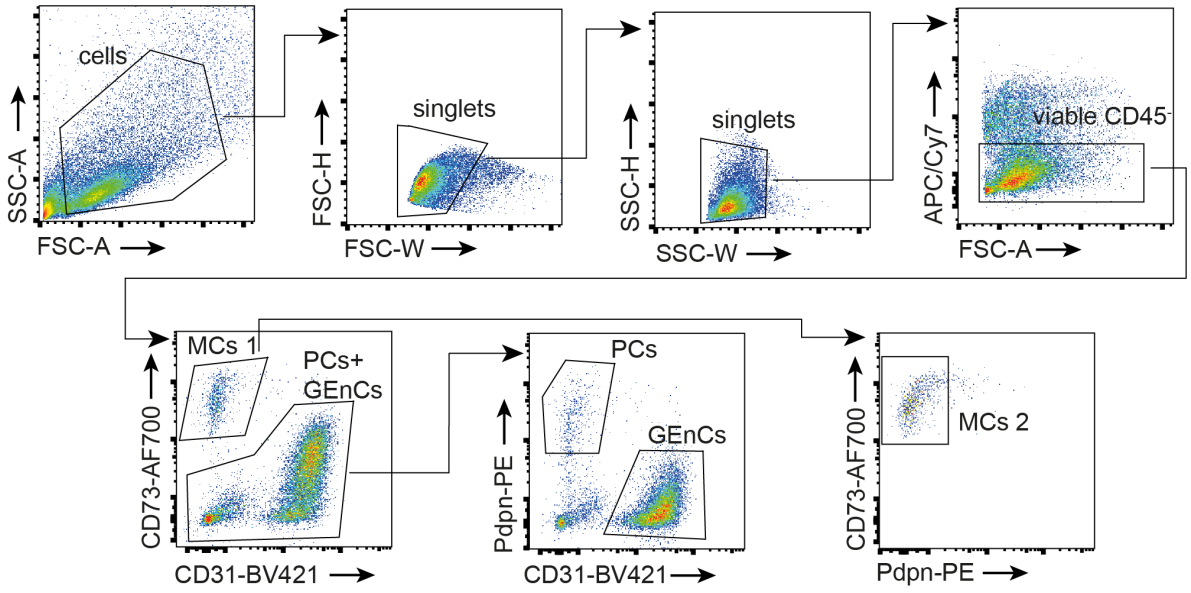

Figure 3-1: Gating strategy for the isolation of glomerular cell types (podocytes, PCs; mesangial cells, MCs, glomerular endothelial cells, GEnCs). After excluding debris, doublets, dead and CD45$^+$ cells, MCs were separated from PCs and GEnCs using CD73-AF700 (MCs 1). MCs were then freed from PC contamination, resulting in the population MCs 2, which was collected for analysis. PCs and GEnCs were separated using Podoplanin (Pdpn) as a PC marker, yielding the three glomerular cell types. Gating strategy was adapted from (108).

In Figure 3-2, the slightly adapted gating scheme used for non-glomerular tissue (non-glomerular kidney fraction, heart, liver and lung) is shown. Cells were separated from debris using an FSC-A vs SSC-A gate, doublets were excluded using both FSC-H vs FSC-W and SSC-H vs SSC-W. Dead cells were excluded using a fixable live/dead stain. In a CD45-AF700 vs CD31-BV421 plot, leukocytes were excluded, and endothelial cells were identified. Finally, lymphatic endothelial cells were excluded using Podoplanin-PE staining to only extract

microvascular endothelial cells. $CD31^+Pdpn^-$ cells were collected as endothelial cells, $CD45^-$ $CD31^-$ cells were collected as non-endothelial control cells from each organ.

After cell sorting, cell suspensions were pelleted for ten minutes at 1500 x *g* and the supernatant was carefully aspirated with a micropipette. Cells were snap frozen and stored at -80°C until further analysis.

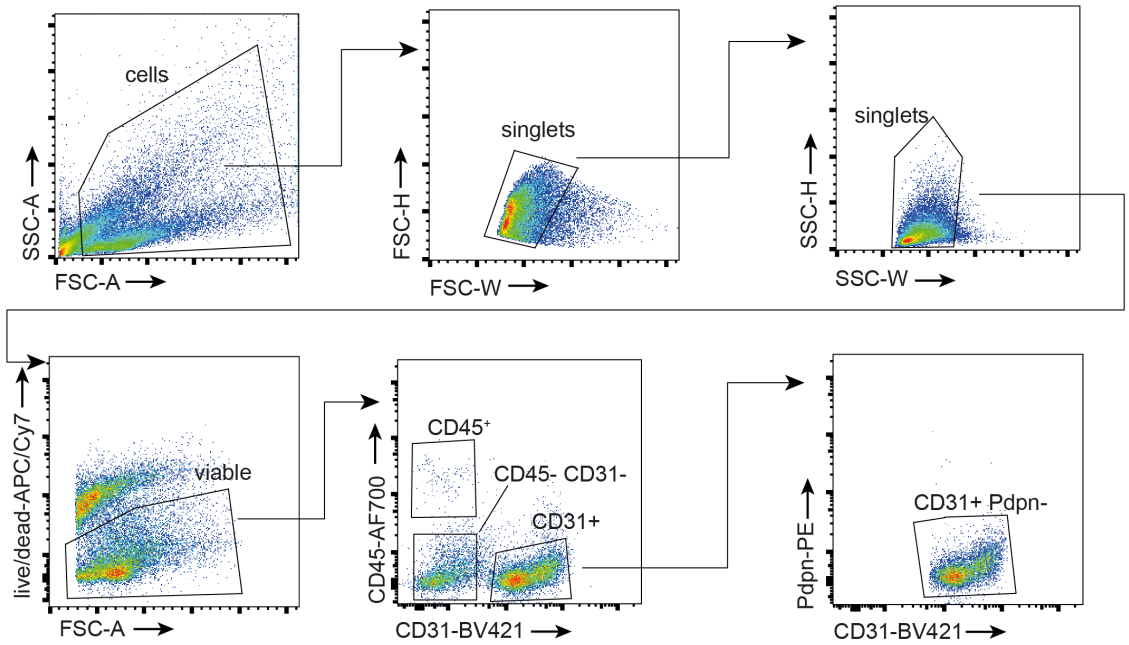

Figure 3-2: For the isolation of endothelial cells from tissue (here shown for kidney peritubular endothelial cells (PtEnCs)), a slightly simplified gating strategy was employed. After the exclusion of debris, doublets and dead cells, $CD45^+$ cells were separated from $CD31^+$ endothelial cells. Finally, $CD31^+Pdpn^+$ cells were excluded to not include lymphatic endothelial cells. The isolated $CD31^+$ $Pdpn^-$ cells were then collected as microvascular endothelial cells. This gating strategy was employed for heart, lung, the non-glomerular kidney fraction and liver, optionally with CD146-bead based pre-enrichment.

3.2.8 Flow cytometric analysis of cells

Flow cytometric analysis of kidney endothelial cells was carried out at either the BD LSRII, BD FACSymphony™ A3 or BD LSRFortessa™ analyser. Figure 3-3 displays the simplified gating scheme used for both GEnCs and PtEnCs. First, viable single cells were identified using the FSC-A and SSC-A parameters and a cell viability dye. $CD45^+$ leukocytes were excluded and from the $CD45^-$ cell population, $CD31^+$ endothelial cells were analysed for the expression of cell surface markers.

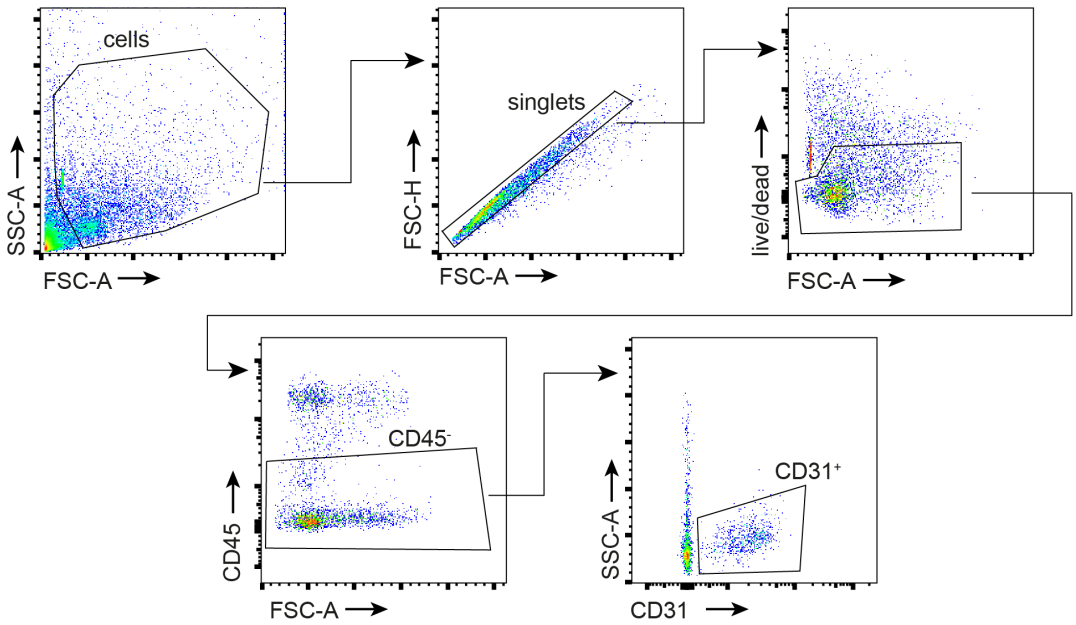

Figure 3-3: Simplified gating scheme used for flow cytometric analysis of both kidney peritubular and glomerular EnCs. After the identification of viable single cells, CD45⁺ leukocytes were excluded. Then, CD31⁺ EnCs were identified and analysed for the expression of cell surface markers.

3.2.9 Cell cycle analysis via flow cytometry

For the flow cytometric assessment of cell cycle state, cells were first stained extracellularly with CD31 and a live/dead stain (1:1000, BioLegend) as described above. Thereafter, cells were fixed and permeabilized with 70% EtOH overnight at -20°C in the dark. Cells were washed twice with MACS buffer and subsequently stained with propidium iodide (PI, Molecular Probes) staining solution (20 µg/ml PI, 200 µg/ml RNase A in PBS) for 30 min at RT. Cells were diluted in PBS and directly analysed at a FACSymphony™ A3 flow cytometer. The PI signal was detected in the PE channel. Cell cycle analysis was performed using FlowJo 10.9.0 using the “Cell Cycle” function and a pragmatic Watson model.

3.2.10 Lysing samples

For protein biochemical analyses, samples were lysed using different lysis buffers depending on the application. The lysis method was adapted both to the type of tissue analysed (glomeruli, isolated primary cells) as well as the type of analysis (immunoblot or activity analysis).

3.2.10.1 Murine glomeruli for immunoblot

TPER lysis buffer:	*100 nM Calyculin A, 1 mM NaF, 1 mM Na_3VO_4, 1x cOmplete™ protease inhibitors in TPER™*

Glomeruli were lysed in a number adapted manner by lysing 5000 glomeruli in 150 µl lysis buffer. Initially, frozen glomeruli were thawed on ice and the pellet crushed with a pestle in 50 µl of TPER lysis buffer, before adding the remaining volume. The suspension was incubated on ice for thirty minutes and ratched over a tube rack every ten minutes. Cell debris was

pelleted for thirty minutes at 16,000 x *g* at 4°C and the supernatant transferred to a fresh tube and either stored at -80°C or directly used for analysis.

3.2.10.2 Murine glomeruli for proteasome activity measurements

TSDG buffer:	*10 mM Tris, pH 7.5, 10 mM NaCl, 25 mM KCl, 1 mM $MgCl_2$, 100 nM EDTA, 10% Glycerol, 1 mM DTT, 2 mM ATP in H_2O*

Glomeruli were lysed in a number adapted manner by lysing 5000 glomeruli in 100 µl lysis buffer. Initially, frozen glomeruli were thawed on ice and the pellet crushed with a pestle in 50 µl of TSDG buffer, before adding the remaining volume. Lysis was performed with seven freeze-thaw cycles between an ethanol-dry ice mixture and a warm water bath. Protein solutions were spun down at 16,000 x *g* for 30 minutes at 4°C to remove cellular debris. Supernatants were transferred to fresh tubes and either analysed directly or stored at -80°C until further processing.

3.2.10.3 Isolated cells for WB

TPER lysis buffer:	*100 nM Calyculin A, 1 mM NaF, 1 mM Na_3VO_4, 1x cOmplete protease inhibitors in TPER™*

Frozen cell pellets were thawed on ice, lysis buffer was added to the pellet, so that 50,000 cells were lysed in 10 µl and the cells were resuspended by vortexing. Cells were incubated on ice for thirty minutes and ratched over a tube rack every ten minutes. Cellular debris was pelleted for 30 minutes at 16,000 x *g* and the supernatant transferred into fresh tubes. Lysates that were not analysed directly were stored at -80°C.

3.2.10.4 Isolated cells for proteasome activity measurements

TSDG buffer:	*10 mM Tris, pH 7.5, 10 mM NaCl, 25 mM KCl, 1 mM $MgCl_2$, 100 nM EDTA, 10% Glycerol, 1 mM DTT, 2 mM ATP in H_2O*

Frozen cell pellets were thawed on ice. The corresponding volume of TSDG lysis buffer was added to the cells and the cells were resuspended via vortexing. For measuring proteasome activity, the volume of the lysis buffer depended on the number of cells per sample. Approximately 200,000 cells were loaded per gel lane. Cells were lysed using seven freeze-thaw cycles between an ethanol-dry ice mixture and a warm water bath. Cellular debris was pelleted at 16,000 x *g* for 30 minutes, the supernatant transferred to fresh tubes and the lysates preferably directly analysed, otherwise stored at -80°C.

3.2.11 Derivatization with activity-based probes

Activity-based probes allow the detection of catalytically active proteasomal subunits. Consisting of a reactive group, a recognition element and a reporter tag, they covalently bind to the active centres of proteasomal subunits and subsequently allow their detection via the reporter (e.g. a fluorophore or biotin) (reviewed in (109)).

TSDG buffer:	*10 mM Tris, pH 7.5, 10 mM NaCl, 25 mM KCl, 1 mM $MgCl_2$, 100 nM EDTA, 10% Glycerol, 1 mM DTT, 2 mM ATP in H_2O*
5x sample buffer:	*50 mM Tris pH6.8, 0.1 M DTT, 2% SDS, 10% Glycerol, 0.05% bromphenolblue in H_2O*
TG running buffer:	*25 mM Trizma base, 192 mM Glycine, 0.1% SDS in H_2O*

Natively lysed samples were used for analyses with activity-based probes. Control samples were treated either with inhibitor (Epoxomicin) or DMSO as a positive control at a concentration of 2 µM for one hour at 37°C. Subsequently, samples were incubated with the activity-based probe (Abp) MVB003 at 0.5 µM for 1 hour at 37°C. After incubation with the Abp, 5x DTT sample buffer was added to the sample and the sample was denatured for 10 minutes at 95°C.

3.2.12 In gel proteasomal activity measurements

ClearNative sample buffer:	*50 mM BisTris, 50 mM NaCl, 10% glycerol, 0.05% bromphenolblue in H_2O*
Native running buffer:	*50 mM BisTris, 50mM Tricin in H_2O*
Substrate incubation buffer:	*20 mM Tris pH 7.4, 5 mM MgCl2, 2 mM ATP, 100 µM Suc-LLVY-Amc in H_2O*

For analysis of the activity of proteasomal complexes, samples were natively lysed as described above. For electrophoretic separation using native polyacrylamide gel electrophoresis (PAGE), samples were mixed with 5x ClearNative sample buffer and separated using 3-12% native gels. Gels ran for 3 hours at constantly 150-200 V in native running buffer at 4°C. After electrophoretic separation, gels were incubated for 20 minutes in substrate incubation buffer. Cleavage of the Suc-LLVY-Amc substrate generates free aminomethylcumarin (Amc), which could then be detected at the Vilber Fusion FX7 imager using excitation at 365 nm and detection at 450 nm. After development of the fluorescent readout, proteins were blotted as detailed in section 3.2.15 for the determination of protein levels.

3.2.13 SDS-PAGE

Sample buffer: *50 mM Tris pH 6.8, 0.1 M DTT, 2% SDS, 10% Glycerol, 0.05% bromphenolblue in H_2O*

Running buffer: *25 mM Tris, 192 mM Glycine, 0.1%SDS in H_2O*

For the separation via denaturing SDS-PAGE, lysates were denatured in sample buffer for 10 minutes at 95°C. After that, samples were loaded onto discontinuous gradient gels from Biorad. Proteins were separated at 100-200 V using a Tris glycine running buffer.

3.2.14 Subunit-specific SDS-PAGE

For analysis of proteasomal subunits via activity-based probes, samples were loaded on self-prepared discontinuous 12.5% Tris glycine gels. Separation was carried out at 120-150 V. Fluorescently labelled proteasomal subunits were then analysed at the Vilber FX7 imager with the corresponding filter sets. After fluorescence detection, immunoblot analysis of proteins of interest were performed as described in section 3.2.15.

3.2.15 Protein detection via immunoblot

Transfer buffer: *25 mM Tris, 192 mM Glycine, 20% EtOH in H_2O in ddH_2O*

TBS-T: *100 mL 10x TBS, 900 mL ddH2O, 0.5 mL Tween-20*

PTSA: *0.01 M PTSA in ddH_2O*

Protein transfer was performed using the BioRad TransBlot Turbo transfer system. 0.45 µm PVDF membranes were activated for two minutes in ethanol and washed twice in H_2O for one minute. The transfer was carried out for 30 min at 25 V in transfer buffer containing 20% EtOH. After completion of the transfer, membranes were stained for ten minutes in 0.2% Ponceau-S staining solution, destained in several rinsing steps with H_2O until the membrane background was white and a clear protein staining was visible. Finally, a colorimetric image of the Ponceau staining was taken. After washing twice for five minutes in tris buffered saline with Tween (TBS-T), membranes were blocked in 5% non-fat dry milk (NFDM)/TBS-T for one hour at room temperature. After washing the membranes three times in TBS-T, membranes were incubated in primary antibodies overnight at 4°C. The next day, four five-minute washing steps at room temperature were followed by incubation of the membranes with the secondary HRP coupled antibodies in 5% NFDM/TBS-T for one hour at room temperature. After washing again four times for five minutes with TBS-T, the membranes were incubated for five minutes in ECL development solution, and the signal was developed at the AI600 or AI800 imager. Optionally, HRP activity was inhibited before the membranes were incubated in the next primary antibody. For this, membranes were treated with 0.01 M para-toluene sulfonic acid (PTSA) for 2 x 5

minutes (110). Membranes were rinsed twice and washed twice for five minutes in TBS-T and subsequently incubated in the new primary antibody as detailed above.

Band intensities obtained from HRP readout, Ponceau staining or fluorescent gel readout were quantified using the “Measure” function from Fiji, with the “Mean” value being used for further analysis. Rectangles of the same size were used for all samples for the same protein on the same gel/blot. Band intensities for the proteins of interest were normalised to the respective β-actin or Ponceau signal and then to the respective controls.

3.2.16 Determination of serum parameters

Serum urea and triglycerides were determined at the Cobas Integra 400 plus analyser (Roche Diagnostics) with the corresponding kits. To convert the serum urea values determined by the Cobas into blood urea nitrogen values, they were multiplied by 0.466, based on the nitrogen content of urea.

3.2.17 uACR Determination

Coating buffer:	*0.5 M Carbonate-Bicarbonate buffer*
10x MAE buffer:	*0.5 M Trizma base, 1.38 M NaCl, 0.027 M KCl, pH 8.0 in H_2O*
Wash buffer:	*0.05% Tween 20 in 1x MAE buffer*
Postcoat:	*1% BSA in 1x MAE buffer*
Conjugate diluent:	*0.005% Tween-20 in Postcoat*
Stopping solution:	*16.85 ml phosphoric acid 85% + 250 ml ddH_20*
Creatinine reagent:	*5 ml alkaline buffer (R1) + 1 ml picric acid (R2)*

Albumin content of murine urine samples was determined using a sandwich ELISA for the detection of murine albumin. Briefly, a high bind 96 well plate was coated with primary antibody 1:100 in coating buffer at 4°C overnight. Surplus primary antibody was removed with three washing steps, after which the plate was incubated with postcoat solution for 30 minutes. Following three washing steps, the plate was incubated with the diluted samples for 1 hour. After washing 5 times with wash buffer, secondary antibody at a dilution of 1:40,000 in conjugate diluent was given to each well and the plate further incubated for 1 hour. After washing 5 times, TMB substrate was added to each well and the reaction allowed to develop for up to five minutes in the dark. Finally, the reaction was stopped using 5.4% H_3PO_4 and the absorbance was measured at 450 nm. Based on a serial dilution standard curve consisting of 7 different concentrations, the albumin concentration of each sample was calculated.

Duplicates were done for each sample. Samples not in the linear range of the standard curve were repeated on a different plate at a different dilution.

The creatinine content of each sample was determined using the kinetic method based on Jaffé with a kit from Hengler analytics. 10 µl of each sample or standard were loaded into a well of a 96 well microtest plate. 50 µl of creatinine reagent was added and the plate incubated for 1 minute at room temperature. Then, the kinetic measurement was started consisting of two measurements five minutes apart. Based on a linear standard curve consisting of 7 different concentrations, the concentration of each sample was calculated. Duplicates were performed for each sample. Based on the albumin and creatinine concentration determined, the urinary albumin-to-creatinine ratio (mg/mg) was calculated.

3.2.18 *In vivo* perfusion of mice with tomato lectin

For the endothelial localisation of accumulated msIgG in the organs, LMP7$^{\Delta EnC}$ mice were perfused with tomato lectin *in vivo*. The abdomen was opened, and the mice perfused with 10 ml 40 µg/ml tomato lectin through the aorta. To retain organ morphology, mice were additionally perfused with 10 ml 4% PFA directly afterwards. Organs were preserved either for cryoblocks, formalin fixed paraffin embedding (FFPE) or zinc-fix analysis.

3.2.19 Immunohistochemical analyses

Zinc fixative:	*3.16 mM $CaCH_3COOH$, 27.4 mM $ZnCH_3COOH$, 36.7 mM ZnCl in 0.1 M Tris*
Blocking buffer:	*5% normal horse serum, 0.05% Triton X-100 in PBS*

Immunohistochemical and immunofluorescence analyses were carried out either on formalin fixed paraffin embedded (FFPE), zinc fixed tissue or cryosections, depending on the staining.

For FFPE sections, organ pieces were fixed in 4% PFA overnight at 4°C and subsequently washed in PBS. Organ pieces were then dehydrated according to the following table and embedded in paraffin. From step 2 on, tissue pieces were handled by an automated tissue processer.

Zinc fixation was used for the assessment of T cell markers and MHC class I and II (111). Tissue pieces were fixed in zinc fixative for 24 hours and stored in 50% EtOH until dehydration according to the following table, followed by paraffin embedding

Table 3-16: Treatment scheme for the paraffin embedding of tissue samples.

Substance	**Duration**
50% EtOH	>2h
60% EtOH	2h30min
70% EtOH	1h
96% EtOH	1h
96% EtOH	1h
100% EtOH	1h
100% EtOH	1h
100% EtOH	1h30min
Xylol	1h
Xylol	1h
Xylol	1h30min
Paraffin	1h
Paraffin	1h30min

For cryosections, tissue pieces were stored in 15% sucrose until they sank to the bottom, then they were stored in 30% sucrose until they sank to the bottom and then they were shock frozen in TissueTek in a 2-methyl butane bath on dry ice. Tissue blocks were then stored at -80°C.

3 µm sections were cut (8 µm for cryosections), fixed on microscope slides and the parrafin sections rehydrated in a descending alcohol series as detailed in table 3-17. Target retrieval was performed according to table 3-4. Sections were incubated with blocking buffer for 30 minutes at room temperature. Sections were incubated overnight at 4°C in primary antibodies. The next day, sections were washed three times for five minutes in PBS and incubated at least 30 minutes in secondary antibody. Sections were washed again and sealed in fluoromount under cover slips. Immunofluorescent stainings were analysed using either the Zeiss LSM800 or Zeiss LSM980 confocal microscope equipped with an AiryScan 1 or 2.

Table 3-17: Steps of the descending alcohol series used to rehydrate paraffin-embedded tissue sections.

Solvent	Duration	repetitions
Xylol	5 min	3x
100% EtOH	5 min	3x
96% EtOH	5 min	2x
70% EtOH	5 min	2x
demineralised water	5 min	2x

To quantify protein intensity based on confocal immunofluorescence images, the mean intensity of the channel of the protein of interest was determined using FIJI. A region of interest was used to only measure intensities in certain areas (e.g. only in glomeruli).

3.2.20 Periodic acid Schiff staining and crescent quantification

For the assessment of general kidney morphology and crescent formation, periodic acid Schiff (PAS) staining of kidney sections was performed. Briefly, 1.5 µm thick sections were cut using a Leica microtome and fixed on microscope slides. Sections were rehydrated using a descending alcohol sequence as detailed in table 3-17 and incubated in periodic acid for 15 minutes at room temperature. Sections were rinsed for three minutes under running tap water and briefly rinsed in demineralised water. After incubation with Schiff's reagent for 40 to 50 minutes, sections were rinsed for seven minutes under running tap water and briefly rinsed in demineralised water. The nuclei were stained using hemalaun solution for approximately 30 seconds and the section rinsed again under running tap water. Sections were differentiated by dipping them in EtOH-HCl. Sections were washed in cold tap water and the nuclei staining was verified under the microscope. Sections were washed again and dehydrated using an ascending alcohol series as detailed in table 3-18. Sections were sealed under cover slips using Eukit. After drying overnight, stainings were ready for evaluation under a light microscope.

For crescent quantification, 30 glomeruli on as PAS-stained section were randomly chosen per mouse. Each glomerulus was classified as either being crescentic or not. The percentage of crescentic glomeruli was used to characterise disease severity.

Table 3-18: Steps of the ascending alcohol series used for dehydrating tissue sections after PAS staining.

solvent	duration	repetitions
70% EtOH	2 min	1x
96% EtOH	2 min	3x
100% EtOH	2 min	1x
100% EtOH	5 min	1x
100% EtOH	10 min	1x
Xylol	5 min	3x

3.2.21 Electron microscopy

Electron microscopy sample workup and analysis was performed by PD Dr. Oliver Kretz, UKE, Hamburg. For electron microscopy, small cortical kidney pieces were fixed in 4% buffered PFA with 1% Glutaraldehyde at 4°C for 24 hours. The tissue was postfixed in 1% osmium in 0.1 M phosphate buffer (PB) and stained with 1% uranyl acetate in 70% ethanol, each for 1h at room temperature. Samples were then dehydrated and embedded in epoxy resin. Ultrathin sections were cut and contrasted with lead citrate. Micrographs were recorded using a Zeiss 910 transmission electron microscope. Glomerular endothelial fenestrations, foot process effacement and GBM swelling were quantified using ImageJ version 1.53t.

3.2.22 RNA isolation for bulk mRNA sequencing

RNA isolation for bulk mRNA sequencing was performed using the Qiagen RNeasy Plus Micro kit according to the manufacturer's instructions. Briefly, cells were lysed and genomic DNA removed using the gDNA eliminator spin columns. Samples were transferred to MinElute spin columns and washed. RNA was eluted with 21 µl of RNase free water. RNA quantity and purity were determined using the DeNovix DS11 spectrophotometer. RNA was stored at -80°C.

3.2.23 Bulk mRNA sequencing

Isolated mRNA was sent to Novogene, Cambridge, UK for library preparation and sequencing. mRNA was isolated from total RNA using poly T-oligo attached magnetic beads. cDNA was synthesized in a non-directional way and the library was quality-controlled and quantified. Paired end 150 bp sequencing was performed on an Illumina platform. Raw reads were quality controlled and mapped to the reference genome. Fragments per kilobases per million mapped reads (FPKM) values were calculated and differentially expressed genes were identified using the DESeq2 R package (1.20.0).

3.2.24 Bottom-up proteomics

Buffer A:	*0.1% Formic acid (FA) in H_2O*
Buffer B:	*0.1% Formic acid (FA) in 80% aceto nitrile*

Cells for mass spectrometric based proteomic analysis were isolated as described in sections 3.2.4 and 3.2.5. Proteomic sample workup, measurements and analysed were performed by the Mass Spectrometric core unit at the UKE, led by Prof. Dr. Hartmut Schlüter. Cells were dissolved in 100 mM triethyl ammonium bicarbonate (TEAB) and 1% w/v sodium deoxycholate (SDC) buffer, boiled at 95°C for 5 min and sonicated. The samples were then pipetted into a 96-well LoBind plate (Eppendorf, Hamburg, Germany) placed on an Andrew+ Pipetting Robot (Waters, Milford, USA), which was used to execute all following steps. Using the robot, disulfide bonds were first reduced in 10 mM dithiothreitol for 30 min at 56°C while shaking at 800 rpm and alkylated in presence of 20 mM iodoacetamide for 30 min at 37°C, again while shaking at

800 rpm. Then, carboxylate modified magnetic E3 and E7 speed beads (Cytiva Sera-Mag™, Marlborough, USA) at 1:1 ratio in LC-MS grade water were added in a 10:1 (beads/protein) ratio to each sample, following the single-pot, solid-phase enhanced sample preparation (SP3)-protocol workflow (112). To bind the proteins to the beads, acetonitrile (ACN) concentration was raised to 50%. Subsequently, samples were shaken at 600 rpm for 18 min at room temperature. Magnetic beads were collected at the magnet and the supernatant was removed. Magnetic beads were further washed two times with 80% Ethanol (EtOH) and then two times with 100% ACN. After resuspension in 100 mM AmBiCa, digestion with trypsin was performed (sequencing grade, Promega) at 1:100 (enzyme:protein) ratio at 37°C overnight while shaking at 500 rpm. The next day, trifluoroacetic acid (TFA) was added to a final concentration of 1% to inactivate trypsin. The samples were then shaken at 500 rpm for 5 min at room temperature. Finally, beads were magnetized, and the supernatant containing tryptic peptides was transferred into a new 96-well LoBind plate, ready for subsequent LC-MS/MS analysis. Chromatographic separation of tryptic peptides was achieved with a two-buffer system (buffer A: 0.1% FA in H2O, buffer B: 0.1% FA (Fisher Chemical, A117-50) in 80% ACN) on a UHPLC (VanquishTM neo UHPLC system, Thermo Fisher). Attached to the UHPLC was a peptide trap (300 µm x 5 mm, C18, PepMap™ Neo Trap Cartridge, Thermo Fisher, 174500) for online desalting and purification, followed by a 25 cm C18 reversed-phase column (75 µm x 250 mm, 130 Å pore size, 1.7 µm particle size, peptide BEH C18, nanoEase, Waters, 186008795). Peptides were separated using an 80 min gradient with linearly increasing ACN concentration from 2% to 30% ACN over 60 minutes.

MS/MS measurements were performed on a quadrupole-orbitrap hybrid mass spectrometer (Exploris 480, Thermo Fisher Scientific). Eluted peptides were ionized using a nano-electrospray ionization source (nano-ESI) with a spray voltage of 1800 V and analysed in data independent acquisition (DIA) mode.

LC-MS/MS data were searched with the DIA-NN algorithm (Version 1.9.1, (113)) against a *mus musculus* database (obtained May 2024, 17005 entries). The oxidation of methionine, the N-terminal methionine excision and the acetylation of the protein N-terminus were allowed as variable modifications. A maximum number of two missing tryptic cleavages was set. Peptides between 7 and 30 amino acids were considered. A strict cutoff (FDR < 0.01) was set for peptide identification in double pass mode. Match between runs was activated. Normalization was performed based on the sample median protein abundance. Obtained protein abundances were log2-transformed, and further statistical testing was performed in Perseus (Maxquant, Max-Planck-Institute of Biochemistry, (114)). Student's T-testing was performed and results of p-values and log2 fold changes were visualized as volcano plots in R Studio.

3.2.25 EA.hy926 cell culture and harvesting

Culture Medium: *IMDM + 50 ml FBS + 5 ml P/S*

Parental and LMP7 knockout EA.hy926 cell lines were a kind gift from Elke Krüger, Greifswald. They were cultured in Iscove's Modified Dulbecco's Medium (IMDM) + 10% FBS + 1% Penicillin/Streptomycin at 37 °C, 5% CO_2 and 100% relative humidity in a cell culture incubator. For passaging, medium was removed and cells washed with DPBS. Cells were detached using Trypsin-EDTA and detachment was verified under a microscope. Cells were diluted using culture medium and seeded into fresh flasks. For protein biochemical analysis, cells were washed twice with ice-cold PBS and harvested in ice-cold PBS with cell scrapers. For flow cytometric analysis, cells were washed in ice-cold PBS. 200 µl Accutase® solution were added to each well of a 12-well plate and successful cell detachment was verified under a microscope. 500 µl PBS were added to each well and the cell suspension transferred to a 1.5 ml tube. Wells were washed once more with 500 µl PBS to gather remaining cells. Fc block was performed using human FcR blocking reagent (130-059-901, Miltenyi BioTec), stained for cell surface markers and analysed at the BD FACSymphony A3 flow cytometer.

3.2.26 Statistical analysis

Statistical analyses and visualization were done using GraphPad Prism. Mann-Whitney U test was used for two-sample comparisons, a Welch-Anova where more than two groups were compared, unless otherwise stated. P values in figures are denoted as follows: ns: $p \geq 0.05$; *: $0.01 < p < 0.05$; **: $0.001 < p < 0.01$; ***: $0.0001 < p < 0.001$; ****: $p < 0.0001$.

More complex datasets, both published and self-generated, were analysed and visualized using R in the R studio environment. Packages used are summarised in Table 3-8 and code can be made available upon reasonable request.

4 Results

4.1 The endothelial immunoproteasome under basal conditions

The immunoproteasome as an alternative form of the proteasome was originally described to be induced by cytokines, most importantly IFNγ (30). It has also been shown to be expressed and relevant in different kind of immune cells (115, 116). Possible functional consequences of this proteasomal switch towards the immuno subunits have only recently been described. Among them is the hypothesis that the immunoproteasome has a higher catalytic capacity than the constitutive proteasome and retains proteostasis under IFNγ induced stress (35). However, increasing evidence suggests that structural cells and especially EnCs express immunoproteasomal subunits also under homeostatic conditions, without cytokine induction. Therefore, this study sought to build on these findings and unravel the functional role of endothelial LMP7 expression.

4.1.1 Endothelial cells basally express immunoproteasomal subunits

Most research conducted on the molecular processes and functional role of the proteasome and especially individual proteasomal subunits has either been performed in yeast and cell lines or constitutive knockout mice. Only very recently, first studies employing cell type specific knockouts have been conducted. Therefore, only very little is known about the organ-, tissue- and cell type specific roles the (immuno)proteasome might play under both homeostatic and pathological conditions. More detailed knowledge about which proteasomal subtypes and –forms are present in which cells are therefore needed to gain a deeper understanding of cellular processes potentially regulated by the immunoproteasome.

The increased use of *omics* technologies in recent years has led to the generation of more and more datasets examining the gene expression or protein abundance in various sample types focussing only on a certain (patho)biological aspect. Some of these datasets contain information about the cell type specific relevance of the proteasome in, among others, endothelial cells. However, since the original publications accompanying these datasets usually did not focus on the UPS or protein degradation, they were originally not analysed regarding the expression of proteasomal genes. As part of this thesis, existing datasets were utilised to discover hidden aspects regarding the proteasome in these publications.

In 2020, Krausgruber *et. al.* published a study describing structural cells (i.e., endothelial cells, epithelial cells and fibroblasts) as important regulators of the immune response in C57BL/6 mice based on a bulk mRNA sequencing (mRNAseq) dataset (22). They did, however, not focus on (immuno)proteasomal genes, especially not under homeostatic conditions. Therefore, the dataset accompanying the publication was analysed in regard to the catalytically active proteasomal subunits. Figure 4-1 shows the relative expression of the three genes

encoding the catalytic subunits of the constitutive (*Psmb5*, *Psmb6* and *Psmb7*) as well as of the immunoproteasome (*Psmb8*, *Psmb9*, *Psmb10*) in the three structural cell types of different murine organs under homeostatic conditions. Notably, in most organs, endothelial cells were the cell population showing the highest expression of immunoproteasomal subunits, compared to epithelial cells and fibroblasts (Figure 4-1, panel A). Only in the liver and in the heart the expression of immunoproteasomal subunits did not appear to predominantly occur in EnCs. In the liver, the expression was more heterogeneous among the cell types, while heart EnCs did not predominantly express any of the three immunoproteasomal subunits. Interestingly, when only comparing the endothelial cells of different organs among each other, the three catalytically active immunoproteasomal subunits were differentially expressed between organs (Figure 4-1, panel B). While, for example, kidney EnCs showed the highest expression of *Psmb10* (β2i), *Psmb9* (β1i) was most highly expressed in lung endothelium. In contrast, *Psmb8* (β5i) expression was more evenly distributed among the endothelia of different organs. Heart and brain seemed to have a slightly lower *Psmb8* (β5i) expression compared to kidney, lung, liver, and skin, which had similar expression levels.

In summary, this dataset indicated that, among structural cells, endothelial cells show the highest expression of immunoproteasomal subunits under homeostatic conditions. Additionally, the different subunits did not seem to be homogeneously expressed between EnCs of different organs.

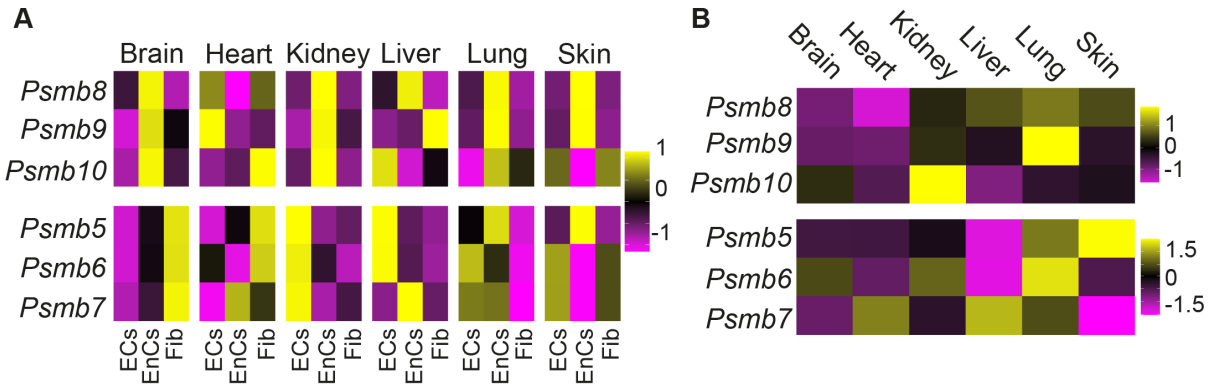

Figure 4-1:Analysis of proteasomal subunit expression in a published bulk mRNAseq dataset comparing three structural cell types, namely epithelial cells (ECs), endothelial cells (EnCs) and fibroblasts (Fib) in different organs of male C57BL/6 mice (22). **(A)** Gene expression levels of the six catalytically active subunits of the constitutive (*Psmb5*, *Psmb6*, *Psmb7*) and immunoproteasome (*Psmb8*, *Psmb9*, *Psmb10*) were z-normalised within each organ and the three structural cell types are shown for six exemplary organs. **(B)** Gene expression levels were z-normalised only within the EnCs from the six different organs shown in (A). Refer to table 1-1 for proteins and subunits corresponding to the gene names.

4.1.2 In the glomerulus, only EnCs express the immunoproteasome

The glomerulus as the place of filtration of blood into primary urine is a functional syncytium formed by three distinct cell types, namely podocytes (PCs), mesangial cells (MCs) and glomerular endothelial cells (GEnCs). The published dataset described above did not analyse these specialised kidney cell types. To examine whether also in this highly specific compartment of the kidney, EnCs are the cell type mainly expressing immunoproteasomal subunits, published kidney datasets were utilised. To this end, the publicly available human scRNAseq data from the kidney precision medicine project (KPMP) was analysed (117). For murine cells, a scRNAseq dataset describing isolated glomerular cells from male C57BL/6J mice (118) was analysed. As shown in figure 4-2, all three catalytically active immunoproteasomal subunits were expressed in GEnCs much more than they were in PCs and MCs in both human and murine samples. As already observed in other organs and total kidney EnCs in figure 4-1, this was not the case for the three catalytically active subunits of the constitutive proteasome. They were expressed more evenly and tended to be more abundant in PCs and MCs. To substantiate the RNA data, an available proteomic dataset comparing the protein expression among isolated glomerular cell types between different mouse strains was analysed (108). These data confirmed the mRNA findings, also showing that the corresponding proteins were present at much higher levels in GEnCs compared to PCs and MCs (Figure 4-2, Panel C). Notably, the three catalytically active subunits of the constitutive proteasome were enriched in PCs in this dataset. Immunofluorescence analyses on human (Figure 4-2, D) and murine (Figure 4-2, E) kidney tissue were performed to assess the expression of LMP7 in glomeruli. These also supported the findings that LMP7 is foremost expressed in GEnCs and to a much lesser extent in PCs and MCs. Therefore, this preferential expression of immunoproteasomal subunits in EnCs over other structural cells was also found within the glomerulus.

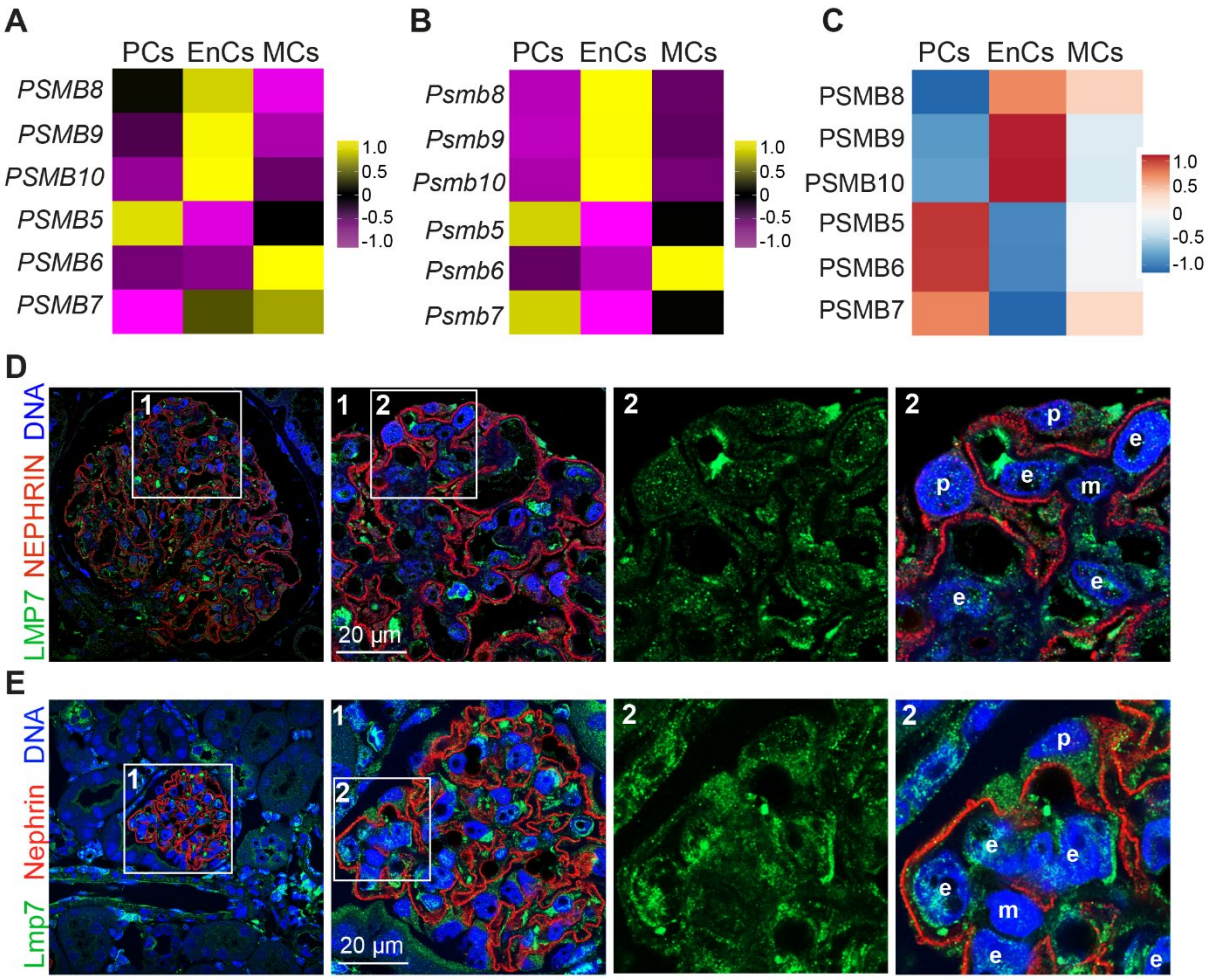

Figure 4-2: Analysis of (immuno)proteasomal subunit expression within the glomerulus. Pseudobulk analysis was performed on published scRNAseq datasets from **(A)** human (data from (117)) and **(B)** murine (data from (36)) and the gene expression z-normalised among the three glomerular cell types. **(C)** Depiction of a published proteomic dataset (data from (108)) showing the protein levels of (immuno)proteasomal subunits. Confocal immunofluorescence stainings on **(D)** human and **(E)** murine kidney tissue were performed using paraffin-embedded tissue sections. Nephrin in red marks the slit diaphragm, DNA in blue marks cell nuclei. Numbers denote magnified excerpts. e: endothelial cell nucleus; m: mesangial cell nucleus; p: podocyte nucleus

These results clearly demonstrated that immunoproteasomal genes were expressed in structural, especially endothelial, cells in different organs and tissues, systematically supporting earlier and already published findings. However, insights into the functional role of the immunoproteasome were not possible using these descriptive datasets. Since most of them are based on mRNA levels, they do not necessarily reflect protein levels in the cell. For proteasomal subunits, this is especially relevant since even the protein levels might not accurately reflect the amount of assembled proteasomal complexes, subunit composition or even proteasomal activity in each cell type.

4.1.3 Validation of the LMP7$^{\Delta EnC}$ mouse line

The functional role of the immunoproteasome in endothelial cells is hardly described. Based on the observations that immunoproteasomal subunits were prominently expressed in EnCs of different organs under homeostatic conditions, a mouse line allowing for the inducible, endothelial specific knockout of LMP7 (β5i) was generated. This mouse line would also allow functional assessment of the immunoproteasome in EnCs. LMP7 was chosen as the immunoproteasomal subunit that harbours the most prominent catalytic activity, namely the chymotrypsin like (CTL) activity. Furthermore, LMP7 has been described to be essential for immunoproteasome assembly, by leading to a preferential incorporation of the immunoproteasomal subunits β1i and β2i into the 20S core particle (40). The absence of LMP7 therefore hinders the assembly of immunoproteasomes, making it a promising target subunit to study potential cellular effects dependent on the immunoproteasome. The mouse line used in this thesis, dubbed LMP7$^{\Delta EnC}$, was generated by crossing *Psmb8*$^{fl/fl}$ mice to *Cdh5*(PAC1)-Cre-ERT2 mice (104, 105). While the former carries a floxxed exon 3 of the *Psmb8* gene encoding LMP7, the latter expresses an inducible Cre recombinase construct under the control of the *Cdh5* promoter, which normally regulates the expression of vascular endothelial cadherin (VE-Cadherin). Therefore, the injection of tamoxifen induces Cre expression and subsequent excision of the exon 3 in *Psmb8* specifically in *Cdh5* expressing cells, namely endothelial cells.

Figure 4-3 shows the basal characterisation of the newly established LMP7$^{\Delta EnC}$ mouse line. Panel A shows the outcome of the genotyping PCRs and the experimental setup. Mice were genotyped for the presence of flox sites within the *Psmb8* gene and the presence of the endothelial specific Cre driver. To assess the successful deletion of LMP7, endothelial cells were isolated via cell sorting as described in sections 3.2.4 and 3.2.5. Cells isolated from kidney (both glomerular (GEnCs) as well as peritubular (PtEnCs)), heart and lung were analysed via immunoblotting and high-resolution immunofluorescence confocal microscopy for LMP7 protein expression (Figure 4-3, panels B - D). Indeed, endothelial cells showed a very robust loss of LMP7. Importantly, other resident cells isolated from the same organ used as control cells (Ctrl) did not show a change in LMP7 levels. Kidney control cells did not show any expression of LMP7 under homeostatic conditions at all. Supporting these findings, high-resolution immunofluorescence confocal microscopy analysis of the studied organs confirmed that LMP7 protein was absent from endothelial cells. Again, LMP7 signal was still observable in non-endothelial cells of these organs, most prominently in the lung. These data confirmed that the newly generated mouse line carried a robust inducible endothelial cell specific LMP7 knockout, making it an appropriate and valuable tool to study the role of the immuno-proteasome in endothelial cells of different organs.

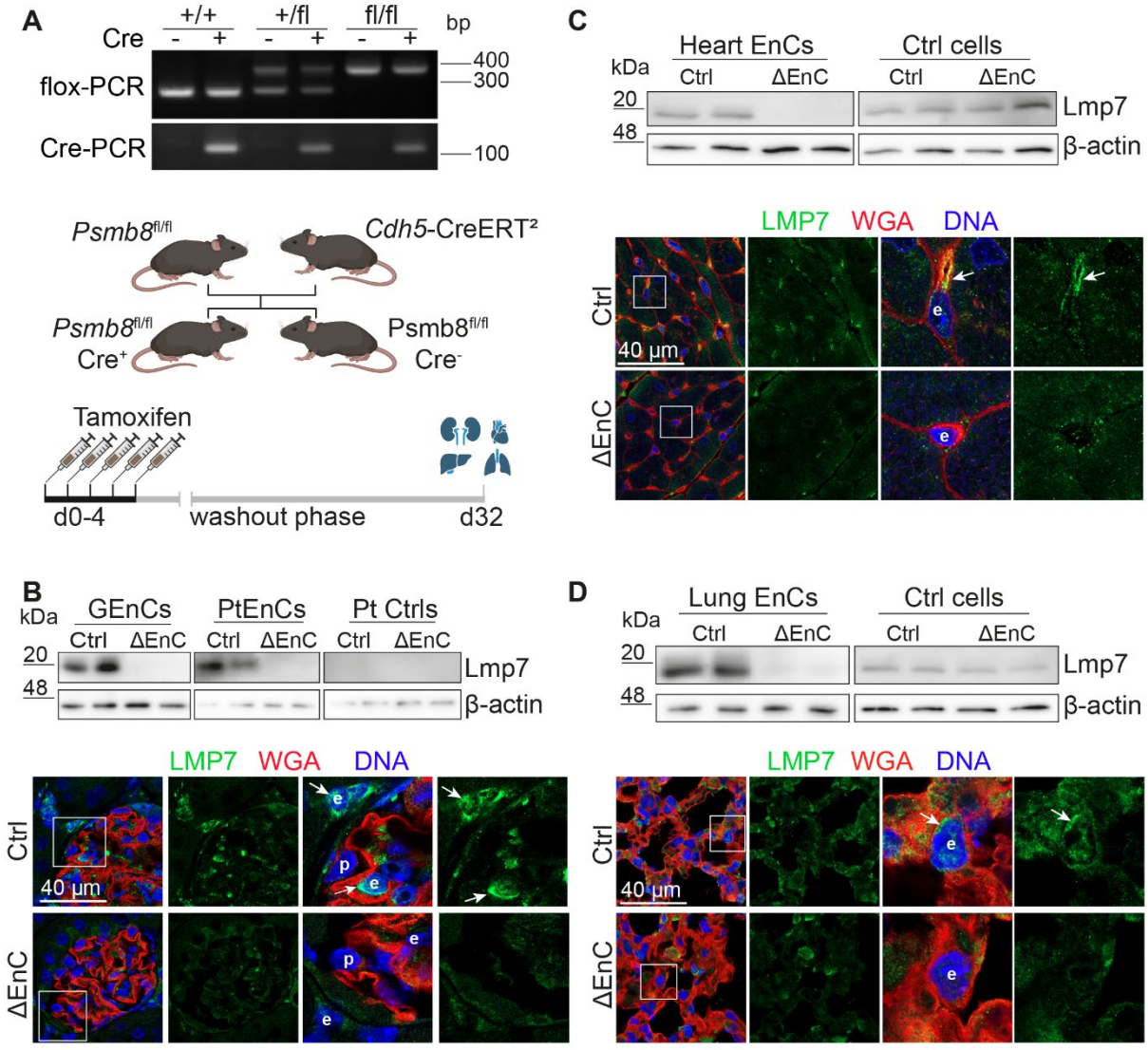

Figure 4-3: Validation of the newly generated LMP7$^{\Delta EnC}$ mouse line. **(A)** Potential outcomes of the PCR-based genotyping approach, breeding strategy and experimental setup for the induction of the knockout. **(B - D)** Both endothelial cells (EnCs) and non-EnC structural cells (Ctrls) were isolated as detailed in sections 3.2.4 and 3.2.5. Immunoblotting analysis for LMP7 and β-actin as a loading control were performed to assess cellular LMP7 levels. Additionally, confocal immunofluorescence microscopy analyses on paraffin-embedded tissue sections were performed for the detection of LMP7 levels. White arrows indicate endothelial LMP7 expression. LMP7 is stained in green, wheat germ agglutinin in red marks cell surfaces, DNA as a nuclear marker is stained in blue. The scheme in panel A was created with Biorender. e: endothelial cell nucleus; p: podocyte nucleus

4.1.4 LMP7$^{\Delta EnC}$ mice grow normally

After specific knockout confirmation, the mice were further observed to determine possible developmental differences in comparison to their littermate controls. Specifically, the mice were initially observed for signs of premature deaths, differences in weight gain and, as a potential kidney specific phenotype, an increase in urinary albumin-to-creatinine ratio (Figure 4-4). Surprisingly, none of these parameters were altered. Although some deaths occurred within four months of intraperitoneal tamoxifen injection, these were very rare and independent of the genotype (Figure 4-4, panel A). When observing mice for up to 50 weeks after LMP7

knockout induction, also no differences in weight gain could be observed. Mice of both genotypes showed the expected weight gain while ageing (Figure 4-4, panel B). Since glomerular endothelial cell LMP7 expression had been found to be very prominent (see Figure 4-2 and Figure 4-3), uACR was analysed to detect a potential impairment of the glomerular filtration barrier (GFB) upon the loss of LMP7 in this special type of endothelial cell. However, no indication of a GFB impairment was observed as the uACR was not significantly altered between the genotypes (Figure 4-4, panel C). These results indicated that LMP7 is not essential for survival or adult development of the LMP7$^{\Delta EnC}$ mouse line and maintenance of the GFB.

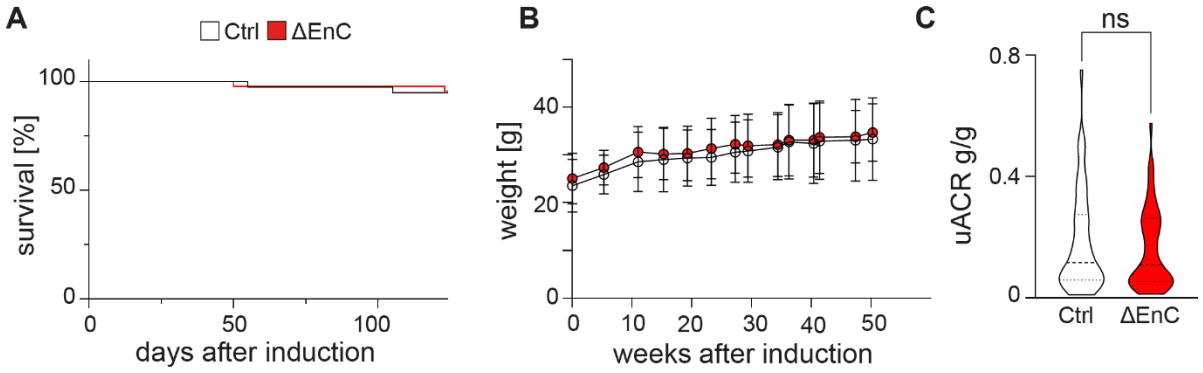

Figure 4-4: Phenotypic evaluation of LMP7$^{\Delta EnC}$ mice after knockout induction. **(A)** Survival curve analysis of LMP7$^{\Delta EnC}$ mice. 40 control mice and 47 LMP7$^{\Delta EnC}$ mice from four independent mouse cohorts and both sexes were included in the analysis. **(B)** Weight gain of an exemplary mouse cohort showing 4-9 mice from both sexes per timepoint. Mean weight per group is given, error bars represent standard deviation (SD). **(C)** Urinary albumin-to-creatinine ratio (uACR) of 47 control littermates and 46 LMP7$^{\Delta EnC}$ mice from seven independent mouse cohort including mice from both sexes was determined at least four weeks after LMP7 knockout induction.

4.1.5 Loss of LMP7 alters cellular phenotype across organs

Since the LMP7$^{\Delta EnC}$ mice allowed for the EnC specific LMP7 knockout and developed normally, EnCs isolated by cell sorting were analysed in more detail to gain insights into cellular mechanisms potentially altered in EnCs upon the loss of LMP7. To this end, endothelial cells were stained for additional surface markers in parallel to the isolation via fluorescent activated cell sorting (FACS). It had been described before that lack of immunoproteasomal subunits resulted in a loss of MHC class I cell surface levels (28). As a crosstalk mechanism between structural and immune cells, this effect is potentially relevant in EnCs. Therefore, cells were stained for H2-K^{b}, the MHC haplotype in C57BL/6 mice. Analysis of the flow cytometric data indeed revealed a drastic decrease of surface MHC class I on EnCs isolated from LMP7$^{\Delta EnC}$ animals compared to cells isolated from control littermates (Figure 4-5, Panel A). Importantly, this effect was observed across different organs and was not present on non-endothelial cells isolated from the same organs. Intriguingly, the degree of MHC class I loss differed between endothelial cells isolated from different organs as summarised in table 4-1. Notably, the relative

loss is similar to the values originally described for other cell types (28). This data nicely showed that loss of LMP7 also results in reduced MHC class I levels on the cell surface of endothelial cells, and even to differing degrees between the analysed organs.

Table 4-1: Summary of the loss of MHC class I surface expression on EnCs from LMP7$^{\Delta EnC}$ mice. EnCs from LMP7$^{\Delta EnC}$ mice lost between 23.7% and 40.0% MHC class I sell surface levels compared to EnCs isolated from control littermates. The 95% confidence interval (CI) is given in the right column.

Tissue	**Mean loss**	**95% CI**
GEnCs	31.2%	23.59% - 38.82%
PtEnCs	37.9%	32.53% - 43.27%
Heart EnCs	40.0%	33.54% – 46.77%
Liver EnCs	26.5%	17.13% – 35.88%
Lung EnCs	23.7%	17.16% – 30.18%

All the structural data published so far indicates that the proteasomal 20S core complex can only be assembled with one copy of all seven subunits present in the two α- and β-rings. Under this assumption, a loss of the LMP7 protein (as the β5i subunit) would require the incorporation of the corresponding constitutive subunit β5c instead. Therefore, after isolation via cell sorting, endothelial cells were analysed for the expression of the constitutive subunit β5c (encoded by *Psmb5*) via immunoblotting. Indeed, a strong enrichment of β5c was present in endothelial cells isolated from LMP7$^{\Delta EnC}$ mice in comparison to EnCs isolated from control mice (Figure 4-5, panels B - D). While the degree of β5c upregulation slightly differed between the examined organs, it was substantially upregulated in all of the examined tissues. Peritubular endothelial cells showed the lowest degree of β5c upregulation (Figure 4-5, Panel B, PtEnCs), while still exhibiting a two-fold increase in β5c levels. Glomerular and lung endothelial cells exhibited the highest degree of upregulation (Figure 4-5, panel B and C, respectively), with an approximate 4-fold increase in β5c levels. Again, these effects were specifically observed in endothelial cells from induced Cre^{+} animals and not present in other control structural cells isolated from the same organs (Ctrls) in LMP7$^{\Delta EnC}$ mice.

These effects of β5c upregulation and MHC class I cell surface loss were shared between EnCs from all the analysed tissues, indicating a very basic reaction of the proteasomal system and antigen presentation machinery to the loss of LMP7.

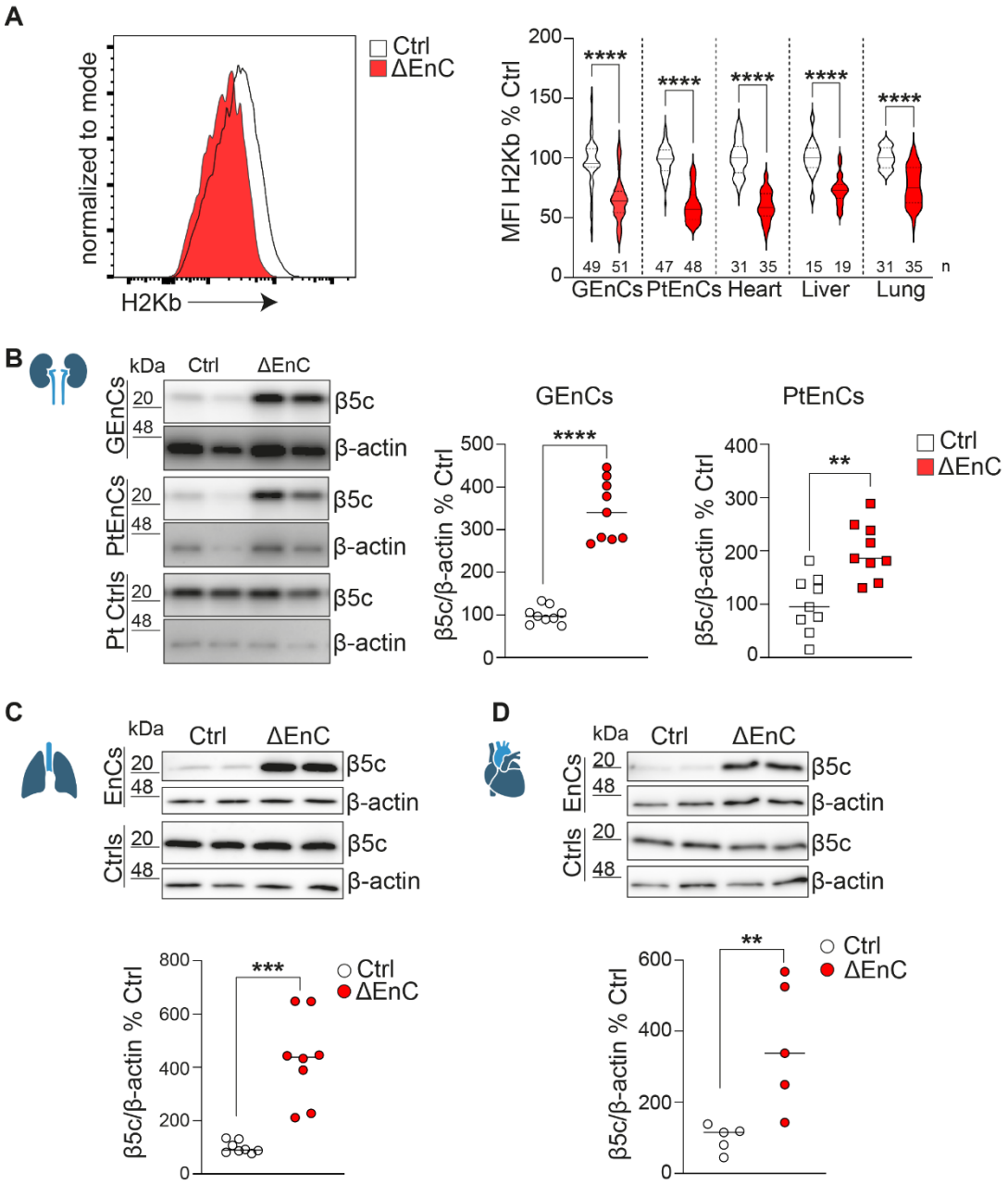

Figure 4-5: Evaluation of MHC class I loss and β5c upregulation in EnCs of LMP7$^{\Delta EnC}$ mice. **(A)** Exemplayry histogram and quantification of flow cytometric MCH class I cell surface level analysis during cell isolation. Small numbers below each violin plot represent the number of mice in that group (n) from at least three independent cohorts. Both sexes were included in the analysis. Immunoblot analysis of β5c expression in EnCs isolated from **(B)** kidney, **(C)** lung and **(D)** heart. Mice of both sexes from at least two independent cohorts were analysed. Quantifications show β5c protein levels normalised to β-actin protein levels relative to EnCs isolated from littermate controls.

4.1.6 The induced knockout is stable over time

The use of an inducible knockout system potentially bears the risk that the knockout might be lost again over time due to cell turnover. Cells and tissues might regenerate from cellular pools that were not targeted by the Cre driver and therefore express the protein of interest again. The very robust loss of cell surface MHC class I observed in EnCs from LMP7$^{\Delta EnC}$ animals offered a good experimental readout to assess the presence of the knockout at the time of sacrifice. Therefore, the MHC class I cell surface levels on kidney cells measured during cell isolation were used as a surrogate measurement to assess the KO status of all LMP7$^{\Delta EnC}$ mice that were experimented during this thesis (Figure 4-6). Indeed, no significant correlation could be observed between time passed since induction and the relative MHC class I levels (Figure 4-6, panel A). However, in mice that had been induced for more than 250 days, some recovering LMP7 expression could be observed via immunoblot analysis, especially in EnCs isolated from the lung (Figure 4-6, panel B). This clearly contrasted the complete loss of LMP7 protein observed in animals that were induced for less than six months. Importantly, this slight LMP7 expression did not immediately lead to an increase in cell surface MHC class I levels. Nevertheless, the LMP7 knockout was stable for up to six months, only after that time a reinduction of the knockout would become necessary.

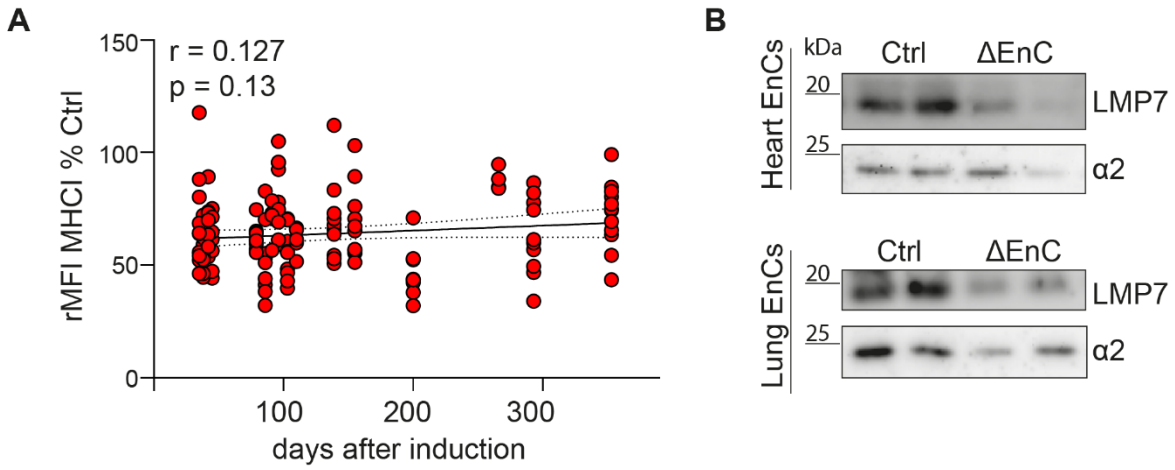

Figure 4-6: The EnC-specific knockout of LMP7 is stable for at least six months after induction via tamoxifen injection. **(A)** Correlation analysis between the MCH class I cell surface levels on EnCs isolated from glomerular, non-glomerular kidney, heart, lung, and liver tissue and the duration of knockout induction at the time of sacrifice. Mice of both sexes from seven independent cohorts were included. **(B)** Cell number adapted immunoblot analysis of LMP7 protein levels in EnCs isolated from heart and lung tissue from mice induced for more than 250 days. α2 represents total proteasome abundance.

4.1.7 Loss of LMP7 alters proteasomal composition and abundance

The upregulation of constitutive subunits as a reaction to the loss of their immuno counterparts has been described before for different kinds of immune cells (119). However, it has not been described in non-immune cells and increased protein levels of subunits cannot be directly related to the composition of functional proteasomal complexes or even proteasomal activity.

Therefore, isolated endothelial cells from different organs were natively lysed and separated on a non-denaturing native gel to assess the composition of assembled proteasomal complexes. In-gel proteasomal activity was determined using the fluorogenic peptide substrate Suc-LLVY-Amc as a measure for the chymotrypsin-like activity of the assembled proteasome. Indeed, the higher levels of the PSMB5 protein also related to higher levels of proteasomes containing the β5c subunit (Figure 4-7, exemplary shown for GEnCs). When normalised to protein levels of the α3 subunit as an indicator of total proteasome abundance, KO cells showed a roughly four-fold increase of incorporated β5c, the same order of magnitude that was observed for the subunit protein levels. Surprisingly, the chymotrypsin-like activity was increased in GEnCs isolated from LMP7$^{\Delta EnC}$ mice compared to control littermates. When normalised to α3, the CTL activity was two times higher (Figure 4-7, panel B). In summary, the more abundant β5c subunit was indeed incorporated into functional proteasomal complexes and led to a higher CTL activity in these cells.

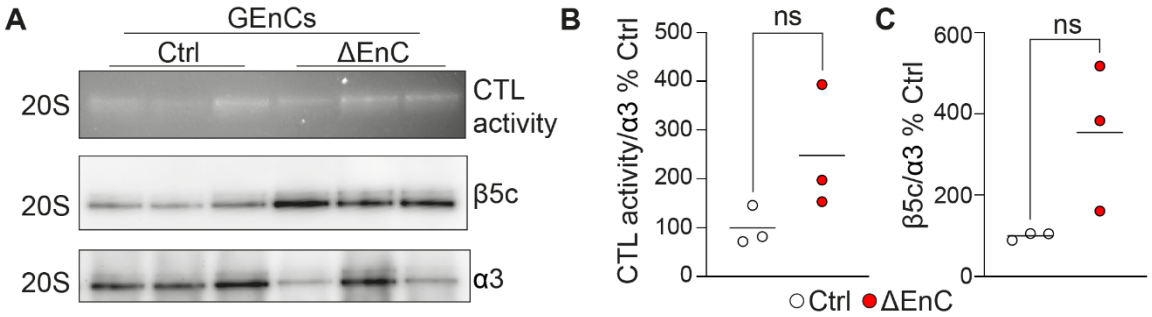

Figure 4-7: Native polyacrylamide gel electrophoresis (PAGE) analysis of isolated glomerular endothelial cells (GEnCs). **(A)** Proteasomal chymotrypsin-like activity (CTL) activity was determined by cleavage of the fluorogenic Suc-LLVY-Amc substrate. Immunoblotting was used to assess the levels of the β5c subunit and the α3 subunit was analysed as an indicator of proteasome abundance. CTL activity was normalised to α3 levels and the quantification is shown in **(B)**. Levels of incorporated β5c subunits were also normalised to α3 and the quantification is shown in **(C)**.

4.1.8 Mouse IgG differentially accumulates in LMP7-KO EnCs

Since the composition and catalytic activity of proteasomal complexes was altered by the loss of LMP7, the isolated cells were further analysed via immunoblot to unravel potential cellular consequences of the observed changes. Surprisingly, a differential alteration of endogenous murine IgG (msIgG) levels was observed in endothelial cells isolated from different organs of LMP7$^{\Delta EnC}$ animals. Immunoblot analysis for msIgG revealed that glomerular endothelial cells showed increased levels of endogenous IgG (Figure 4-8, panel A), while PtEnCs showed lower levels (panel B), a trend also observed in EnCs from heart and lung (panel C and D, respectively). To confirm these results, LMP7$^{\Delta EnC}$ mice were *in vivo* perfused with tomato lectin to stain the endothelial glycocalyx. Additional immunofluorescence staining for msIgG in kidney tissue isolated from these mice allowed the localisation of msIgG. Indeed, this analysis confirmed the accumulation of endogenous msIgG in the endothelial cells of glomerular

capillaries, while no msIgG staining could be observed on kidney sections from control animals (Figure 4-8, panel E).

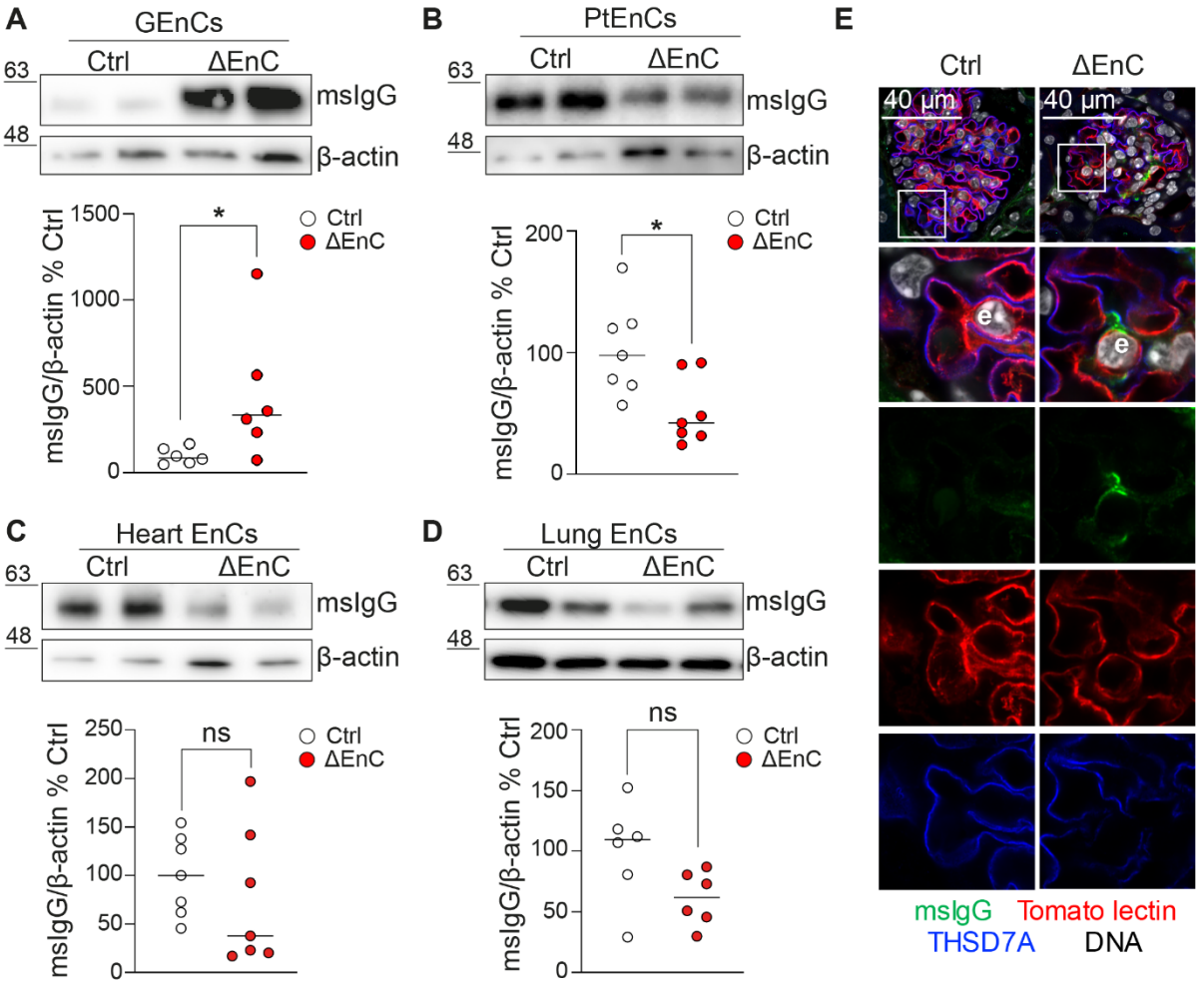

Figure 4-8: Assessment of msIgG accumulation in EnCs isolated from LMP7$^{\Delta EnC}$ mice. Immunoblot analyses of msIgG levels in **(A)** glomerular endothelial cells (GEnCs), **(B)** peritubular endothelial cells (PtEnCs), **(C)** heart EnCs and **(D)** lung EnCs isolated from LMP7$^{\Delta EnC}$ mice and control littermates. β-actin was used as a loading control. Quantifications show endothelial msIgG levels normalised to β-actin relative to EnCs isolated from control littermates. Mice from both sexes and at least three independent cohorts were included in the analysis. **(E)** Confocal immunofluorescence microscopy on zinc-fixed paraffin embedded tissue sections was used to determine the localisation of msIgG in glomerular tissue. Tomato lectin was used to mark endothelial glycocalyx *in vivo* directly before sacrificing the mice, THSD7A marks podocyte foot processes. e: endothelial cell nucleus

4.1.9 Organotypic EnCs show differential reaction to loss of LMP7

To unravel potential explanations for the tissue-specific changes of msIgG levels in endothelial cells, the flow cytometric data was analysed in more detail. During isolation via cell sorting, both forward scatter-area (FSC-A) and sideward scatter-area (SSC-A) were recorded which can be used to assess cell size and granularity, respectively, as measures of basic cell morphology. Surprisingly, analysis of this cytometric data revealed a significant increase in both cell size and granularity for the analysed types of kidney endothelial cells (GEnCs and PtEnCs), but for none of the other organs (heart, liver and lung) (Figure 4-9).

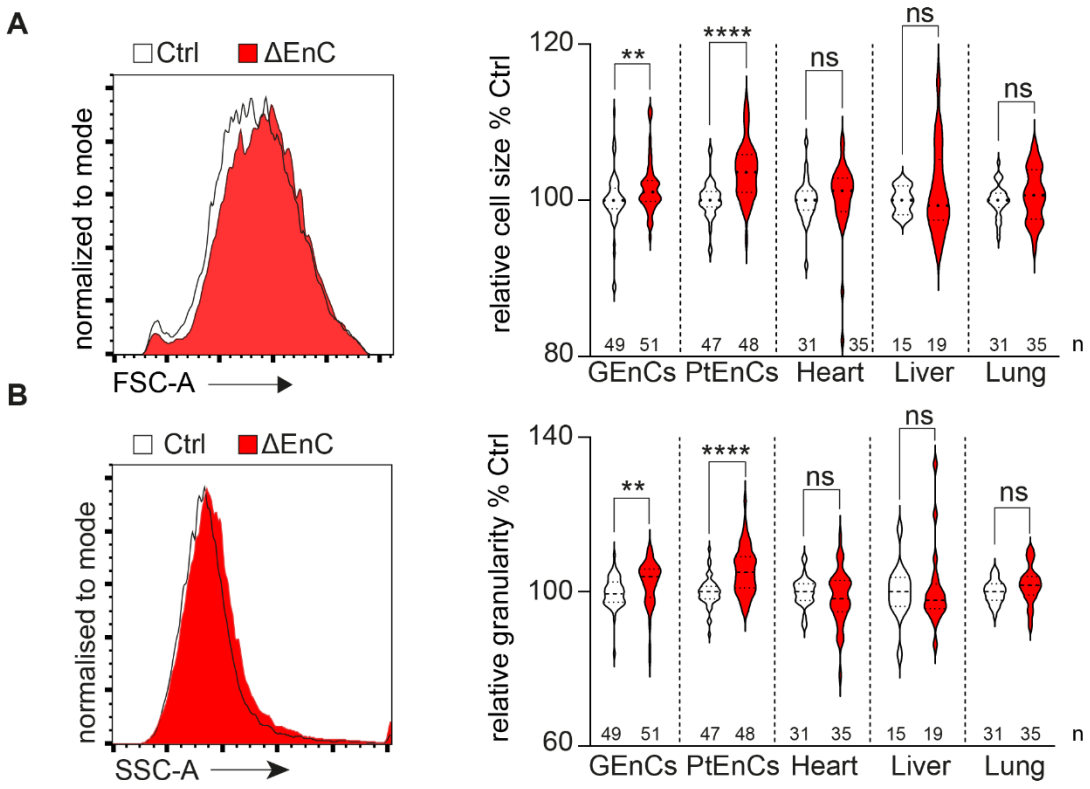

Figure 4-9: Flow cytometric assessment of changes in forward scatter-area (FSC-A) and sideward scatter area (SSC-A) in endothelial cells isolated from different organs from LMP7$^{\Delta EnC}$ animals. **(A)** Exemplary flow cytometry histogram and quantifications of the FSC-A parameter. **(B)** Exemplary histogram and quantifications of the SSC-A parameter. Quantifications show relative FSC-A/SSC-A as % of EnCs isolated from control littermates. Small numbers below each violin represent the number of mice in each group (n). Mice of both sexes from at least three independent mouse cohorts were included.

Among the two kidney cell types, PtEnCs appeared to react slightly more sensitively to the loss of LMP7 with more drastic increases in both parameters (Table 4-2). Interestingly, the granularity was altered more drastically by the loss of LMP7 than the cell size. In both cell types, the relative changes of SSC-A were stronger than the relative changes in FSC-A (Table 4-2). Since both kidney cell types increased in size, but only GEnCs showed an accumulation of msIgG, the increased cell size could not be explained by msIgG accumulation.

Table 4-2: Summary of the changes in cell size (FSC-A) and cell granularity (SSC-A) caused by the loss of LMP7 in kidney EnCs. Given are the % increase in LMP7$^{\Delta EnC}$ animals compared to WT animals as well as he 95% confidence interval (CI).

Celltype	**Parameter**	**Change**	**95% CI**
GEnCs	FSC-A	1.81 (± 0.70) %	0.42% - 3.21%
GEnCs	SSC-A	2.50 (± 0.99) %	0.51% - 4.48%
PtEnCs	FSC-A	3.80 (± 0.63) %	2.55% - 5.05%
PtEnCs	SSC-A	5.57 (± 1.045) %	3.49% - 7.65%

This increase in cell size as a consequence of LMP7 deficiency was a new phenomenon that had not been described so far. One possible mechanism linking this effect to the induced knockout could be the accumulation of proteasomal substrates. It has been proposed that the immunoproteasome has a higher proteolytic capacity and therefore allows cells to more efficiently degrade proteasomal substrates, making the immunoproteasome relevant for proteostasis (34, 35). Based on this hypothesis, a loss of immunoproteasomal degradation in cells should lead to an accumulation of proteins, potentially leading to an increased cell size. To address this question, the levels of K48-polyubiquitinated proteins, the most described proteasomal substrate, were determined in isolated EnCs via immunoblotting. Surprisingly, no accumulation of K48-polyubiquitinated proteins in endothelial cells isolated from any of the studied organs could be detected. Instead, a minute trend towards higher K48-pUb levels was observed in GEnCs and no change was visible in PtEnCs and lung EnCs whereas heart EnCs even had decreased levels of K48-polyubiquitinated proteins (Figure 4-10).

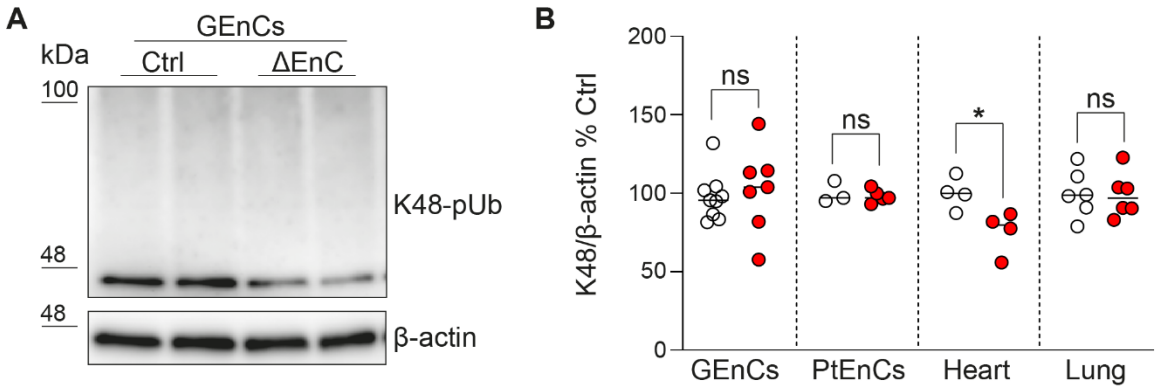

Figure 4-10: Assessment of K48-polyubiquitinated (pUb) protein levels in EnCs isolated from LMP7$^{\Delta EnC}$ mice. **(A)** Exemplary image of an immunoblot experiment determining the cellular levels of the proteasomal substrate K48-pUb in GEnCs. β-actin was used as a loading control. **(B)** Quantifications show K48-pUb levels normalised to β-actin relative to EnCS isolated from littermate controls. Mice from at least two independent cohorts were included in the analysis.

The changed msIgG levels and increased cell size in the absence of proteasomal substrate accumulation raised the question of the functional mechanism linking the loss of LMP7 to these differential reactions. The increased cell granularity as determined via flow cytometry indicated a higher vesicle content of the cells, potentially implicating the immunoproteasome in regulation of vesicular trafficking. Altered vesicular trafficking could potentially, among other processes, impact the delivery of proteins to the cell surface. Therefore, MHC class II levels on the surface of endothelial cells were analysed to examine whether the changed levels of cell surface markers might be a more general effect not only limited to MHC class I. Surprisingly, a statistically significant decrease of MHC class II surface levels could only be observed on PtEnCs, but on none of the other studied organs (Figure 4-11). Liver EnCs might also show a decreased expression of MHC class II, however, this change did not reach statistical significance, most likely due to fewer mice being included in this group. Therefore,

the immunoproteasome on PtEnCs and liver EnCs appears to influence not only MHC class I, but also class II cell surface levels. However, since this effect was again tissue specific, but did not show the same tissue specificity as the increase in cell size, it cannot (only) rely on the same cellular mechanisms.

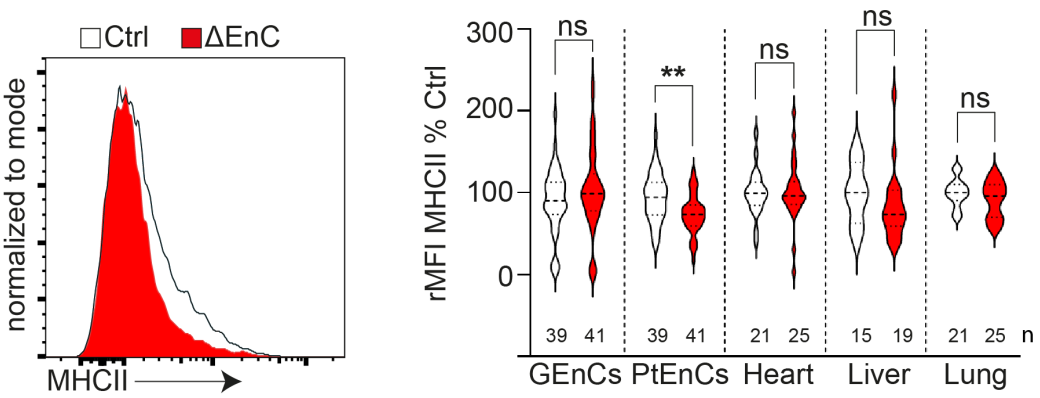

Figure 4-11: Flow cytometric assessment of MHC class II cell surface levels. **(A)** Exemplary histogram of the flow cytometric analysis of MHC class II cell surface levels on PtEnCs. **(B)** Quantification of the MHC class II cell surface levels relative to EnCs isolated from control littermates. Small numbers below each violin represent the number of mice included in each group. Mice from both sexes and at least three independent mouse cohorts were included in the analysis.

4.1.10 Influence of the LMP7-KO on kidney cells

The results on cellular changes caused by the loss of the immunoproteasome highlight a particularly high dependence on LMP7 of kidney endothelial cells. Several parameters, like the cell size, are only altered in GEnCs and/or PtEnCs. Even between these two kidney endothelial cell populations, differences were observed, as cell surface levels of MCH class II were only altered on PtEnCs, but not on GEnCs. The predominant expression of immunoproteasomal subunits in endothelial cells within the glomerulus, together with the kidney specific effects of the loss of LMP7 is intriguing. Considering the earlier observations that the mice did not develop a phenotype under homeostatic conditions, this raised the question which function the (glomerular) endothelial immunoproteasome expression fulfils in the kidney. Based on the results that kidney cells seem to react more sensitively to the loss of LMP7, both GEnCs and PtEnCs were analysed in more detail.

Since no accumulations of (immuno)proteasomal substrates could be observed that potentially explained the increase in cell size, cell cycle progression was analysed in these cells. It has been described that a cell cycle arrest can lead to cellular overgrowth, concomitant osmotic stress and cellular senescence (120). Therefore, isolated kidney endothelial cells were examined for their cell cycle state using a flow cytometry-based approach using propidium iodide (PI) staining. Using this approach, PI fluorescence intensity was used to measure the DNA content of cells. Based on the DNA content, cell cycle phases could be determined. The cell cycle of neither GEnCs nor PtEnCs was altered by the loss of LMP7 (Figure 4-12). Most

cells from both cell types were in the G1 phase, with only a very small percentage being in the G2 phase and even fewer cells in the S phase. Therefore, also a change in cell cycle progression did not explain the observed increase in cell size and granularity.

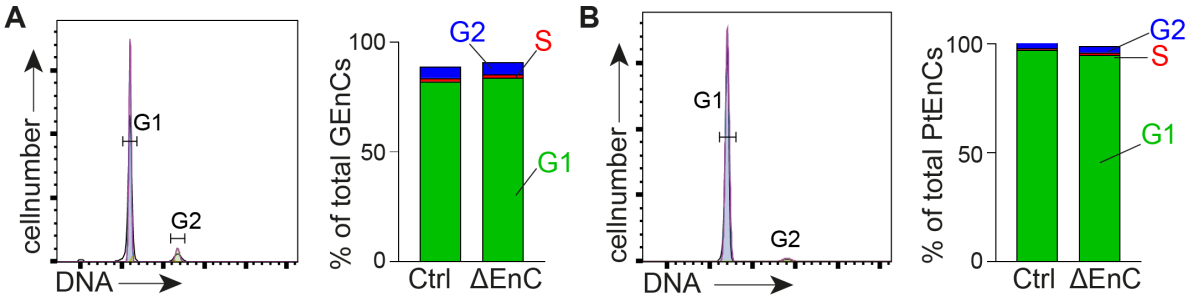

Figure 4-12: Flow cytometric assessment of cell cycle in kidney endothelial cells. DNA amount was measured using propidium iodide (PI) fluorescence. Exemplary PI histogram and quantifications for **(A)** GEnCs and **(B)** PtEnCs are shown. Stacked bargraphs depict percentages of endothelial cells (EnCs) in the labelled cell cycle phase from total EnCs. Five male mice from one mouse cohort were included in the analysis.

None of the analyses performed so far could explain the kidney specific effects of the LMP7 loss. To gain further insights into the glomerular reaction, ultrastructural analyses using electron microscopy (EM) on kidney tissue from LMP7$^{\Delta EnC}$ mice were performed by Oliver Kretz, III. Medical Clinic, UKE. Figure 4-13 shows exemplary EM micrographs as well as quantifications of parameters of the glomerular filtration barrier (GFB). Astonishingly, the GFB ultrastructure was drastically altered by the loss of endothelial LMP7. Firstly, GEnCs lost their characteristic fenestrations, an important morphological feature of the glomerular capillaries relevant for their function as part of the GFB. Secondly, the loss of endothelial LMP7 led to podocyte foot process effacement, a hallmark feature of podocyte injury. The thickness of the GBM as the third GFB layer was not significantly altered, even though an increase in width and GBM splitting was focally observed. The loss of endothelial immunoproteasome expression therefore appeared to affect both endothelial cells and podocytes. This GFB impairment, especially the podocyte foot process effacement was in stark contrast to the lack of albuminuria observed in these mice (Figure 4-4).

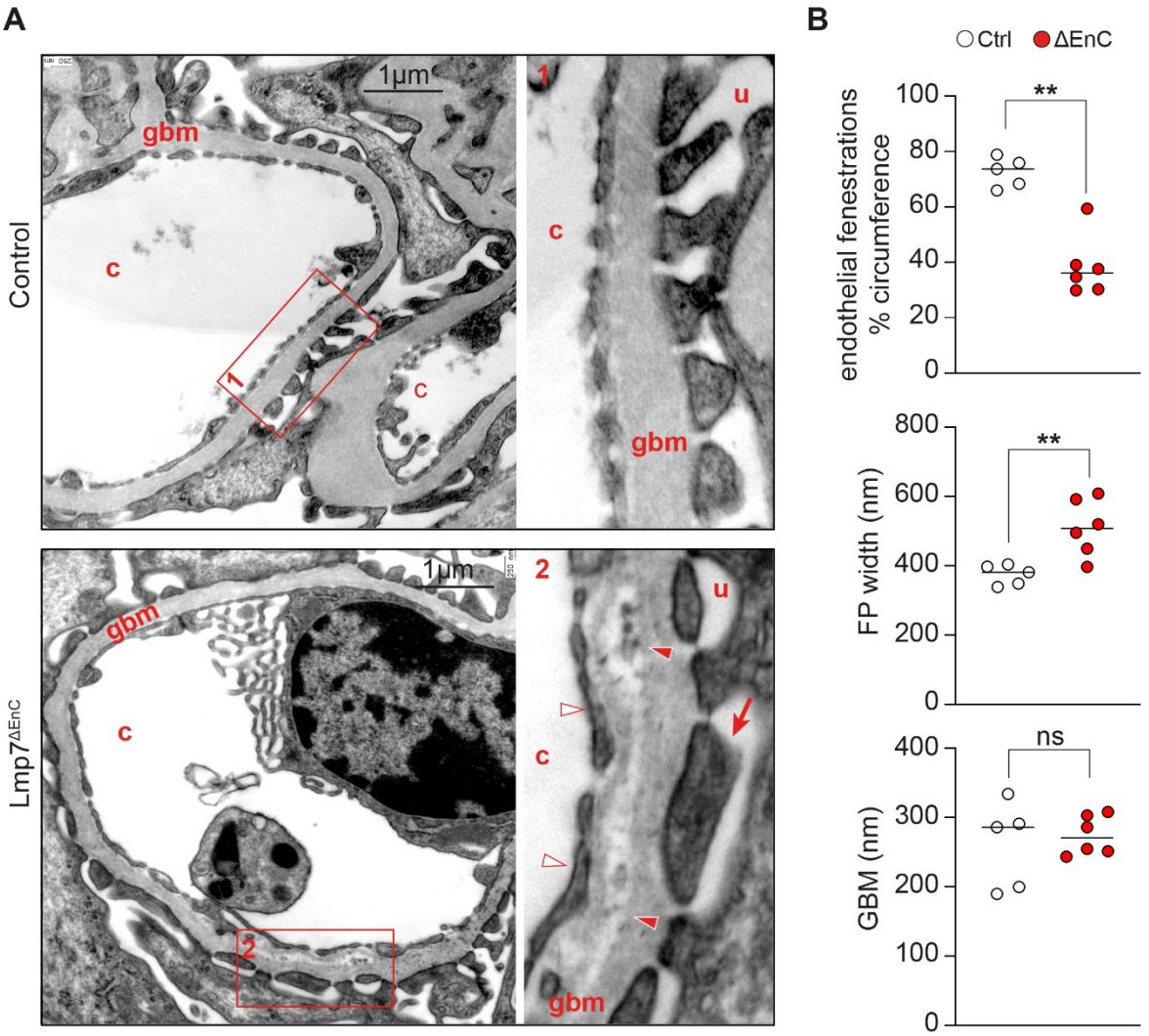

Figure 4-13: Ultrastructural analysis of glomerular filtration barrier (GFB) integrity in LMP7$^{\Delta EnC}$ mice. **(A)** Exemplary electron microscopy (EM) micrographs showing the GFB in one control (to panel) and one LMP7$^{\Delta EnC}$ (lower panel) mouse. Empty arrowheads highlight loss of endothelial fenestrations, filled arrows highlight podocyte foot process effacement (FPE). Filled arrowheads highlight focal splitting and thickening of the glomerular basement membrane (GBM). **(B)** Quantification of GBM parameters. Both male and female mice from two independent mouse cohorts were included in the analyses. Numbers depict magnified excerpts. c: capillary lumen; gbm: glomerular basement membrane; u: urinary space.

4.1.11 Vesicle trafficking in LMP7$^{\Delta EnC}$ mice

The increased cell granularity, the altered msIgG handling and the changed levels of cell surface proteins in combination with the severe ultrastructural alterations of the GFB could be explained by changed intracellular trafficking pathways. To unravel potentially affected vesicular trafficking, the neonatal Fc receptor (FcRn) was analysed using flow cytometry and immunoblotting to assess membrane dynamics. FcRn is responsible for the recycling of endogenous IgG molecules to the cell surface after their internalisation and its cell surface levels therefore depend both on endocytic and exocytic pathways. Figure 4-14 shows the immunoblot analysis of total cellular protein levels of FcRn. When normalised to β-actin, total cellular FcRn levels were reduced in both GEnCs and PtEnCs isolated from LMP7$^{\Delta EnC}$ animals

in comparison to littermate controls (Figure 4-14, panels A and B). To analyse if the reduced total FcRn levels also related to altered cell surface levels, FcRn surface levels were analysed during cell sorting. Surprisingly, the LMP7 knockout did not result in an altered FcRn surface abundance (Figure 4-14, panels C and D). While both GEnCs and PtEnCs showed a small trend towards altered cell surface levels, this was not statistically significant for either cell type. Total cellular and cell surface levels did not seem to directly relate to one another based on these analyses, indicating a change in relative subcellular distribution of FcRn.

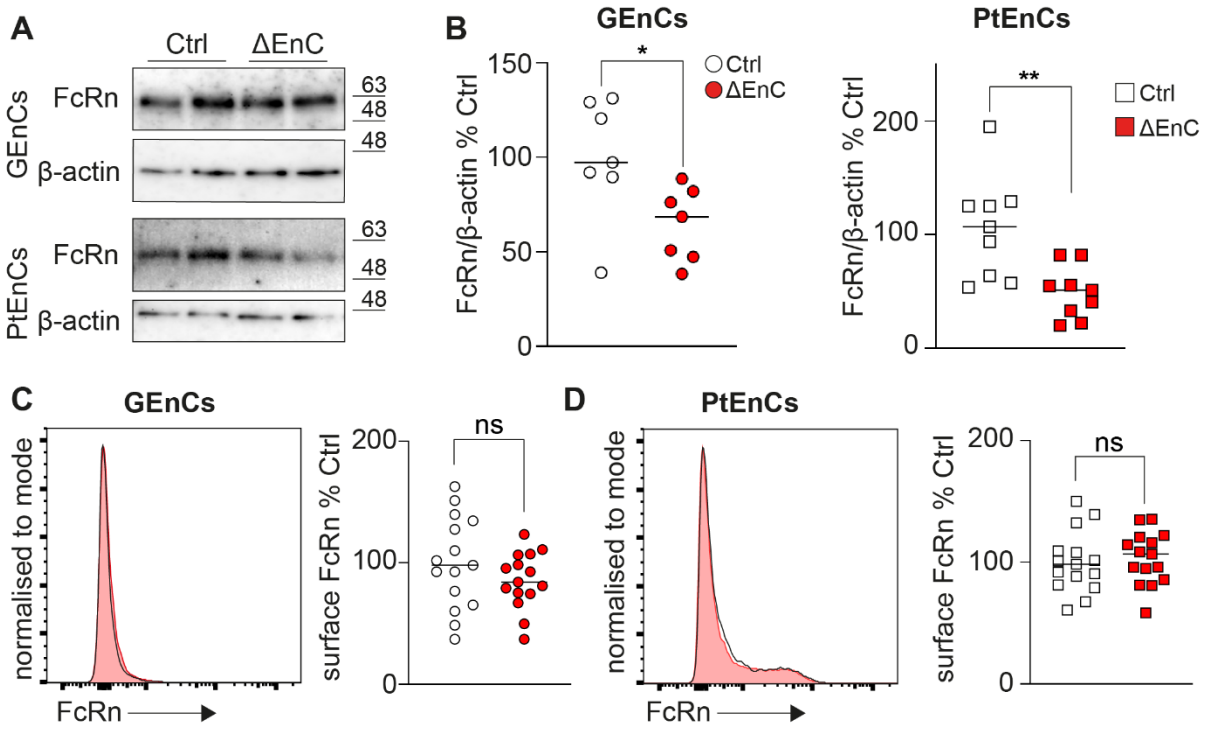

Figure 4-14: Assessment of total and cell surface FcRn levels in glomerular endothelial cells (GEnCs) and peritubular endothelial cells (PtEnCs) isolated from LMP7$^{\Delta EnC}$ mice and control littermates. **(A)** Exemplary immunoblot analysis of FcRn levels in both GEnCs and PtEnCs. β-actin was used as a loading control. **(B)** Quantifications of FcRn levels normalised to β-actin in % of the levels in EnCs isolated from control littermates. Flow cytometric analysis of FcRn cell surface levels on **(C)** GEnCs and **(D)** PtEnCs. The quantifications represent relative mean fluorescence intensity (MFI) in % of MFI on cells isolated from control littermates. Mice from both sexes and at least two independent cohorts were included in the analyses.

These changes in cellular FcRn levels further indicated potential alteration in cellular trafficking. Therefore, proteins involved in vesicular trafficking were analysed. Figure 4-15 shows the analysis of total cellular levels of Rab7, a protein involved in endosome maturation. While levels were significantly increased in GEnCs, PtEnCs had rather lower levels, albeit not significantly within the small sample size (Figure 4-15, panel B). However, these levels indicated a differential reaction of Rab7 levels to the loss of LMP7 between kidney endothelial cell types and therefore supported an alteration of vesicular trafficking, but the exact mechanism remained unclear.

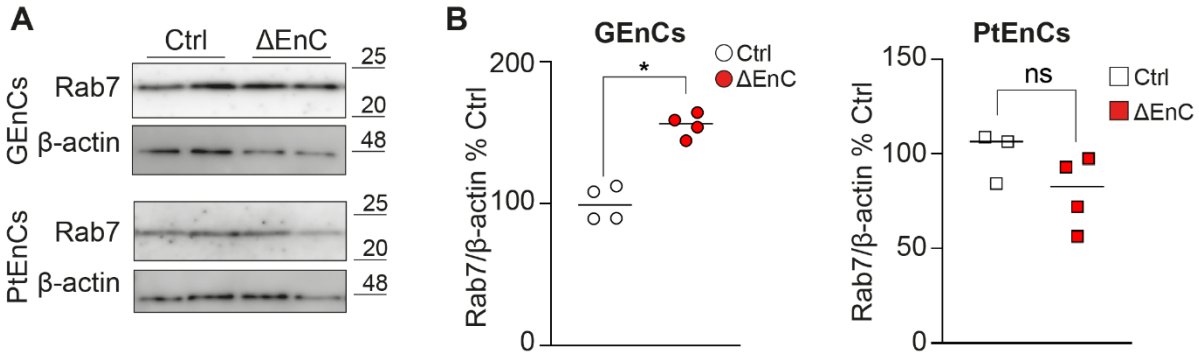

Figure 4-15: Assessment of total cellular levels of Rab7. **(A)** Exemplary immunoblot experiment showing Rab7 levels in both glomerular endothelial cells (GEnCs) and peritubular endothelial cells (PtEnCs). β-actin was used as a loading control. **(B)** Quantifications represent relative protein levels normalised to β-actin in % of levels in EnCs isolated from control littermates. Female mice from one cohort were included in the analysis.

4.2 Untargeted analyses of LMP7$^{\Delta EnC}$ mice

The observed changes induced by the loss of immunoproteasomal subunit expression in (kidney) endothelial cells and on the glomerular filtration barrier even under homeostatic conditions had not been described before. Since no indications towards the responsible mechanism could be observed using targeted approaches, both untargeted transcriptomic and proteomic analyses of isolated endothelial cells from LMP7$^{\Delta EnC}$ and control mice were employed to shed light on a possible mechanism linking the immunoproteasome to cell size and granularity and immunoglobulin handling.

4.2.1 Transcriptomic analyses

First, bulk mRNA sequencing was employed to compare the reactions to LMP7 loss between the two kidney endothelial cell types, GEnCs and PtEnCs. Four male mice five months after LMP7 knockout induction per group were included in the analysis. Figure 4-16 shows the principal component analysis (PCA) of the transcriptomes from both GEnCs and PtEnCs from naïve control and LMP7$^{\Delta EnC}$ mice. Notably, GEnCs and PtEnCs were clearly clustered separately from one another, indicating a heterogeneity in gene expression profiles between these two kidney endothelial cell types. However, within each cell type, the cells were not clearly separated by genotype, indicating a limited effect of the LMP7 loss on the cells' transcriptomes. Nevertheless, it is intriguing that the control cells clustered relatively close together whereas the cells isolated from LMP7$^{\Delta EnC}$ mice had a more variable transcriptomic profile. While this observation was more pronounced in PtEnCs, it was present in both kidney cell types.

Despite the lack of discrimination based on the genotype in the PCA analysis, both cell types showed differentially expressed genes (DEGs) between EnCs isolated from control and LMP7$^{\Delta EnC}$ animals, as shown in the volcano plots in Figure 4-16. In both cell types, similar

amounts of genes were up- or downregulated at the mRNA level, while PtEnCs showed more DEGs in total.

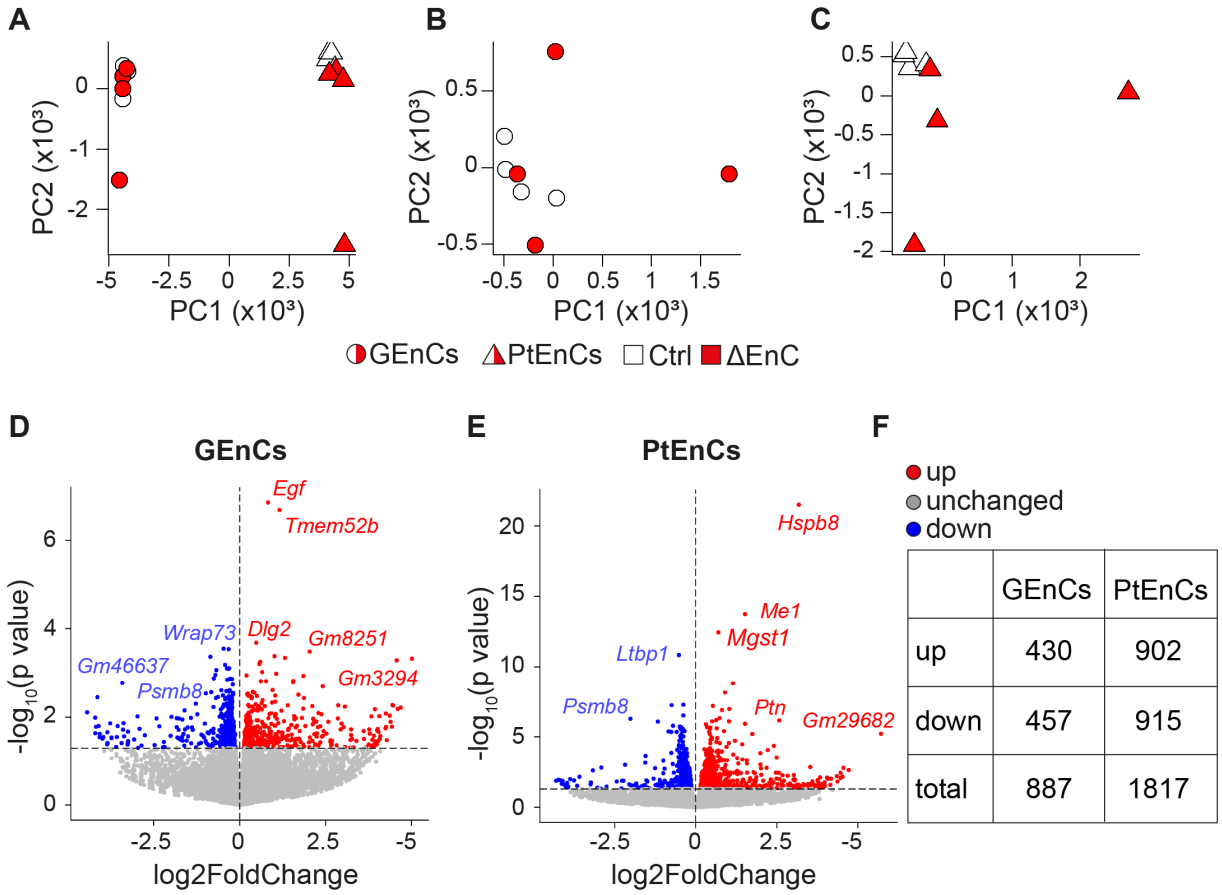

	GEnCs	PtEnCs
up	430	902
down	457	915
total	887	1817

Figure 4-16: Transcriptomic analysis of kidney endothelial cells (EnCs) isolated from control and LMP7$^{\Delta EnC}$ mice. Four male mice from both genotypes were analysed five months after knockout induction. Principal component analysis (PCA) of **(A)** both kidney endothelial cell (EnC) types, **(B)** only glomerular EnCs (GEnCs) and **(C)** only peritubular EnCs (PtEnCs). Volcano plots show differentially expressed genes (DEGs) in both **(D)** GEnCs and **(E)** PtEnCs. The total number of DEGs for both cell types are given in the table in **(F)**.

To unravel potentially altered cellular processes, gene ontology enrichment analysis was performed on the genes altered by the loss of LMP7 in both GEnCs and PtEnCs. In line with the lack of clear clustering in the PCA, only few GO terms were significantly altered between EnCs isolated from control and LMP7$^{\Delta EnC}$ animals. Within the upregulated genes in GEnCs, genes associated with membrane compartments and vesicles were significantly enriched (see Table 4-3). Surprisingly, only in PtEnCs genes associated with the proteasomal complex were upregulated. Genes/proteins that were detected to be altered in both the transcriptomic and the following proteomic analysis are listed in Table 7-11 for GEnCs and Table 7-12 for PtEnCs. Additionally, some DEGs mirrored observations made in other experimental approaches (e.g. flow cytometry) and will be discussed there.

Table 4-3: Gene ontology terms significantly enriched within the genes upregulated in GEnCs upon loss of LMP7.

ID	Description	pvalue	p.adjust
GO:0007588	excretion	2.7E-05	0.011253164
GO:0045177	apical part of cell	1.59E-07	5.62396E-05
GO:0009925	basal plasma membrane	4.59E-07	8.12597E-05
GO:0045178	basal part of cell	1.27E-06	0.000113162
GO:0016323	basolateral plasma membrane	1.28E-06	0.000113162
GO:0016324	apical plasma membrane	3.45E-06	0.000244583
GO:0016328	lateral plasma membrane	5.19E-06	0.000306381
GO:1903561	extracellular vesicle	2.08E-05	0.001050249
GO:0043230	extracellular organelle	4.54E-05	0.001784778
GO:0065010	extracellular membrane-bounded organelle	4.54E-05	0.001784778
GO:0045121	membrane raft	0.000318	0.010594474
GO:0098857	membrane microdomain	0.000329	0.010594474
GO:0005901	caveola	0.000605	0.0178359
GO:0070062	extracellular exosome	0.001503	0.040916794

4.2.2 Proteomic analysis of LMP7$^{\Delta EnC}$ endothelial cells

To complement the mRNA sequencing data, bottom-up proteomic analysis of isolated endothelial cells was performed. In this analysis, endothelial cells isolated from kidney (GEnCs and PtEnCs), heart, liver and lung of both LMP7$^{\Delta EnC}$ and control animals were included. Both male and female mice and at least three animals per group were included in the final analysis. LMP7 knockout had been induced three months before sacrificing the mice and isolating endothelial cells.

Firstly, as an additional measure of total protein amount per cell, the total ion chromatograms (TIC) between samples were compared. If the lack of immunoproteasomal activity leads to an accumulation of (K48-pUb) proteins targeted for proteasomal degradation, this would most likely result in an overall increased protein amount per cell. Therefore, the TIC was normalised to the cell number in each sample and relatively compared to EnCs isolated from the same organs from control littermates. In line with the earlier findings, also this approach did not indicate an increased protein amount in the cells upon the loss of LMP7 (Figure 4-17). EnCs isolated from lung tissue from LMP7$^{\Delta EnC}$ mice even had lower protein amounts per cell than EnCs isolated from control littermates. It is, however, noteworthy that there seems to be a difference in protein amount per cell between organs (Figure 4-17, panel B). Here, the total TIC per cell was analysed to compare the organs with each other. GEnCs seem to have the highest protein content per cell, while liver EnCs seem to have the lowest, with PtEnCs, heart and lung having intermediate values. Of note, these differences do not relate to differences in

cell size as determined by flow cytometry. However, this finding adds to the organ-specific differences observed in endothelial cells.

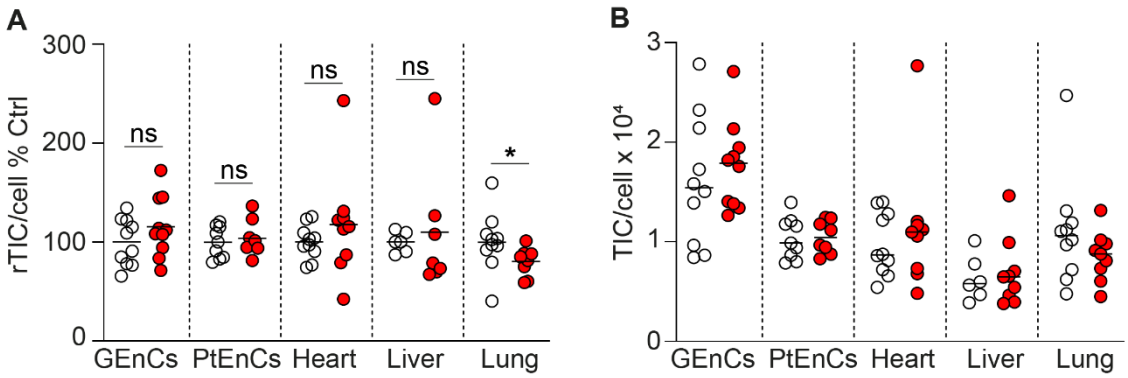

Figure 4-17: Total ion current chromatogram (TIC) was used as a measure of protein amount per cell. Both male and female mice were included in the analysis from two independent mouse cohorts. **(A)** Relative TIC was calculated as the relative amount compared to EnCs isolated from control littermates. **(B)** Without the normalisation to control EnCs from the same organ, interorgan differences were observed.

Secondly, principal component analysis on the proteomics data was performed to see how the protein expression differed between organs and how the loss of LMP7 influenced the global protein expression. Interestingly, in both sexes, EnCs isolated from the heart of both KO and control animals clustered away from all other organs (Figure 4-18, panel A). While this difference was present in both sexes, the other organs did not necessarily show the same behaviour between male and female mice. Only in male mice, the liver EnCs clustered away from lung and kidney EnCs, while in female mice glomerular endothelial cells clustered away from lung, liver and PtEnCs, albeit not as clearly as the liver EnCs in male mice. Therefore, the PCA already indicated both similarities as well as differences between the endothelial cells from different organs and sexes.

Mirroring the results from bulk mRNA sequencing, the LMP7 knockout appeared to have a limited effect on the global protein expression profile of endothelial cells across organs. In none of the examined organs the cells lacking LMP7 clustered away from the control cells. To avoid missing potential differences that were covered up by interorgan differences, also only data from EnCs from individual organs were subjected to PCA. Exemplary, the PCA only for glomerular endothelial cells are shown (Figure 4-18, panel B). But even in this case, no clear separation between the genotypes could be observed, showing that the loss of LMP7 had a limited effect on the global proteome of endothelial cells. This lack of clear impact of the LMP7 knockout on the global proteome was consistent across the five analysed organs.

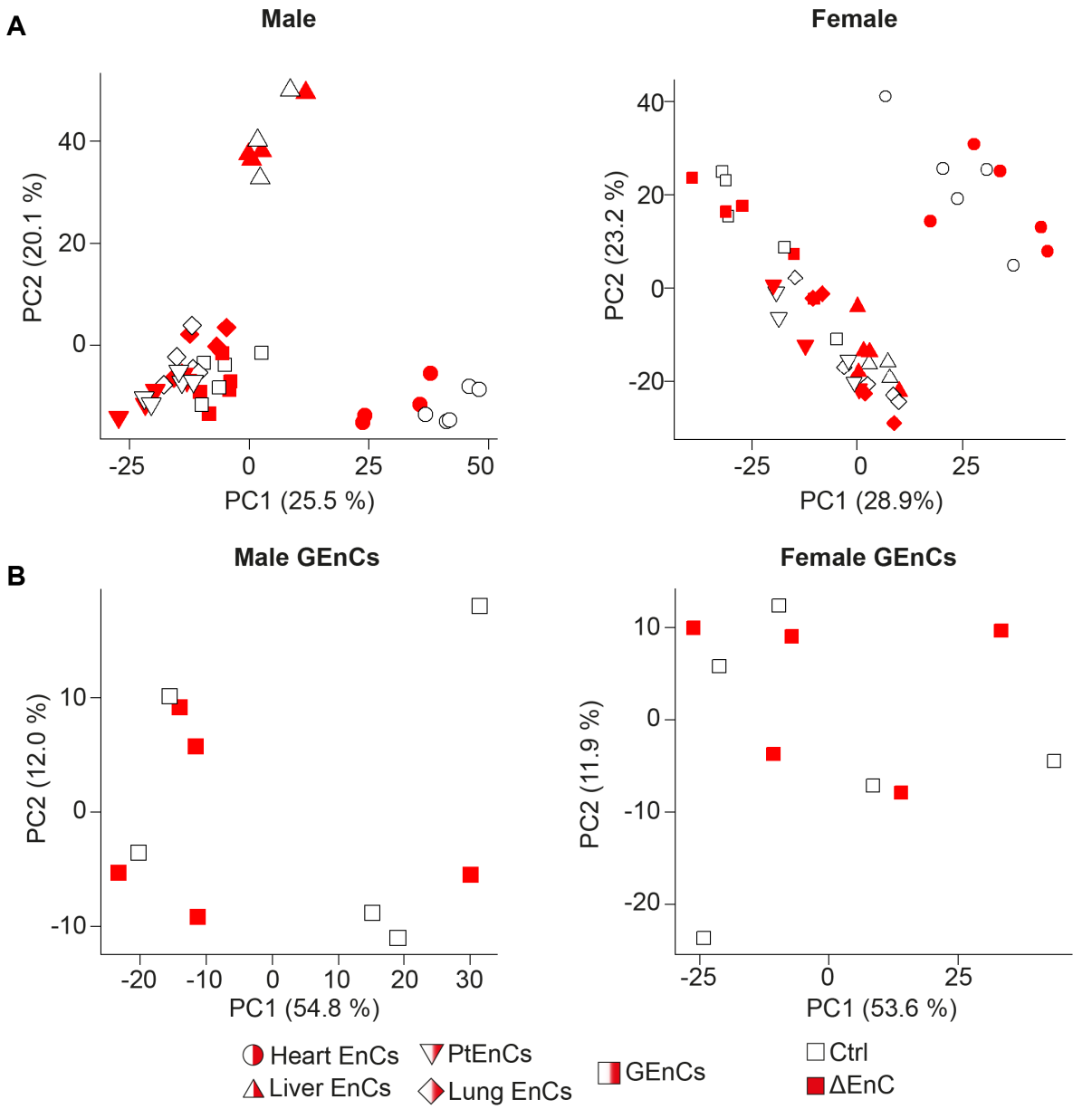

Figure 4-18: Principal component analysis (PCA) of mass spectrometric proteomic data from EnCs isolated from five mouse organs. Both male and female mice were included in the analysis with at least three mice per group **(A)** PCA of EnCs isolated from all five organs from both control littermates and LMP7$^{\Delta EnC}$ mice. **(B)** PCA plot only for GEnCs from male and female mice.

Despite the lack of clear genotype-dependent clustering in the PCA analysis, EnCs isolated from all five organs showed significantly changed proteins, both proteasomal and non-proteasomal ones. Figure 4-19 shows the volcano plots for glomerular, heart, liver, lung and peritubular EnCs. The proteomic data confirmed the observations that β5c (encoded by *Psmb5*) is more abundant in EnCs isolated from LMP7$^{\Delta EnC}$ animals in all five tissues. The total number of changed proteins differed between the organs, indicating differential reactions. While PtEnCs and EnCs isolated from the heart showed a higher number of proteins that were more abundant, GEnCs as well as EnCs isolated from the liver and the lung had more downregulated than upregulated proteins (table in Figure 4-19).

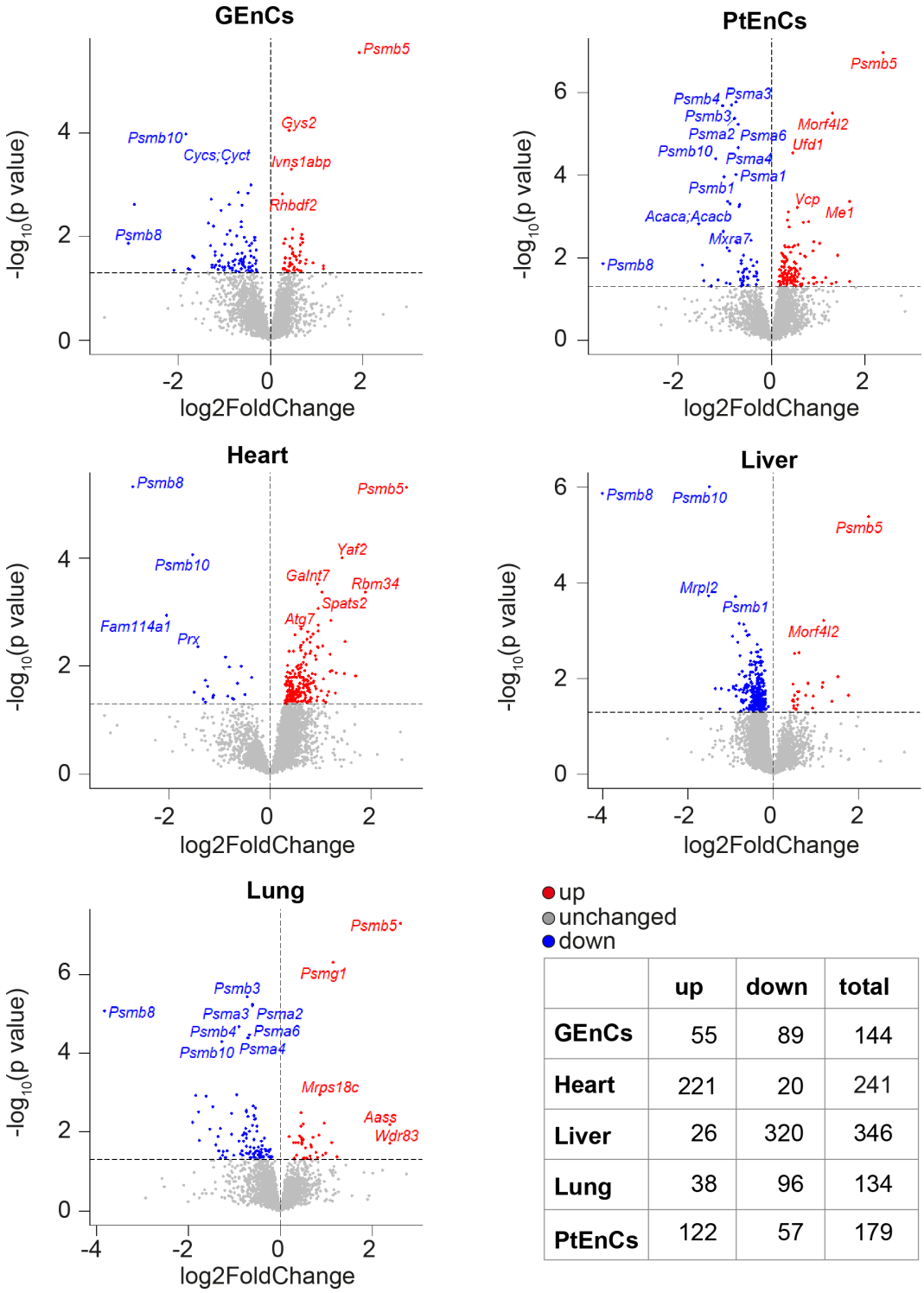

	up	down	total
GEnCs	55	89	144
Heart	221	20	241
Liver	26	320	346
Lung	38	96	134
PtEnCs	122	57	179

Figure 4-19: Volcano plots of the proteomic analysis of EnCs isolated from five different mouse organs. In all analysed organs, both significantly up- and downregulated proteins were detected. Upregulated proteins are marked with red dots, downregulated proteins with blue dots. Labels represent gene names encoding the detected proteins. The numbers of up- and downregulated proteins per organ are given in the table.

Next, the reaction of (immuno)proteasomal subunits of the 20S core particle were analysed and summarised in a heatmap. Notably, only looking at 20S subunits, control and KO animals were grouped in distinct clusters by the Euclidian distance clustering algorithm, contrary to the PCA run on all detected proteins (Figure 4-20, panel A). Confirming the results obtained via immunoblotting, β5c levels were higher in all tissues when LMP7 was missing. Surprisingly, almost all other 20S core particle subunits, both of the α- and β-ring, were also downregulated together with LMP7. Complementing the targeted analysis of LMP7 (Figure 4-3) and β5c (Figure 4-5), the proteomic analysis successfully detected all six catalytically active subunits from both proteasomal subtypes. Especially GEnCs showed a drastic loss of PSMB9 and PSMB10, the other two immunoproteasomal subunits, but also in EnCs from the other organs these subunits were present at lower levels. Only the two β-subunits PSMB6 and PSMB7 deviated from this pattern and were more heterogeneously regulated with no clear pattern between the organs. But apart from these two, all other β- and α-subunits were present at lower levels in EnCs isolated from LMP7$^{\Delta EnC}$ animals compared to control littermates. Therefore, the loss of LMP7 in endothelial cells from different organs resulted in a downregulation of both other immuno- and generally most 20S proteasomal subunits.

The broad decrease of proteasomal subunits could indicate a proteasome assembly defect. Therefore, changes in the protein levels of chaperones involved in proteasome complex assembly were analysed (Figure 4-20, panel B). The proteasome assembly chaperone 1 (PAC1, encoded by *Psmg1*) was significantly upregulated in all knockout cells. Additionally, the proteasome maturation protein (Pomp) was almost exclusively detected in cells isolated from LMP7$^{\Delta EnC}$ animals. Only in EnCs isolated from lung tissue it was also detected in one control animal, albeit at lower levels than in the LMP7 KO EnCs. Higher levels of these two proteasomal chaperones substantiate the indications of a proteasome assembly defect.

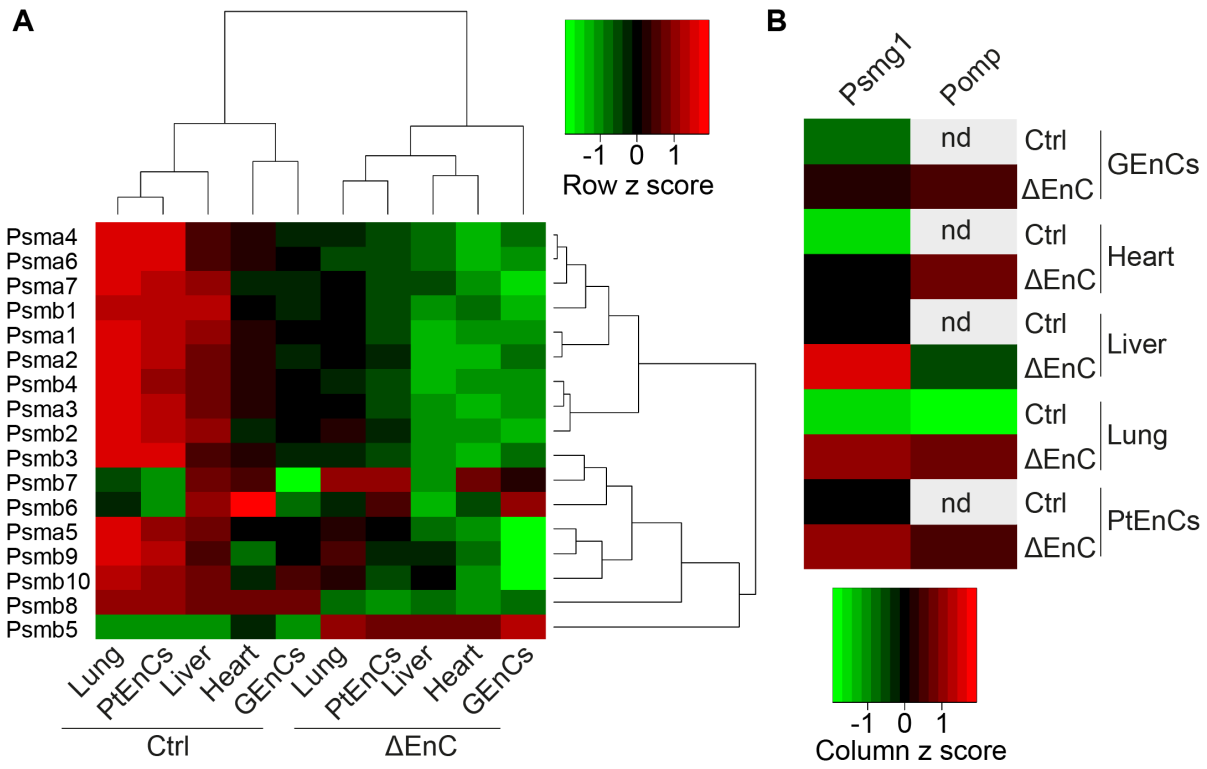

Figure 4-20: Proteomic analysis of proteasome related proteins. **(A)** Heatmap of 20S core particle subunits. Protein intensities were z-normalised among EnCs isolated from the different organs and genotypes. **(B)** Proteomic analysis of proteasomal chaperones. Protein intensities were again z-normalised among the different conditions. Red marks higher intensities, green lower relative intensities. nd: not detected

Interestingly, the levels of two additional proteins were significantly changed by the LMP7 knockout in all five analysed organs, indicating a robust link between LMP7 and their protein levels. In line with the reduced MHC class I cell surface levels determined via flow cytometry, total cellular levels of H2-K1, a component of the MHC class I complex, were also reduced in the mass spectrometric analysis in isolated EnCs from all five organs. Additionally, the protein MORF4L2 (also called MRGX) was more abundant in all EnCs isolated from knockout animals compared to EnCs from control littermates (Figure 4-21). MORF4L2 has been described to be part of several nuclear protein complexes with diverse functions in histone modification and DNA repair (121). Interestingly, the predicted AlphaFold structure for MORF4L2 contains a large N-terminal intrinsically disordered region (IDR), which is not present in the close homologue MORF4L1 (Figure 4-21, panel B). Such regions have been shown to be specifically cleaved by 20S proteasomes (57). Indeed, the peptides detected to be changed in abundance in the mass spectrometric analysis all localised to this IDR (highlighted in red). Two peptides from other regions of the protein were either not reliably detected in all samples or unchanged in abundance (highlighted in black). This is intriguing as it could indicate a specific proteolytic modifcation of MORF4L2 by the i20S, but not or at least to a lesser degree by the c20S. While these data need to be verified via independent experimental approaches, the prior description

of IDRs as targets of the 20S proteasome makes this initial find a very promising starting point for future investigations.

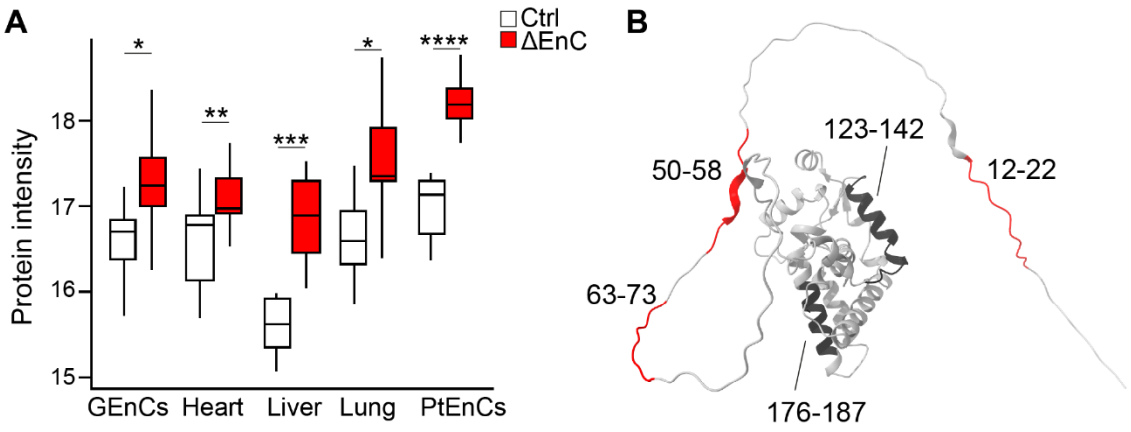

Figure 4-21: MORF4L2 as a potential immunoproteasomal substrate. **(A)** LFQ protein intensity of MORF4L2 in EnCs isolated from five mouse organs. **(B)** Localisation of the peptides detected in the mass spectrometric analysis within the predicted MORF4L2 structure. Peptides that were more abundant in EnCs isolated from LMP7$^{\Delta EnC}$ mice are highlighted in red, other peptides in black. Structure: AF-Q9R0Q4-F1.

Apart from proteasomal genes, MHC class I levels and MORF4L2, no common reaction to the loss of LMP7 across all five organs was observed. This notion was also supported by gene ontology (GO) term enrichment analyses of the altered proteasomal signatures. Only very few GO terms were shown to be altered in more than one tissue type, and these were all directly related to proteasomal composition or assembly. However, additional GO terms were significantly enriched in the affected proteins for individual tissues, indicating specific reactions to the loss of LMP7 in endothelial cells of the corresponding organ. The most prominent alterations observed in EnCs from each organ are briefly summarised in the following paragraphs. Tables containing the top 10 most significantly altered GO terms per ontology for each organ can be found in table 7-1 to table 7-10.

In GEnCs, proteins associated with antigen processing and presentation were less abundant, caused by lower levels of proteasomal subunits and MHC class I proteins. There were indications that vesicular trafficking was altered, with e.g. BET1L being less abundant, a Golgi SNARE protein involved in retrograde vesicular trafficking. In line with the observation that there were fewer upregulated than downregulated proteins in GEnCs of LMP7$^{\Delta EnC}$ mice, (see Figure 4-19), no GO terms passed strict statistical criteria in the upregulated genes. However, some indications occurred that membrane transport was altered with both UBR3 and PKD2 being more abundant in GEnCs isolated from LMP7$^{\Delta ENC}$ mice – a finding potentially complementing the observations made on mRNA level.

In EnCs isolated from the heart, no GO term alterations passed strict statistic criteria. The ones that did seem to be altered were mostly caused by the lower levels of proteasomal proteins and those related to MHC class I. However, also in the heart some indications were observed that retrograde vesicle transport might be altered with GOLPH3L being less and GOLPH3 being more abundant in EnCs isolated from hearts of LMP7$^{\Delta EnC}$ mice.

Overall, liver EnCs reacted with the strongest alteration in their global proteome to the loss of LMP7, in line with the high total number of significantly altered proteins (Figure 4-19). Strong downregulation of proteins involved in cytoskeletal organisation and cell adhesion (e.g. ACTN4, ITGAV) and vesicular trafficking (e.g. SNX9, RAB27B) were detected. MORF4L2, CREBBP and KAT8 were more abundant in liver EnCs isolated from LMP7$^{\Delta EnC}$ mice, leading to the statistically significant alteration of GO terms associated with acetyltransferase complexes.

In EnCs isolated from the lung of LMP7$^{\Delta EnC}$ mice, mostly proteins directly associated with proteasomal composition and immune regulation (H2-K1) were downregulated. Significantly upregulated were proteasomal chaperones (e.g. PSMG1, PSMG3). Additionally, some proteins associated with cytoplasmic stress granules were upregulated, e.g. TIA1 and YTHDF2, potentially indicating a proteostatic impairment in lung EnCs.

In PtEnCs, also a broad downregulation of proteasomal subunit proteins and MHC class I related proteins was observed. As in GEnCs and the heart, there were some indications of Golgi and vesicle involvement. Interestingly, proteins associated with glutathione metabolism (e.g. MGST1 and GSTA4) and pUb- binding proteins (e.g. UFD1 and VCP) were more abundant.

In summary, EnCs isolated from all organs showed reactions to the loss of LMP7 in this proteomic analysis, some of which could explain the phenotypic alterations observed in isolated EnCs. A downregulation of proteasomal subunits beyond LMP7 was observed in several organs. Of note, also proteins involved in (retrograde) vesicle transport were detected to be differently abundant between EnCs isolated from LMP7$^{\Delta EnC}$ mice and control littermates in several organs, potentially explaining some of the phenotypic observations made in the targeted analyses.

4.2.3 Common genes between proteomics and transcriptomics

For the two kidney endothelial cell types, GEnCs and PtEnCs, both mRNA and proteomic data were gathered during this thesis. Interestingly, some genes were detected to be significantly altered on both levels in kidney EnCs isolated from LMP7$^{\Delta EnC}$ mice, strongly indicating a functional link between the observed regulation and the loss of LMP7. For GEnCs, this is only the case for three genes: *Uqcc2*, *Smim12* and *Rflnb*. *Morf4l2* was not detected to be regulated

on mRNA level in GEnCs and neither were the proteasomal genes. Unfortunately, very little is known about both *Rflnb* and *Smim12*, making their functional role in immunoproteasome impairment currently unclear.

However, for PtEnCs, many more genes and proteins were altered in both datasets and some of them have been linked to cellular processes potentially explaining phenotypes that were observed in targeted analyses. As such, *Cyth3* and *Vat1* are involved in vesicular trafficking and protein sorting, whereas *Sgk1* and *Sgk3* are known to be involved in ion channel regulation, potentially explaining the cell size phenotype observed in kidney EnCs (see Figure 4-9).

The complete lists of genes that were altered on both mRNA and protein level in GEnCs and PtEnCs can be found in table 7-11 and table 7-12, respectively.

4.3 An LMP7 deficient endothelial cell culture system

The observations made in isolated endothelial cells from LMP7$^{\Delta EnC}$ mice strongly indicated an effect of the LMP7 loss on (intracellular) vesicular trafficking. Mechanistic studies on this link in primary EnCs are challenging, mostly due to the limited sample material and the small size of the EnCs. However, directly analysing vesicular trafficking via live cell imaging would be a promising approach to gain further insight into the responsible mechanism. To complement the *in vivo* data generated from isolated murine EnCs, a human endothelial cell culture model with a knockout for *PSMB8* was established. CRISPR/Cas9 mediated genome editing was utilised to interrupt the *PSMB8* gene in EA.hy926 cells. The parental cell line as well as two CRISPR clones (C#6 and C#9) and were analysed in further experiments.

Firstly, the successful knockout and direct reaction already observed in murine EnCs were analysed. Indeed, the parental cell line expressed LMP7 whereas both clones showed a complete loss of the protein, verifying a successful *PSMB8* knockout via CRISPR/Cas9 (Figure 4-22, panels A and B). While these findings nicely mirrored the results from isolated murine endothelial cells, the upregulation of β5c in the knockout cells was not comparable between the two clones. While C#6 exhibited approximately two-fold increased β5c levels, this effect was much smaller in C#9, indicating clonal differences between the two. Therefore, in this aspect, C#6 reflected the situation in murine EnCs more closely.

Secondly, the effects of the altered proteasomal subunit expression on proteasomal activity were analysed using native polyacrylamide gel electrophoresis (PAGE) and the fluorescent peptide substrate Suc-LLVY-Amc. In neither of the clones, a decrease in proteasomal activity was observed (Figure 4-22, panels C and D). While in the isolated murine EnCs, activity was even slightly increased (see Figure 4-7), also the human cultured EnCs (EA.hy926) showed

no proteasomal impairment by the loss of LMP7. Corroborating the levels of the β5c subunit as determined via immunoblot, also β5c levels in assembled proteasomal complexes were found to be increased via native PAGE analysis in both clones. While a trend was observable for both clones in both 20S and 26S complexes, it was only statistically significant for C#6 in the 20S and for C#9 in the 26S complex, potentially indicating different proteasomal species in these two cell lines.

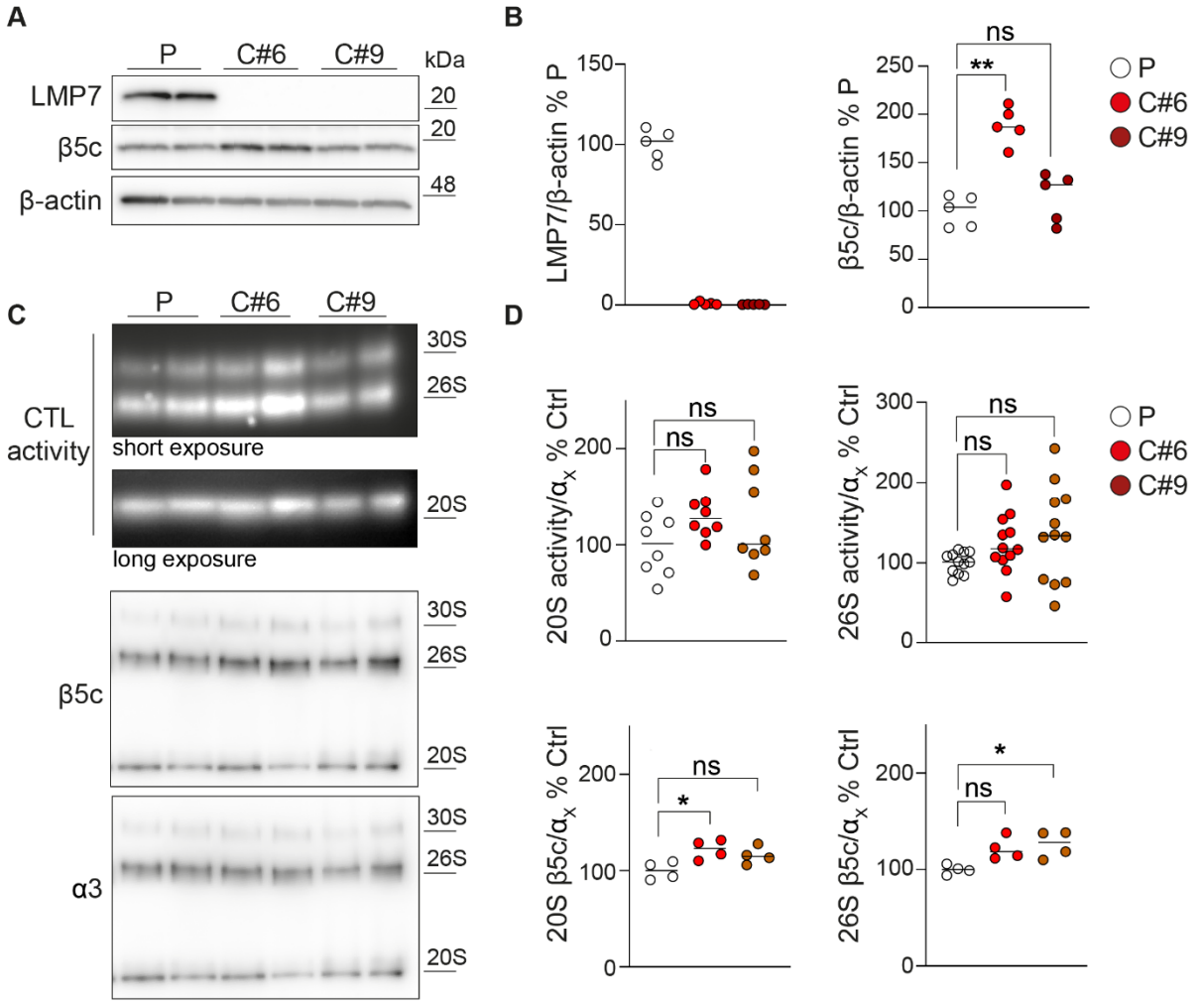

Figure 4-22: Validation of a human endothelial *PSMB8*-KO cell culture system. **(A)** Immunoblot analysis of LMP7 and β5c expression on the parental (P) EA.hy926 cell line and two CRISPR knockout clones (C#6 and C#9). **(B)** Quantifications of these immunoblot analyses from two independent experiments. Depicted are protein levels normalised to β-actin relative to the parental cell line. **(C)** In-gel analysis of proteasomal activity using the fluorescent peptide substrate Suc-LLVY-Amc followed by immunoblot analysis of β5c and α3 protein levels. α3 was used to determine proteasome abundance. **(D)** Quantifications of proteasome in-gel activity and incorporated β5c levels for 20S and 26S proteasomal complexes. Cells from at least two independent experiments were included in the analysis. P: Parental; α_x: normalisations to both α_2 and α_3 as indicators of proteasome abundance were used.

After verifying that the cell culture system reliably lacked LMP7 and at least partially mirrored observations made in the murine setting (β5c upregulation, no loss of proteasomal activity), they were more closely analysed regarding cellular processes potentially explaining the alterations observed in mouse endothelial cells. As some of the data gathered using mouse EnCs indicated an involvement of endocytosis, EA.hy926 cells were analysed via flow

cytometry and immunoblotting for the cell surface and total cellular levels of endocytosis related proteins. Interestingly, they also showed alterations in some endocytosis related proteins, although the alterations did not necessarily directly mirror the effects observed in murine EnCs. While FcRn cell surface levels determined via flow cytometry were unaltered in murine EnCs, both EA.hy926 KO cells had higher FcRn levels at the cell surface (Figure 4-23, panel C). Clone #6 shared the lower total cellular FcRn levels with GEnCs and PtEnCs, whereas this effect could not be observed for clone #9 (Figure 4-23, panel A and B). Changes in the levels of the analysed Rab proteins were much less clear than in the mouse EnCs (Figure 4-23, panels D and E).

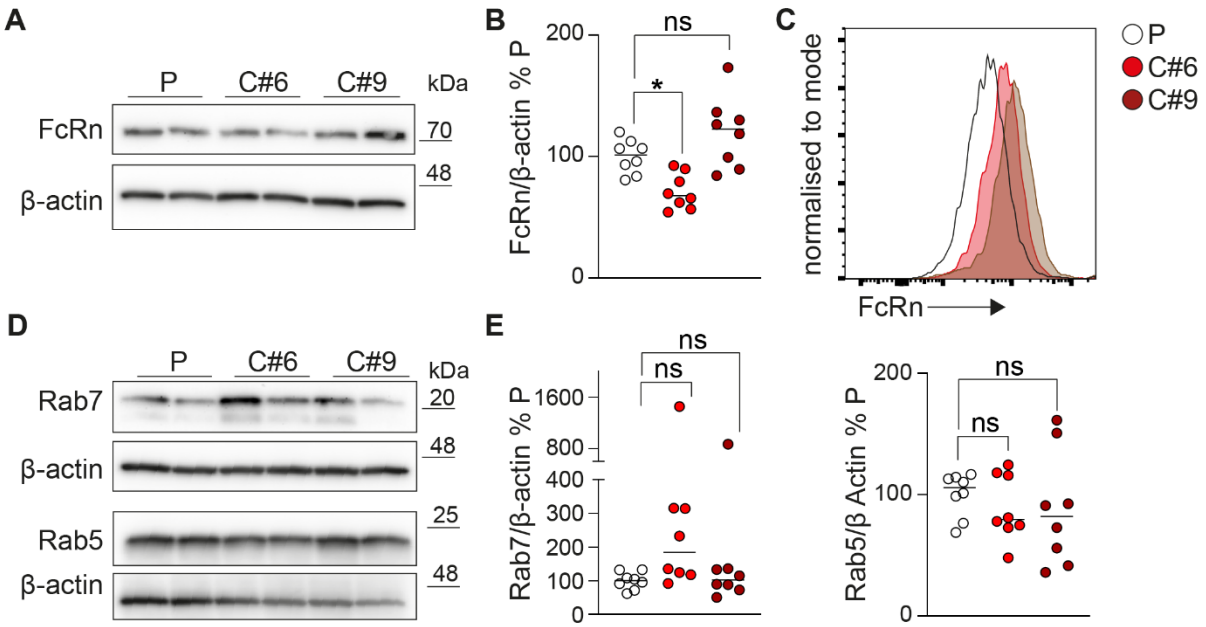

Figure 4-23: Analysis of protein related to vesicular trafficking in EA.hy926 cells. **(A)** Exemplary immunoblot analysis of total FcRn levels in parental and LMP7 knockout EA.hy926 cells, quantified in **(B)**. **(C)** Exemplary histogram of flow cytometric analysis of FcRn cell surface levels on the three cell lines. **(D)** Immunoblot analysis of total Rab5 and Rab7 level in the three cell lines, quantified in **(E)**. β-actin was used as a loading control. P: Parental

Mirroring some of the results observed in EnCs isolated from LMP7$^{\Delta EnC}$ mice, the EA.hy926 cells displaying an LMP7 knockout are a valuable experimental setup for future experiments.

4.4 LMP7 in endothelial cells during disease

The results from naïve LMP7$^{\Delta EnC}$ mice showed that EnCs from different organs were perturbed by the loss of the immunoproteasomal subunit LMP7. Analyses on both murine and cultured human cells indicated an alteration of vesicular trafficking processes, potentially explaining the antibody accumulation in murine GEnCs. However, the mice did not show a clear phenotype upon knockout induction. Furthermore, principal component analysis of both transcriptomic and proteomic data showed that the loss of LMP7 only had a limited influence on the global cellular transcriptome and proteome. To further unravel the consequences of immunoproteasome deficiency in kidney EnCs, the expression and functional role of immunoproteasomal subunits, especially LMP7, in different disease conditions were explored. It had already been shown before that the (immuno)proteasomal system is regulated in persistent, but not transient glomerular diseases (122). However, these analyses were performed on total glomeruli, leaving the cellular distribution within the glomerulus unclear.

4.4.1 LMP7 is upregulated in human disease

As a first step, human kidney biopsies from patients with different kidney diseases were analysed for their expression of LMP7 (Figure 4-24). Confirming the observations made in murine samples, also control biopsies from healthy human kidneys showed an endothelial expression of LMP7 (top row). This was, however, markedly increased in biopsies from diseased kidneys. Especially in anti-glomerular basement membrane glomerulonephritis (anti-GBM-GN) and diabetic nephropathy (DN), there was a strong increase in glomerular LMP7 signal, while this difference was less pronounced in an anti-neutrophil cytoplasmic antigen glomerulonephritis (ANCA-GN) patient. Importantly, this upregulation was mostly localised to endothelial cells in anti-GBM-GN and ANCA-GN, whereas in diabetic nephropathy, podocytes additionally showed an increased expression of LMP7.

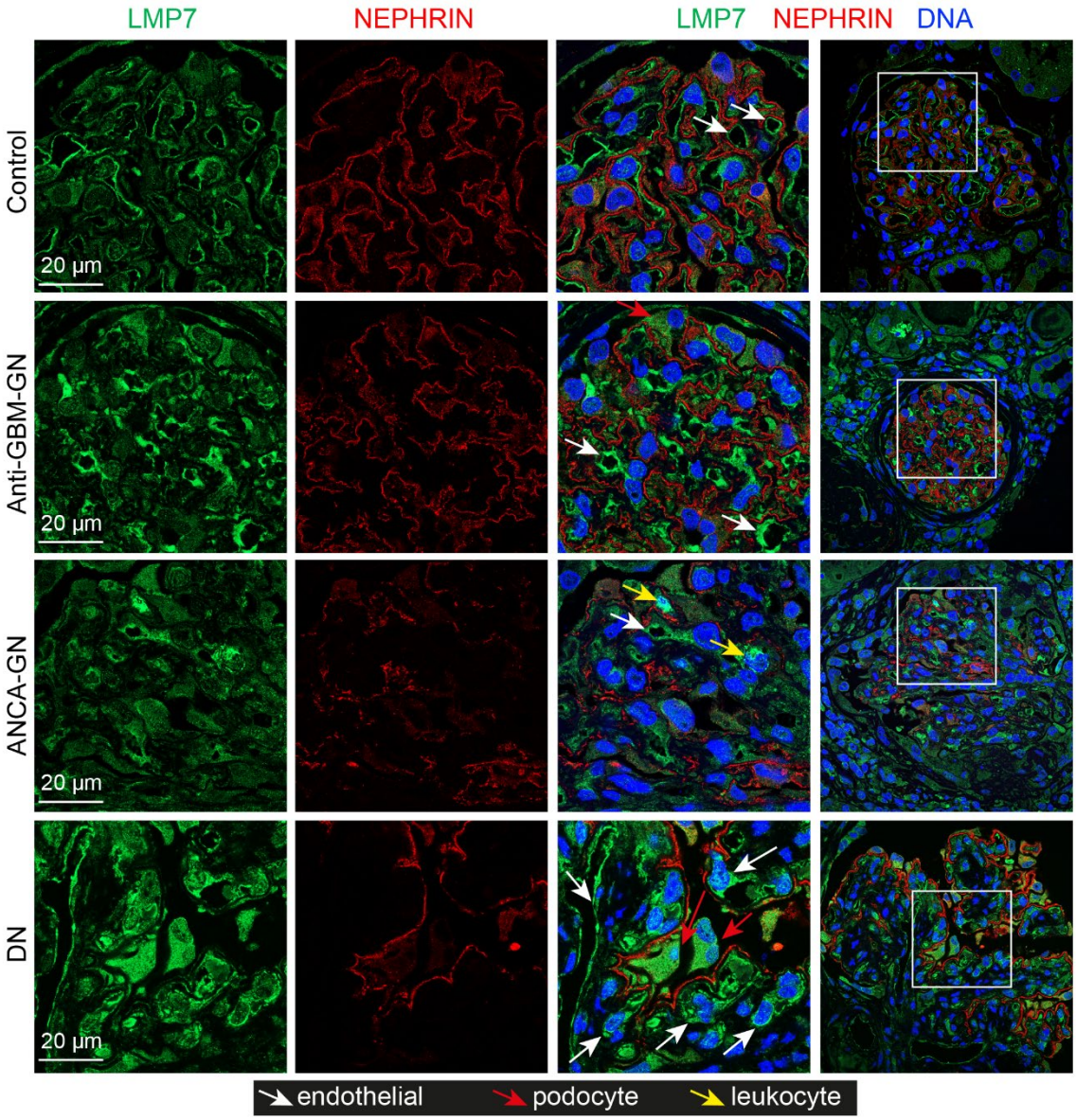

Figure 4-24: Analysis of LMP7 expression in human kidney disease. Confocal microscopy images of formalin-fixed paraffin-embedded (FFPE) tissue sections from human kidney biopsies from a healthy kidney (Control), an anti-glomerular basement membrane glomerulonephritis (anti-GBM-GN) patient, an anti-neutrophile cytoplasmic antigen glomerulonephritis (ANCA-GN) patient and a diabetic nephropathy (DN) patient. LMP7 is stained in green, Nephrin in red marks the slit diaphragm at podocyte foot processes. Cell nuclei are stained in blue using Hoechst.

4.4.2 The UPS in murine diabetes

Among the analysed biopsies from human patients, diabetic nephropathy showed a prominent upregulation of LMP7 in glomerular EnCs and podocytes. To analyse the role of LMP7 in diabetes in more detail, the BTBR *ob/ob* mouse line, a well-established model of type 2 diabetes exhibiting many features of the human disease, was used (96, 123). Firstly, the weight and uACR of the mice were analysed at two timepoints (8 weeks and 20 weeks as early and late-stage diabetic nephropathy, respectively) to confirm the development of disease in the mice (Figure 4-25). Indeed, BTBR *ob/ob* mice were much heavier (panel A) and showed a

higher uACR (panel B) than control mice at both 8 and 20 weeks of age (Figure 4-25). The increased uACR indicated an impairment of the glomerular filtration barrier.

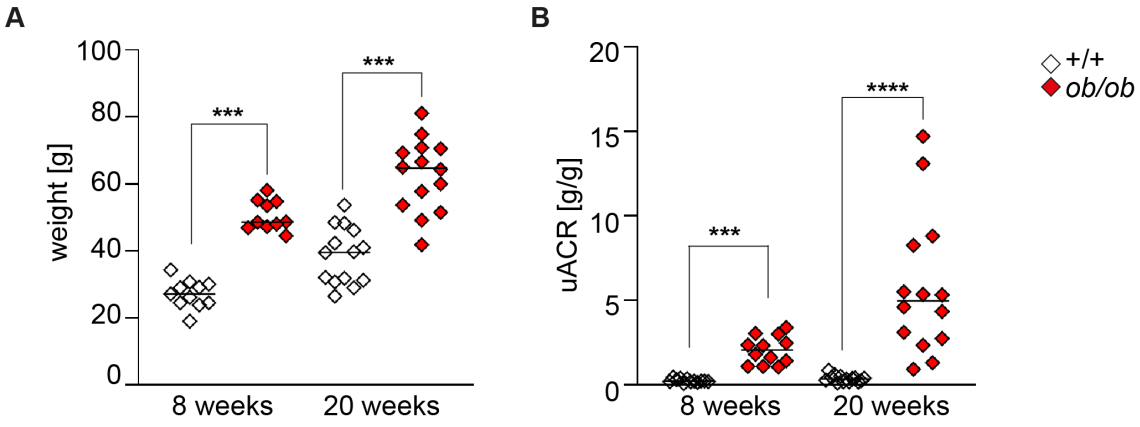

Figure 4-25: Phenotypic assessment of BTBR *ob/ob* mice. **(A)** Body weight of BTBR *ob/ob* mice and control littermates at 8 and 20 weeks of age. **(B)** Urinary albumin-to-creatinine ratio of BTBR *ob/ob* mice and control littermates at 8 and 20 weeks of age.

First, the glomerular expression of the immunoproteasomal subunit β5i was assessed to verify that the murine disease model mimics the human disease in this aspect. To this end, glomeruli isolated from diabetic mice were analysed by immunoblotting for LMP7 protein levels. Indeed, slightly increased levels of LMP7 were observed in glomeruli of both 8- and 20-week-old diabetic mice. Confirming these results, an accumulation of LMP7 was observed in podocytes and glomerular endothelial cells via immunofluorescence microscopy (Figure 4-26, A and B, respectively). In podocytes, the increased LMP7 signal in BTBR *ob/ob* mice did not appear to be cytoplasmic but rather at the foot processes as it did not colocalise with α-tubulin, but instead was localised adjacent to the nephrin signal. In the naïve setting of LMP7$^{\Delta EnC}$ mice, a reciprocal relationship between LMP7 and β5c protein levels had been observed. To assess if a similar relationship was present in murine diabetic nephropathy, the levels of β5c were examined. Interestingly, β5c protein levels were not decreased in glomeruli from diabetic mice, despite the upregulation of LMP7. While the protein levels determined via immunoblotting did not show a clear increase, the immunofluorescence microscopy revealed a more granular pattern of β5c in glomerular endothelial cells in diabetic animals compared to WT controls.

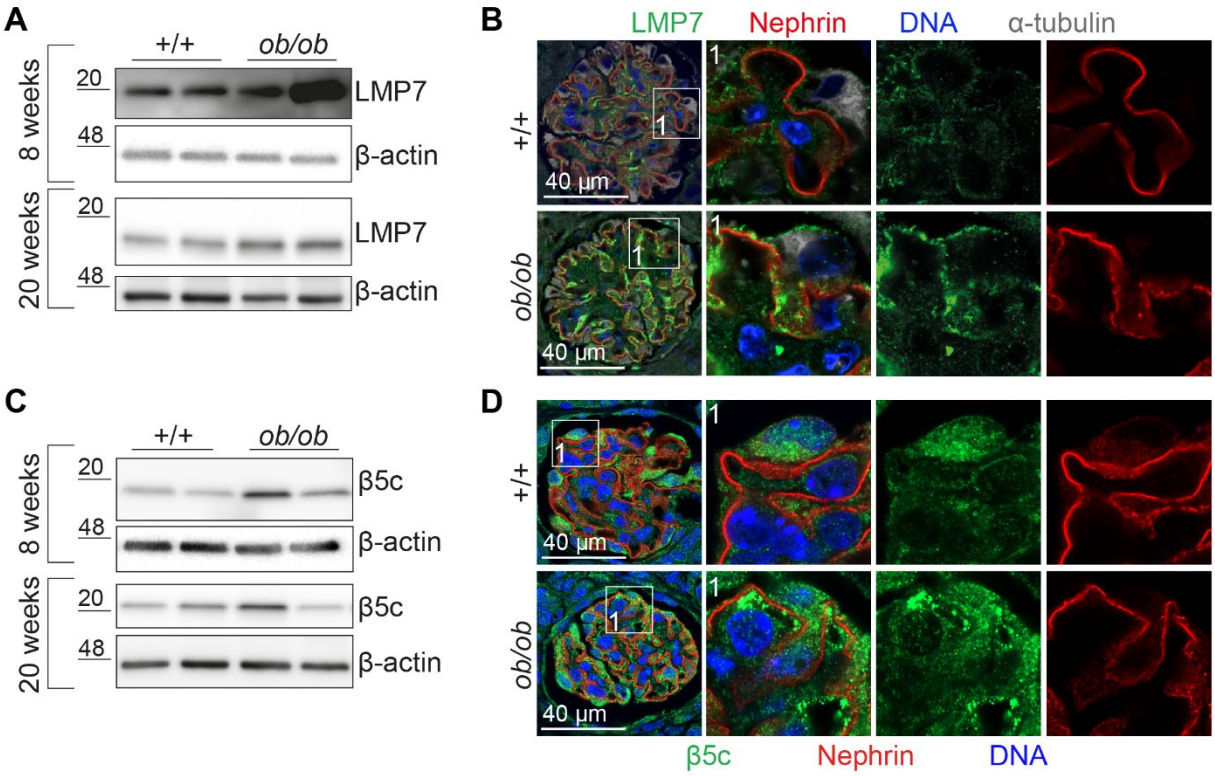

Figure 4-26: Assessment of β5c and LMP7 levels in glomeruli of BTBR *ob/ob* mice. **(A)** Immunoblot analysis of LMP7 protein levels in isolated glomeruli of BTBR *ob/ob* mice and control littermates (+/+) at 8 and 20 weeks of age. β-actin was used as a loading control. **(B)** Immunofluorescence analysis of LMP7 in glomerular tissue of on exemplary mouse per genotype. **(C)** Immunoblot analysis of β5c in isolated glomeruli of BTBR *ob/ob* mice and control littermates. **(D)** Immunofluorescence microscopy analysis of β5c in glomerular tissue of one exemplary mouse per genotype. Protein of interest is stained in green, Nephrin in red marks podocyte foot processes. DNA in blue depicts cell nuclei and α-tubulin in grey depicts podocyte cytoplasm in the LMP7 stained samples.

Increased protein levels of (immuno)proteasomal subunits could, but don't necessarily, relate to increased proteasomal activity. To assess the status of the degradative systems in isolated glomeruli of diabetic mice, proteasomal activities were analysed. In line with the protein levels of the subunits LMP7 and β5c, total proteasomal activity were increased as determined by fluorescence-based activity readouts at both the complex (with Suc-LLVY-Amc) and the subunit level (with the activity-based probe MVB003) (Figure 4-27, panel A). However, total proteasomal amount as determined via the subunit α2 was also increased. Therefore, proteasomal activity was normalised to the levels of α2. Indeed, a very heterogeneous change of proteasomal activity per proteasome was observed in early DN at 8 weeks (Figure 4-27, panel B). However, in glomeruli from 20-week-old BTBR *ob/ob* mice, 20S proteasomal activity was clearly reduced compared to BTBR +/+ littermates, indicating an impairment of proteasomal activity. Subunit activity determined using an activity-based probe revealed no difference in activity of the β5 subunits, indicating that individual subunits were not impaired in their catalytic function (Figure 4-27, panels C and D).

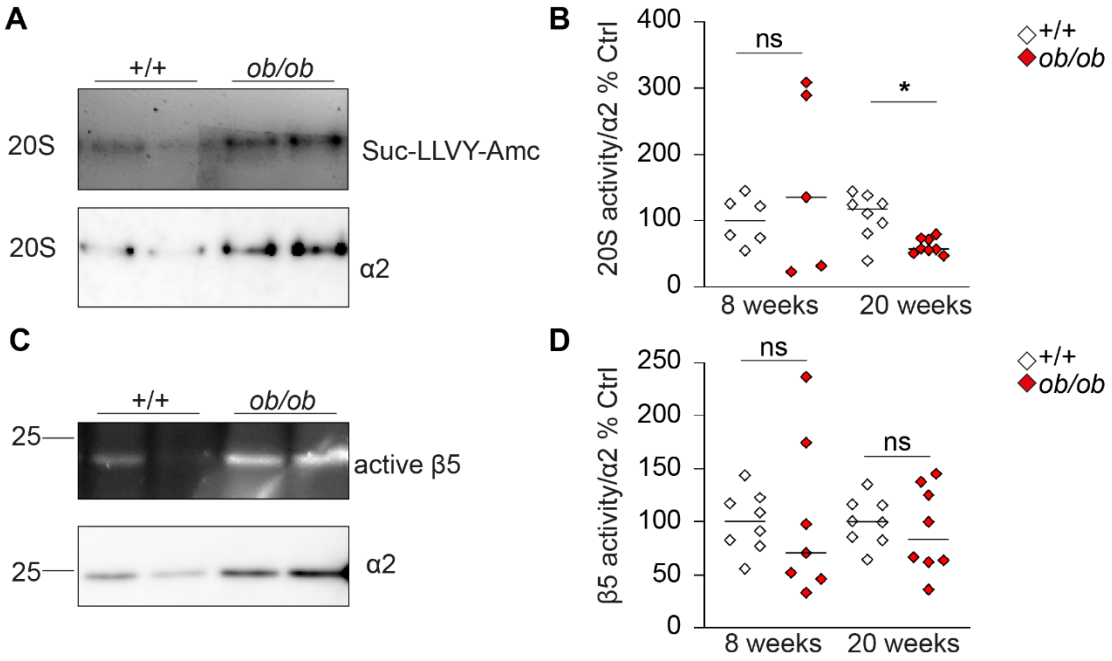

Figure 4-27: Assessment of proteasomal activity in isolated glomeruli of BTBR *ob/ob* mice and control littermates. **(A)** In gel activity analysis of proteasomal activity using the fluorescent peptide substrate Suc-LLVY-Amc. α_2 was used to determine total proteasome abundance. **(B)** Quantification of 20S proteasomal activity normalised to α_2 as % of activity in glomeruli isolated from control littermates. **(C)** Assessment of subunit specific activity of the β5 subunits using the activity-based probe MVB003. α_2 was used to determine total proteasome abundance. **(D)** Quantification of the subunit specific activity. Both male and female mice from at least three independent mouse cohorts were included in the analysis.

To assess the impact of the altered proteasomal composition and activities on cellular proteostasis, the protein levels of K48- and K63- polyubiquitylated (pUb) proteins were analysed by immunoblotting. Both K48 and K63- pUb proteins have been described to mediate protein degradation via different pathways and were analysed here as markers of cellular proteostasis (68). Surprisingly, no clear accumulation of polyubiquitylated proteins could be observed in glomeruli of BTBR *ob/ob* mice. While K48-pUb slightly accumulated in 8-week-old mice, this effect was not present at 20 weeks (Figure 4-28, panels A and B). Surprisingly, the opposite was observed for levels of K63-pUb. While no accumulation was present at 8 weeks, diabetic animals exhibited slightly higher levels of glomerular K63-linked polyubiquitin at 20 weeks (Figure 4-28, panels C and D).

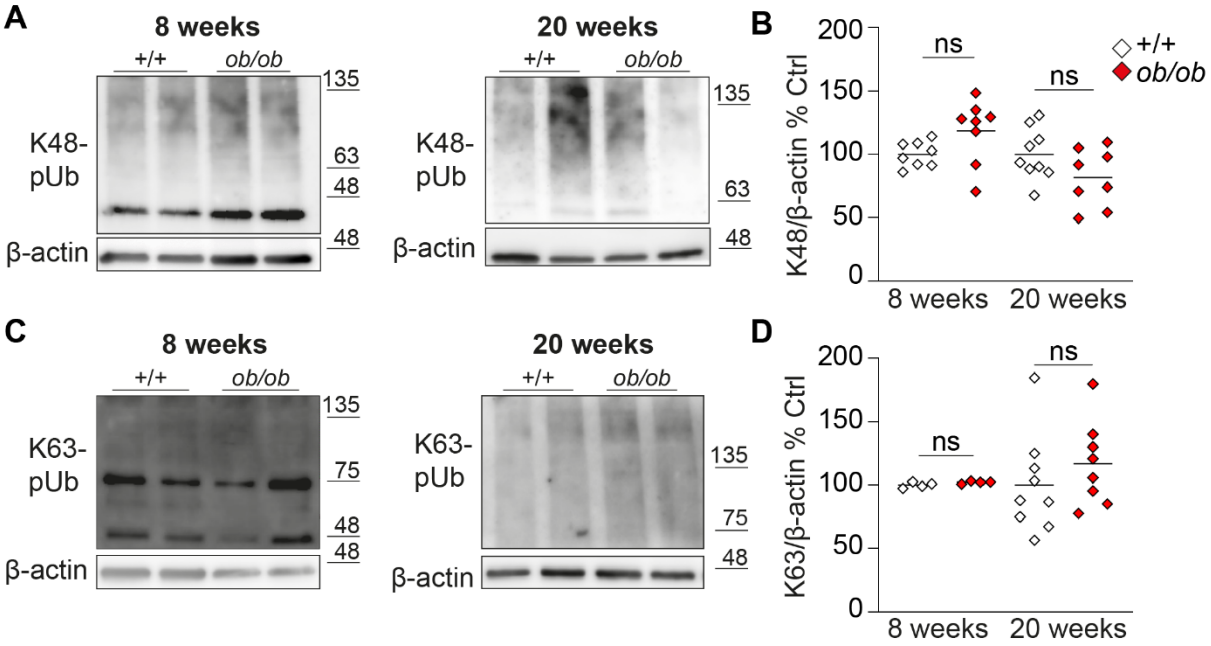

Figure 4-28: Assessment of accumulation of polyubiquitin (pUb) chains in isolated glomeruli of BTBR ob/ob mice and control littermates (+/+).**(A)** Exemplary immunoblots of K48-pUb in isolated glomeruli from 8- and 20-week-old BTBR *ob/ob* mice and control littermates. **(B)** Quantifications of the K48-pUb levels normalised to β-actin as % of levels in glomeruli isolated from control littermates. **(C)** Exemplary immunoblots of K63-pUb in isolated glomeruli from 8- and 20-week-old BTBR *ob/ob* mice and control littermates. **(D)** Quantifications of the K63-pUb levels normalised to β-actin as % of levels in glomeruli isolated from control littermates. Both male and female mice from 1-3 independent cohorts were included in the analysis.

The lack of clear accumulation and the different patterns of K48- and K63-pUb protein accumulation potentially indicate some compensatory reaction of the proteostatic system in the disease course. Potentially, the upregulation of proteasomal subunits detected in glomeruli of BTBR *ob/ob* mice rescued the impaired activity per proteasome.

4.4.3 Endothelial LMP7 in NTN

The upregulation of LMP7 in human kidney disease and the impaired proteasome function in murine diabetes indicated an involvement of the immunoproteasome in these different kinds of glomerular disease. However, no K48-pUb accumulation as a likely result of proteasomal impairment could be observed and immunoproteasomal subunits were upregulated. Together, these findings could indicate a regulatory reaction to the proteasomal impairment preventing accumulation of proteasomal substrates. If these observations were directly related to the disease course and whether they represent beneficial or detrimental reactions, remained unclear. To mechanistically examine the possible relevance of endothelial immunoproteasome expression in disease states, the nephrotoxic nephritis (NTN) mouse model of rapidly progressive glomerulonephritis (RPGN) was induced in the LMP7$^{\Delta EnC}$ mouse line. To this end, mice were injected with nephrotoxic serum four weeks after the induction of the LMP7 knockout. NTN is a well-established mouse model of antibody-mediated auto immune kidney

disease. Mice were observed for ten days after injection with nephrotoxic serum. Urine samples were taken during the disease course, and the mice were sacrificed on day 10. Urinary albumin-to-creatinine ratio, blood urea nitrogen, serum cholesterol and crescent formation were used to assess disease severity. Interestingly, mice lacking endothelial LMP7 showed an exacerbated disease progression in this mouse model of kidney disease (Figure 4-29). While control littermates recovered from initially high uACR as has been described before (94), this was not the case for LMP7$^{\Delta EnC}$ mice. Instead, the albuminuria stayed high and even slightly increased from day 2 to day 10 (Figure 4-29, panel B). In line with this, serum parameters also indicated a worse clinical outcome for LMP7$^{\Delta EnC}$ mice compared to control littermates (panel C). Importantly, more glomeruli showed crescent formation in histological analysis on periodic acid Schiff (PAS)stained sections (panel D).

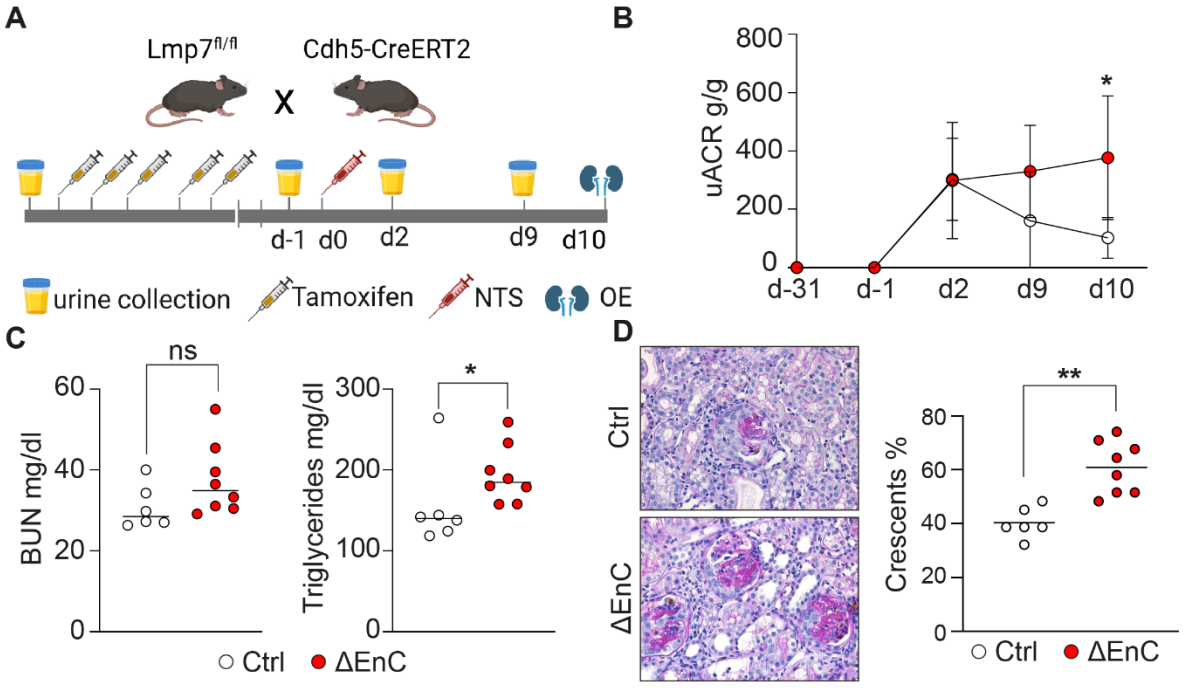

Figure 4-29: Experimental setup and disease course of a murine model of crescentic glomerulonephritis in LMP7$^{\Delta EnC}$ mice. **(A)** Breeding scheme and experimental setup of nephrotoxic nephritis (NTN) induction in LMP7$^{\Delta EnC}$ mice. **(B)** Time course of the urinary albumin-to-creatinine ratio (uACR) in LMP7$^{\Delta EnC}$ mice and control littermates. **(C)** Analysis of blood urea nitrogen (BUN) and serum triglyceride levels. **(D)** Exemplary periodic acid schiff staining (PAS) stainings showing glomerular crescent formation. Quantification shows the proportion of crescented glomeruli from 30 glomeruli counted per mouse. The experimental scheme in panel A was generated with Biorender. Male mice from one mouse cohort were included in the analysis.

Since the immunoproteasome might influence several cellular pathways possibly affecting the reaction to NTN, the response of resident kidney cells and how they depend on the presence of LMP7 was analysed. Interestingly, glomerular endothelial cells were most affected by the loss of endothelial LMP7 when challenged with NTN (Figure 4-30). From diseased mice, significantly lower numbers of GEnCs could be isolated compared to control littermates. This was not the case for PCs and MCs, ruling out the explanation that this was a direct result of

lower numbers of glomeruli isolated from diseased mice. While the CD31 surface levels per cell were unchanged in flow cytometric analyses, histological analyses showed larger areas with absent CD31 staining, in line with the higher crescent formation described above. The same effect was observed for the nephrin staining as a marker of the slit diaphragm at podocyte foot processes. Interestingly, no cleaved caspase 3 signal as an apoptosis marker could be observed in endothelial cells via immunofluorescence microscopy (Figure 4-30, panel B).The loss of endothelial LMP7 therefore also influenced podocyte health in the NTN model as was already observed under homeostatic conditions. Tubular injury determined by immunofluorescence microscopy of kidney injury molecule 1 (Kim1) and kidney fibrosis as determined by α smooth muscle actin (αSMA) expression revealed focal kidney damage and did not show significant differences between genotypes.

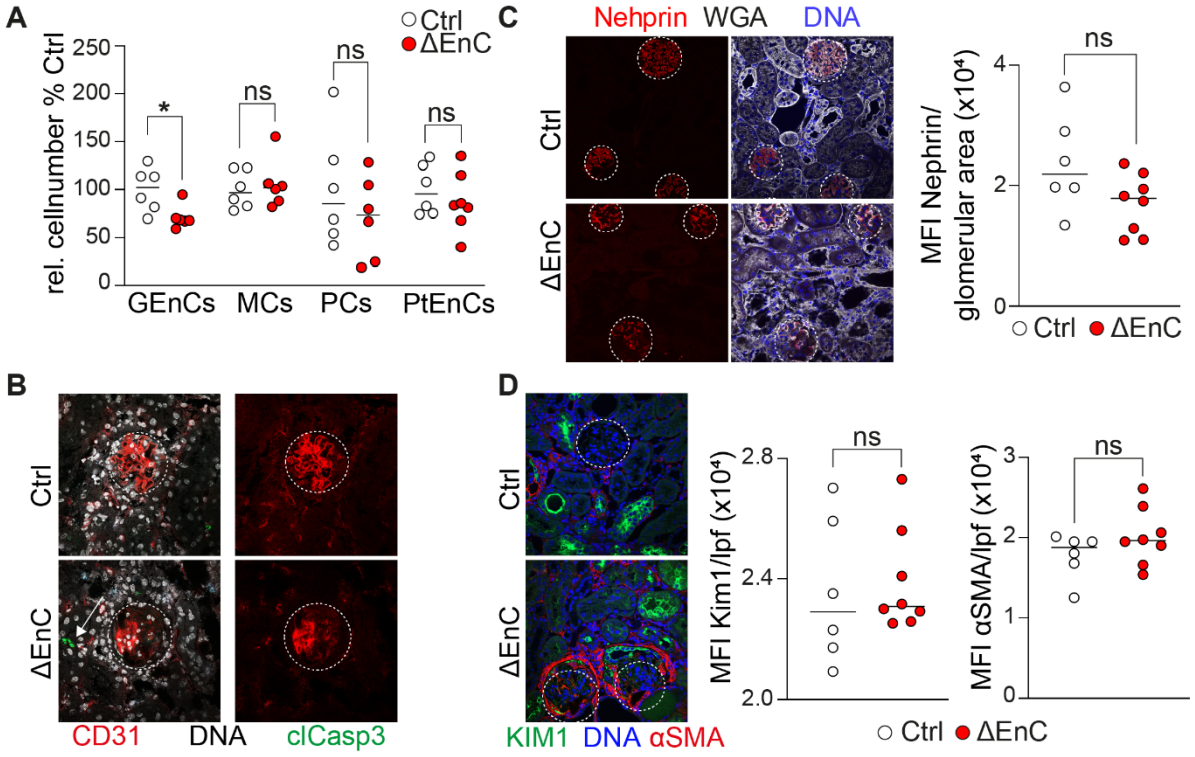

Figure 4-30: Assessment of cellular damage in the nephrotoxic nephritis (NTN) model of crescentic glomerulonephritis. **(A)** Relative cell numbers as % of cells isolated from control littermates for the three glomerular cell types and peritubular endothelial cells (PtEnCs). **(B)** Exemplary immunofluorescent microscopy images of CD31 protein levels in glomeruli of LMP7$^{\Delta EnC}$ mice and control littermates as an indicator of endothelial damage. Cleaved caspase 3 (clCasp3) was stained as an apoptosis marker. **(C)** Exemplary immunofluorescent microscopy images of Nephrin as a marker of podocyte damage. Quantification shows the nephrin mean fluorescent intensity (MFI) per glomerular area. **(D)** Exemplary immunofluorescent microscopy images of kidney injury molecule 1 (KIM1) and α smooth muscle actin (αSMA). Quantification show MFI of both proteins per view area. lpf: low power field; WGA: wheat germ agglutinin

4.4.4 Problems with the LMP7$^{\Delta EnC}$ mouse line background

This initial description of an exacerbated disease course in LMP7$^{\Delta EnC}$ mice compared to control littermates indicated a protective role of the immunoproteasome in NTN. However, when more mice were analysed to unravel the mechanism behind this effect, the exacerbated disease course could not be reproduced. Instead, all mice showed much lower proteinuria during disease and lower crescent formation than before. Importantly, this was even the case for control animals, that did not carry the LMP7 KO (Figure 4-31). While all mice did initially develop proteinuria on day 2, the absolute level was already lower than in the cohort before (Figure 4-31) and uACR almost reached zero on day 9. Serum parameters were also different, with BUN now being significantly lower in LMP7$^{\Delta EnC}$ mice and triglycerides not showing a difference anymore. Basically, none of the disease parameters that are considered hallmarks in NTN developed as before. The NTN disease model is well established in BL/6 mice and cooperating working groups were simultaneously successfully employing it in their experimental setups. Therefore, several parameters were ruled out as a possible cause of this puzzling lack of reproducibility. Different lots of nephrotoxic serum were used, larger amounts of antibodies were injected and even different experimenters carried out the serum injections. However, none of these changes were successful in re-establishing the NTN disease course as disease parameters still reflected a very mild or even absent development of disease.

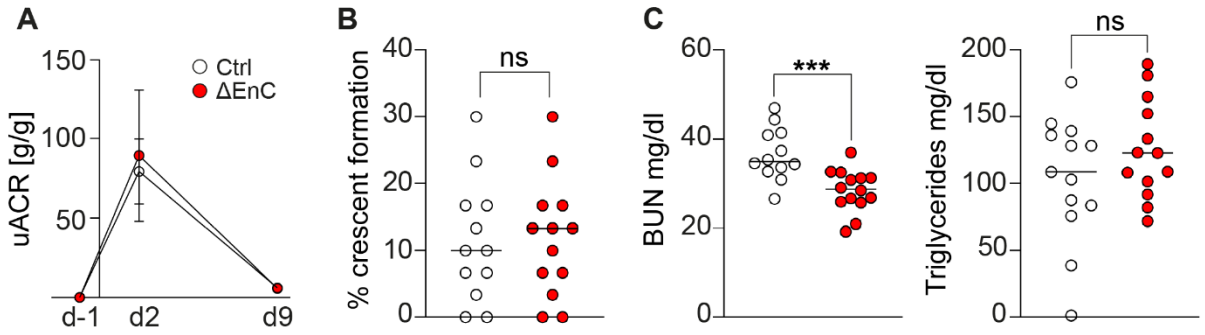

Figure 4-31: Assessment of disease progression in mild NTN cohorts. **(A)** Urinary albumin-to-creatinine ratio (uACR) was determined. **(B)** Percentage of crescentic glomeruli in LMP7$^{\Delta EnC}$ mice and control littermates. **(C)** Serum parameters blood urea nitrogen (BUN) and triglycerides as markers of disease severity. Male mice from four independent cohorts were included in the analysis.

Since all the most likely possible causes had been excluded, tail biopsies were sent to Charles River for a SNP-based mouse background analysis. Surprisingly, the results clearly showed that the mice were not on a (pure) C57BL/6J background (anymore). The SNP analysis only showed 54.4% overlap with the reference panel. For comparison, a mouse line that was used by colleagues for NTN experiments at the time, was also analysed. In this mouse line, the NTN model had recently still been shown to work with the same serum. This mouse showed a notably higher match rate with the reference SNP panel than the LMP7$^{\Delta EnC}$ mouse, albeit it also appeared to be on a mixed background.

Table 4-4: Percentages of identical, homozygous mismatched and heterozygous mismatched SNPs in comparison to a BL/6 reference panel of one control mouse from colleagues and one LMP7$^{\Delta EnC}$ mouse. The results clearly showed that the LMP7$^{\Delta EnC}$ mouse line was on a mixed background.

Mouse	**% Match**	**% heterozygous**	**% mismatch**
Mouse from colleagues	74.0	1.6	25.2
LMP7$^{\Delta EnC}$	54.4	21.4	34.9

4.4.5 Immune regulatory markers on LMP7 deficient EnCs

While the disease progression was much milder than in earlier experiments, the initial antibody-mediated stress was present, as the mice developed strong proteinuria on day 2 after injection of the nephrotoxic serum. Since the initial reaction to the nephrotoxic serum was intact, albeit less pronounced compared to the first set of experiments (Figure 4-29), expression of potentially immune-regulating cell surface molecules was analysed on isolated glomerular and peritubular endothelial cells via flow cytometry. A difference in endothelial – immune cell crosstalk could explain the more severe disease course observed in the initial NTN experiment. Therefore, cell surface levels of immune regulatory molecules on kidney EnCs were analysed via flow cytometry. Figure 4-32 shows exemplary scatterplots as well as quantifications of MHCII^{+} and CD74^{+} EnCs among GEnCs and PtEnCs. These two molecules were reduced on PtEnCs, but not on GEnCs, adding to the vascular bed specific immune modulatory effects of the LMP7 knockout. These findings were in line with the reduced levels of MHCII on PtEnCs isolated from naïve mice described earlier (see Figure 4-11). Of note, also higher percentage of PtEnCs than GEnCs was MHC class II and CD74 positive. Interestingly, CD74 is another protein with an altered expression on the cell surface upon loss of LMP7. Surprisingly, CD74 mRNA was also identified to be reduced in the RNA sequencing analysis specifically in PtEnCs, indicating a transcriptional regulation of this protein by the immunoproteasome.

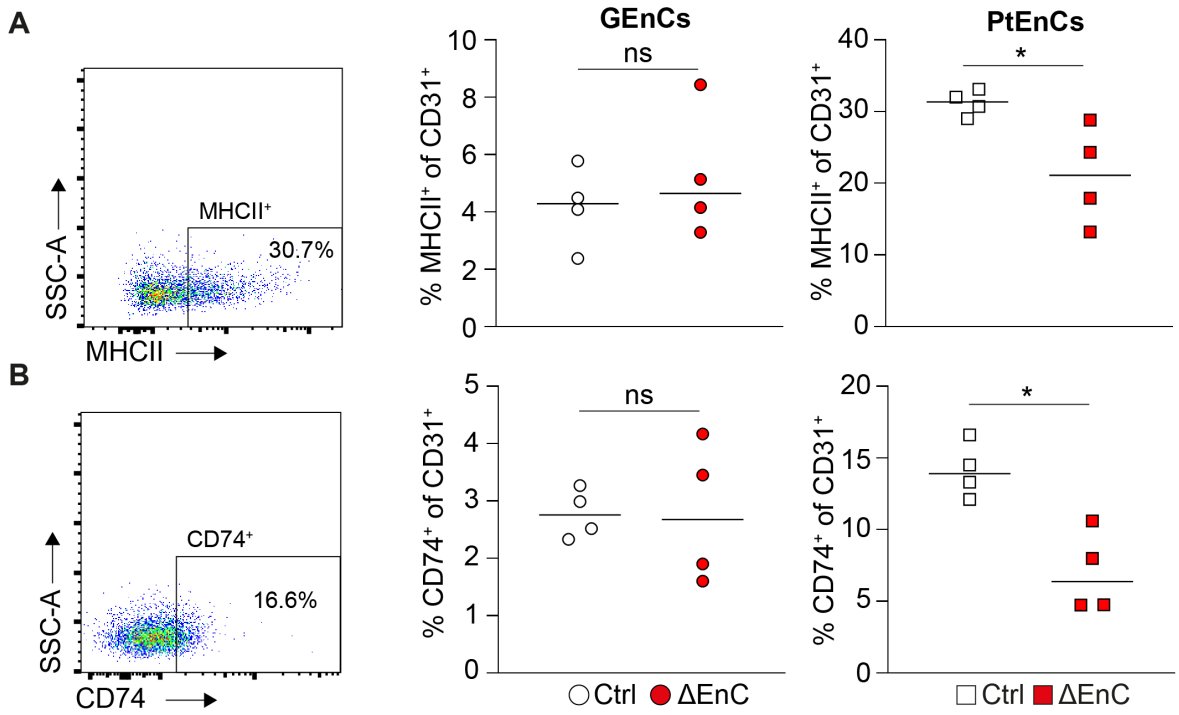

Figure 4-32: Flow cytometric assessment of cell surface levels of immune modulatory proteins on glomerular endothelial cells (GEnCs) and peritubular endothelial cells (PtEnCs) isolated from LMP7$^{\Delta EnC}$ mice and control littermates in a mild NTN model. (**A)** Exemplary scatterplot and quantifications of MHC class II positive GEnCs and PtEnCs. **(B)** Exemplary scatterplot and quantifications of CD74^{+} GEnCs and PtEnCs. Four male mice from one cohort were included in the analysis.

In summary, the experiments on the role of endothelial LMP7 expression presented in this thesis clearly showed perturbations of cellular properties by the loss of LMP7. While some reactions (MHC class I loss, β5c upregulation) were conserved across organs, others revealed a particular dependence on LMP7 by kidney EnCs (changes in cell size, MHC class II loss). The analysis of LMP7 in kidney disease models revealed a potential involvement of this immunoproteasomal subunit in disease progression of both non-inflammatory and inflammatory kidney disease models.

5 Discussion

The ubiquitin proteasome system (UPS) is one of the two major protein degradation pathways in mammalian cells. Together with the autophagosomal-lysosomal pathway (ALP) it is responsible for the degradation of the vast majority of cellular proteins. Combined, these two systems play a major role in proteostasis, the process by which a cell balances its proteome and adapts it to the current conditions. The proteasome is the catalytic complex at the heart of the UPS, being responsible for the proteolytic degradation of proteins that are damaged or not required in the cells' current status. It is formed by the 20S core particle (CP) that can associate with different caps, depending on the cell type and external as well as internal cues. Importantly, the 20S CP harbours three different subunits that carry proteolytically active centres. These three subunits can be replaced by counterparts, the so called immunosubunits to form the immunoproteasome. The immunoproteasome has been described to be involved in numerous cellular processes, most recently in the development of hypertension in mice (21). Much of the studies on molecular properties, however, have been done in cell culture systems or on yeast or archaeal proteasomes. The intricate nature of this protein complex makes studies on murine or human material technically challenging. Therefore, the functional role in mammalian tissue has hardly been directly investigated, even though the expression of the immunoproteasome in structural and especially endothelial cells (EnCs) is increasingly recognised. This study has, for the first time, systematically assessed possible functions of the immunoproteasomal subunit LMP7 (β5i) in EnCs.

5.1 LMP7 in EnCs under basal conditions

Analyses of published datasets performed during this thesis showed expression of immunoproteasomal subunits in EnCs of different organs. Across several organs, EnCs were the cell type showing the highest expression of immunoproteasomal subunits compared to epithelial cells and fibroblasts. Furthermore, even in the functional syncytium of the glomerulus, it was almost exclusively the EnCs that expressed immunoproteasomal subunits, not podocytes (PCs) or mesangial cells (MCs). However, the functional role of the immunoproteasome in EnCs still remains largely enigmatic.

To shed light on the cell type specific role the immunoproteasome plays in EnCs, a new mouse line, the LMP7$^{\Delta EnC}$ mouse line, was established during this project. To this end, LMP7$^{fl/fl}$ mice were crossed with Cdh5-CreERT2 mice, resulting in a mouse line that deletes exon 3 of the *Psmb8* gene in *Cdh5* expressing cells upon induction with tamoxifen (20). The use of an inducible Cre driver allowed the analysis of LMP7 dependent effects in mature endothelium while not interfering with potential roles of LMP7 during vascular development. Initial characterisation of this mouse line showed a robust and cell type specific knockout of the basal

LMP7 expression in EnCs across organs. Non-endothelial cells isolated from the same organs did not show alterations in LMP7 expression. Interestingly, the mice did not exhibit an obvious basal phenotype, as they grew normally and did not show any signs of disease after the knockout induction. *PSMB8* mutations in humans have been well described to lead to CANDLE/PRAAS, an auto inflammatory disease related to altered immune cell function and type I interferon (IFN) signalling (124). None of the related symptoms like dermatosis or lipodystrophy were observed in LMP7$^{\Delta EnC}$ mice, indicating that loss of endothelial LMP7 does not contribute to this disease. However, whether this is due to the cell specific knockout, timing of endothelial LMP7 deletion, or due to the complete loss of the protein compared to the presence of a dysfunctional protein, remains unclear. Since no mouse model for CANDLE/PRAAS has been reported so far, the species difference could also explain the lack of disease manifestation in mice. Importantly, mice completely lacking all three immunoproteasomal subunits have also been described to not show symptoms of disease (125).

Further analyses of EnCs isolated from LMP7$^{\Delta EnC}$ mice offered, for the first time, in depth functional insights into the role of LMP7 in organotypic endothelium. Importantly, the endothelial specific knockout was shown to be stable for up to six months, allowing functional studies into the role of endothelial LMP7 also in other (disease) models and contexts. Despite the lack of a clear phenotype in LMP7$^{\Delta EnC}$ mice, several properties of EnCs were altered by the loss of LMP7.

5.1.1 Reduced MHC class I (and II) levels

Along with the isolation of EnCs via cell sorting, the MHC class I cell surface levels were analysed on both EnCs and control cells. On all analysed EnCs, MHC class I cell surface levels were strongly reduced when LMP7 was missing. It has already been described that immunoproteasomal impairment leads to reduced MHC class I cell surface levels (28), whereas activation of immunoproteasomal activity boosts MHC class I mediated peptide presentation (126). It was postulated very early that the immunoproteasome plays an important role for the generation of peptide antigens, as this process was drastically altered in mice completely lacking immunoproteasomes (125). Early biochemical evidence indicated that immunoproteasomes produce peptides with terminal amino acids that are more suitable for binding to MHC class I molecules (127), potentially explaining the observed alterations in antigen presentation. Additionally, it was shown that the MHC class I cell surface levels rely on all three catalytically active immunoproteasomal subunits, β5i, β2i and β1i (128). The substrate binding pockets of the immunoproteasomal subunits, most importantly LMP7, preferentially produce peptides with bulky amino acids in the S1 position and such peptides are particularly well suited to bind to MHC class I molecules. MHC class I complexes that are

not loaded with peptides have been shown to be retained within the endoplasmic reticulum (ER) (129). Combining these different lines of evidence, a common hypothesis is therefore that a lack of immunoproteasomal activity leads to a diminished generation of peptides suitable for loading on MHC class I molecules, which are therefore retained in the ER. However, this does not fit the data gathered in this project that also total levels of MHC class I are reduced, which should be unchanged if MCH class I localisation merely changes from the plasma membrane to the ER. Furthermore, the massive upregulation of β5c and the increased overall activity of the proteasome should at least partially compensate for the loss of LMP7 activity, making the drastic loss (20 - 40%, depending on the organ) of MHC class I on the cell surface implausible. Additionally, studies have been published that also clearly challenge the paradigm that different peptide pools between the two proteasomal subtypes are directly related to altered presentation on MHC class I molecules. As such, it was found that the two proteasomal subtypes, constitutive proteasomes (cPs) and immunoproteasomes (iPs), produce largely overlapping peptide pools with only some distinct differences (37). While the iP did show a higher preference for amino acids that are good anchors in the MHC class I groove, the corresponding peptides were found to only represent a minute proportion of total MHC class I presented peptides. Therefore, that study concluded that both the cP and the iP specifically produce certain epitopes, broadening the peptide repertoire, but do not globally differ in their peptide production. This seriously questions the widely accepted paradigm on the link between the immunoproteasome and MHC class I peptide loading. Of note, the original study proposing this mechanism used splenocytes that are potentially capable of cross presenting peptides taken up externally (28). Therefore, the observed rescue of MHC class I cell surface level upon addition of extracellular peptides might be a splenocyte specific effect, not necessarily true for other cell types like EnCs. In conclusion, the mechanism linking immunoproteasomal deficiency and reduced cell surface levels of MHC class I molecules on murine EnCs is not fully clear. While only immunopeptidomic analysis of peptides presented on MCH class I molecules would refute the abovementioned hypothesis, the mechanism linking immunoproteasomal impairment and MCH class I most likely includes other aspects besides peptide generation, some of which will be discussed below.

It must be noted, however, that the specific generation of certain epitopes by one of the proteasomal subtypes might already have consequences for biological functions. As such, it has recently been described that the processing of isolevuglandin-adducted proteins by the immunoproteasome and the presentation of the resulting peptides on MHC class I promotes hypertension (21, 130). Furthermore, the presentation of certain e.g. viral epitopes might elicit a more specific and powerful immune response than would be possible with peptides only generated by the constitutive immunoproteasome (131).

Surprisingly, flow cytometric analyses of isolated EnCs showed that on peritubular endothelial cells (PtEnCs) and liver EnCs, MHC class II levels were reduced in addition to MHC class I levels. Additionally, CD74 was reduced both transcriptionally and as a protein on the cell surface of PtEnCs in a mild setting of crescentic glomerulonephritis. This link between the (immuno)proteasome and MHC class II is even less described than for MHC class I. While a connection between the immunoproteasome and MHC class II dependent peptide presentation has been described in dendritic cells (132), the mechanism behind this is completely unknown. Even more intriguing is the fact that this effect was not observed on all the studied EnCs, making it a tissue specific effect. Therefore, it obviously depends on other factors besides the presence of LMP7 and immunoproteasomal activity. These results seem to strengthen the case that proteasomal function is also linked to MHC class II (and not just class I) mediated peptide presentation, at least in endothelial cells. This in turn emphasizes the EnCs' role as antigen presenting cells (reviewed in (95)). As such, it makes studying the alteration of immune cell infiltration of underlying tissue caused by immunoproteasomal alterations in disease models even more interesting.

5.1.2 Protein accumulation as a result of LMP7 loss

One of the main functions often attributed to the immunoproteasome is its specific role in proteostasis. As such, it has been reported to maintain proteostasis in situations of oxidative stress due to a higher catalytic activity compared to the constitutive proteasome (15). In line with this, it has been reported that under IFNγ induced oxidative stress, the immunoproteasome maintains the cells' proteostasis (35). However, others could not reproduce and instead challenged those findings, claiming that the constitutive and immunoproteasomes do not differ in the degradation of ubiquitinated proteins (36). Whether the immunoproteasome really has an intrinsically higher catalytic capacity to degrade proteins, is therefore unclear. Importantly, experimental setups approaching this question differ regarding the time of IFNγ induction. While some studies used short term treatment of cultured cells, the *in vivo* experiments performed during this thesis represent a long-term impairment of immunoproteasomal activity.

During this project, no indications could be observed that the complete loss of LMP7 disturbs the proteostasis of endothelial cells. Protein attached lysine 48-linked polyubiquitin chains (K48-pUb), the most commonly described proteasomal substrate, did not accumulate in EnCs isolated from any of the studied organs. Furthermore, as part of the proteomic analysis, the total amount of protein per cell was also unchanged. This indicates that EnCs do not express the immunoproteasome to deal with a higher degree of protein turnover compared to other structural cells. Alternatively, the EnCs might have upregulated other degradative pathways or even decreased protein synthesis, a reaction already described in other situations of

proteostatic impairment (69). However, also no indications for strong alterations in the autophagosomal-lysosomal pathway (ALP), the ubiquitination machinery or deubiquitinating enzymes were observed in the proteomic analysis. Only the observed upregulation of β5c could partially compensate for a loss in proteostatic capacity caused by loss of LMP7. In summary, the immunoproteasome does not seem to be essential for global proteostasis in murine EnCs of the studied organs under physiologic conditions.

Interestingly, absolute protein content per cell was observed to differ between EnCs isolated from different organs. While glomerular endothelial cells (GEnCs) showed the highest protein content per cell, liver showed the lowest, with lung, heart and PtEnCs showing intermediate values. The biological relevance of this effect remains unclear. The protein abundances did not correlate to changes in cell size between the EnCs isolated from different organs. While maintaining endothelial fenestrae could potentially require a high protein content, this hypothesis is refuted by the relative protein content of glomerular and liver EnCs. Since both are highly fenestrated (133, 134), but do not show the same relative protein content compared to the other organs, the fenestrae cannot be the explanation for this observation.

5.1.3 Effect of the LMP7 loss on vesicular trafficking

The effect of LMP7 loss on cell surface proteins in this study was not limited to MHC class I, but, depending on the cell type, also affected MHC class II proteins and the neonatal Fc receptor (FcRn). FcRn on endothelial cells is responsible for recycling circulating IgG, substantially prolonging its half-life (reviewed in (135)). Therefore, it is a protein heavily relying on intracellular vesicular trafficking and potentially being responsible for the observed msIgG accumulation. In addition to the observed changes in cell surface molecules, the internal structure of the cells seemed to be altered as granularity determined by the flow cytometric parameter sideward scatter-area (SSC-A) was increased in kidney endothelial cells. This evidence strengthens earlier studies linking the proteasome and vesicular trafficking (136), but the direct link is still unclear. Importantly, no differentiation between the proteasomal subtypes was performed in that study. Both the UPS and the endocytic system are highly complex and regulated at multiple levels. An impairment at any point of the vesicular (recycling) pathway would also affect the proteins relying on this process to reach the cell surface or be internalized from the cell surface. The amount of sample material, small cell size of EnCs and limited possibilities to pharmacologically target the proteasome, make unravelling this mechanism *in vivo* technically challenging. A broader approach assessing cell surface protein levels could be a valuable step, narrowing down which cell surface proteins are affected and which might not. Additionally, employing *in vitro* cell culture models could offer alternative experimental setups to tackle these questions (discussed below).

5.1.4 Limited KO effect on cellular gene and protein levels

The expression of immunoproteasomal subunits in endothelial cells is a phenomenon that has only recently been described. Data gathered during this thesis support the presence and functional relevance of LMP7 in EnCs. Contrasting this, in both the bulk mRNA sequencing and the proteomic analysis, the loss of LMP7 only induced limited reactions shared between EnCs isolated from different organs on the global mRNA and protein levels. In both datasets, principal component analysis was not able to clearly differentiate between knockout (KO) and control cells from the same sex and organ. Possibly, the global transcriptome and proteome of EnCs lacking LMP7 are only significantly affected by the knockout in stressed or diseased conditions – performing similar analyses in diseased mice in the future might therefore resolve this apparent contradiction. Nevertheless, EnCs from all tissues showed both altered genes and proteins, indicating that they are indeed affected by the loss of LMP7. Importantly, some processes appeared to be altered in EnCs isolated from different organs. As such, proteins associated with (retrograde) vesicle transport were detected to be altered in EnCs isolated from glomeruli (BET1L), the heart (GOLPH3(L)) and the liver (SNX9).

Another possibility why the global proteome alterations were only limited is that the immunoproteasome does not regulate total protein abundance. It has been described that the 20S proteasome specifically cleaves certain proteins instead of completely degrading them. This has potential effects on their function and subcellular localisation without necessarily affecting their total levels. A possible example of this was also observed in the proteomic dataset generated during this project – MORF4L2.

5.1.5 The immunoproteasome and MORF4L2

Besides proteins directly related to the proteasomal complex, only MORF4L2 was found to be altered in abundance in isolated EnCs from all tissues via the mass spectrometric analysis. Intriguingly, the peptide data indicated that MORF4L2 is not completely degraded by the proteasome, but instead specifically cleaved within its N-terminal intrinsically disordered region (IDR). While this specific cleavage of IDRs by the proteasome has been described (57), a preferential modification of certain substrates by different proteasome subtypes has not. The effect described in this thesis that a lack of LMP7 leads to a significant increase in MORF4L2 is therefore a new phenomenon and would be, if confirmed, the first description of an immunoproteasome specific substrate. Interestingly, MORF4L2 has been shown to be part of nuclear histone methyl transferase complexes (121), fitting earlier reports that nuclear intrinsically disordered proteins (IDPs) are enriched within 20S proteasome substrates (57). It must, however, be kept in mind that this data is preliminary, especially since peptides from regions of the protein outside the IDR were not reliably detected. Careful validation is therefore necessary. Nonetheless, the preferential modification of proteins by certain proteasome

subtypes would be in line with descriptions that also certain viral epitopes for presentation via MHC class I are preferentially produced (or destroyed) by certain proteasome subtypes (137, 138). That such a substrate has not been described so far is likely due to two reasons: 1) Only few studies have been conducted directly comparing the effects of proteasome subtype differences on the global proteome of cells, especially in tissue and cell type specific contexts and 2) these modifications affect, per definition, only certain parts of the target protein. That reduces the likelihood of these proteins to be detected as changed in abundance, because specifically these peptides would need to be detected in both targeted and untargeted analyses. Furthermore, since other parts of the protein are not affected, these proteins might not pass statistic criteria in e.g. mass spectrometric analysis, letting the modifications go unnoticed. Its role in a nuclear histone acetyl transferase complex could potentially explain why an altered regulation of MORF4L2 does not directly lead to strictly regulated alterations in the cells' transcriptomes and proteomes. As an epigenetic regulator, how it effects gene expression and thus protein levels might also rely on the cell's current condition. Additionally, the effects of the observed proteolytic modification on MORF4L2 function are unclear – it could potentially abrogate or enhance its function, change its localisation or interaction partners. Therefore, the observed indications for MORF4L2 to be specifically modified by the immunoproteasome need to be verified but are very promising to be studied in more detail.

5.1.6 Alterations on kidney EnC morphology

The loss of MHC class II molecules specifically on PtEnCs (next to liver EnCs) was a first indication that EnCs in the kidney depend on the immunoproteasome more than EnCs from other organs. Adding to this, flow cytometric analysis of EnCs isolated from LMP7$^{\Delta EnC}$ mice revealed that both types of analysed kidney EnCs, GEnCs and PtEnCs, showed increases in cell size and granularity, indicating changes in the inner structure of the cell. Neither of these parameters was altered in EnCs isolated from any other organ. Plausible explanations for this phenotype would be the accumulation of proteins upon proteasomal impairment or a cell cycle arrest. However, both these hypotheses were refuted experimentally. First, flow cytometric analysis showed no difference in cell cycle progression between the genotypes. Secondly, protein accumulation could also not be observed, neither via immunoblotting nor via mass spectrometry, as discussed above. While some genes or proteins were found in the untargeted analysis that potentially explain these phenotypes (e.g. *Sgk1* and *Sgk3* as ion channel regulators, potentially regulating cell volume), their exact role in this context remains unclear.

Interestingly, an increased cell size beyond the normal range for a specific cell type was found to contribute to cellular senescence in yeast and human fibroblasts (139). Conversely, senescent cells from different organs in mice were found to be larger than non-senescent cells (140). Glomerular endothelial cell senescence has already been shown to lead do

podocyte damage mediated by PAI-1 (88). Furthermore, cell enlargement has been described to induce the senescence-associated secretory phenotype (SASP) (141). Both effects could potentially contribute to the observed impairment of the glomerular filtration barrier (GFB) by altering the GEnC-PC crosstalk. Analysing whether kidney EnCs in LMP7$^{\Delta EnC}$ mice are indeed senescent could therefore offer valuable clues towards (the kidney specific) function of the immunoproteasome in endothelial cells. Assessment of the nuclear envelope, analysing lysosomal alterations via β-galactosidase levels or the SASP are common experimental approaches to determine cellular senescence (reviewed in (142)).

5.1.7 Alterations in the glomerular filtration barrier

In line with the kidney specific cellular alterations, profound alterations of the glomerular filtration barrier (GFB) ultrastructure were observed by electron microscopy. While the glomerular endothelium lost its characteristic fenestrations upon LMP7 loss, the podocytes were also affected and showed substantial foot process effacement (FPE). Considering the drastic alterations in GFB ultrastructure, the lack of albuminuria in LMP7$^{\Delta EnC}$ mice is surprising as damage to any of the GFB layers can lead to proteinuria and especially FPE is considered a hallmark of GFB integrity loss (reviewed in (143)). However, some studies have already questioned the direct link between FPE and proteinuria (144-146). The observations made in this study add to the evidence that FPE does not immediately cause proteinuria and that there must be other renal or glomerular effects causing the leakage of protein into the urine. Physiologically low levels of filtered albumin have already been shown to be reabsorbed in the proximal tubulus (reviewed in (147)). Whether and which other effects are usually responsible for proteinuria in addition to FPE and are not present in LMP7$^{\Delta EnC}$ mice is unclear and requires further studies.

Nevertheless, from the data provided it is clear that the loss of LMP7 in EnCs does not only affect the glomerular endothelium itself, but at the very least also the podocytes. This finding is intriguing and indicates an alteration of the crosstalk between glomerular cell types. The mechanism through which the loss of LMP7 influences this crosstalk remains unclear, but several ways are imaginable:

1. Loss of LMP7 alters pathways in GEnCs which in turn affect glomerular crosstalk.
2. Changes in vesicular trafficking/exocytosis affect the secretion of glomerular crosstalk mediators.
3. Peptides generated by the (immuno)proteasome are directly involved in glomerular crosstalk.

That generally impaired GEnC health alters pathways of glomerular crosstalk is likely, as GEnC senescence has already been shown to also affect podocyte health (88). An impairment of vesicular trafficking could also very well result in changed secretion of mediators between the

glomerular cell types. The potential effects on vesicular trafficking in GEnCs have already been discussed above.

A direct role of proteasome generated peptides in glomerular cell crosstalk is the least described possibility. However, peptides generated by the proteasome have already been shown to exert cellular functions beyond MHC class I peptide loading and amino acid recycling. As such, a membrane bound neuronal proteasome was shown to produce peptides that influence neuronal signalling and are relevant for neuronal plasticity (148-150). However, proof of a membrane bound proteasome in the kidney as a prerequisite for such a direct effect of generated peptides is lacking. The intricate morphology and small size of GEnCs makes such a proof technically challenging. Immunogold electron microscopy (EM) with antibodies directed against proteasomal subunits would allow such experimental proof *in vivo* and would be a valuable next step. A membrane bound (immuno)proteasome in GEnCs, especially on their basolateral side, would be a prime candidate for mediating GEnC-PC crosstalk directly through the generated peptides.

5.1.8 Proteasome catalysed peptide splicing

Another process that might be altered by the loss of immunoproteasomal activity is the presence of spliced peptides produced by the proteasome. It has been described that the proteasome does not only cleave peptide bonds, but that it can also catalyse the formation of new peptide bonds. This can lead to either cis- or trans spliced peptides, linking distant parts of the same or even different proteins, respectively (151). Such peptides could potentially explain some of the alterations discussed above. If proteasome derived peptides directly exert cellular functions, the lack of spliced peptides might be responsible for changes in EnC morphology or glomerular cell crosstalk (discussed in sections 5.1.6 and 5.1.7). A specific modification of proteins as observed for MORF4L2 (section 5.1.5) could also involve peptide splicing. The presentation of spliced peptides to cytotoxic T lymphocytes via MHC class I molecules *in vivo* has been described (152, 153), but was also challenged (reviewed in (154)). However, increasing evidence supports the observation that both cis and trans splicing does occur during protein degradation. Importantly, it has also been described that the generation of specific spliced peptides greatly varies between the proteasomal subtypes (155). Combining these phenomena, it is well imaginable that (immuno)proteasome-derived spliced peptides might also influence cellular pathways in endothelial cells. It is also possible that spliced peptides mediate crosstalk between glomerular cell types as discussed above and are therefore responsible for e.g. the altered GFB structure. However, direct evidence for this is still lacking, requiring further studies.

5.1.9 *PSMB8*-KO EA.hy926

The cellular mechanisms behind some of the observations made in isolated mouse EnCs (e.g. alterations in vesicular trafficking) are difficult to determine *in vivo*. Cell culture endothelial cells potentially provide a complementary experimental system to obtain data that cannot be obtained in mice. Therefore, human *PSMB8* knockout EA.hy926 cells were characterised as an additional experimental tool during this thesis. The robust knockout of LMP7 lead to upregulation of β5c, mirroring the reaction observed in mouse EnCs. However, the upregulation was weaker than in mouse EnCs and differed between the two analysed clones. Importantly, β5c was also incorporated into functional proteasomal complexes and proteasomal activity was not reduced when LMP7 was missing. Additionally, FcRn cell surface and total levels were determined to be altered by flow cytometric and immunoblot analyses, potentially indicating an alteration of vesicular trafficking as already observed in the mouse EnCs. Interestingly, cell surface levels seem to be increased, whereas total cellular levels are decreased, at least in clone #6. Therefore, this endothelial cell culture system mimics important aspects of LMP7 deficiency observed in the LMP7$^{\Delta EnC}$ mice. Analysing vesicular movement by live cell imaging could give more insights into the endocytic alterations that cannot be obtained in murine EnCs. The retransfection with (mutated) *PSMB8* plasmids could also be useful to define which effects rely on LMP7 activity and which effects might rely on its structural integration into the proteasomal complex. Due to the higher amount of sample material compared to isolated primary EnCs, this system also allows for a more comprehensive characterisation of the proteasomal composition in EnCs upon LMP7 deletion. All in all, the established PSMB8-KO cell lines nicely complement the *in vivo* experimental approaches presented during this thesis and, in the future, can help to further unravel the role of LMP7 in EnCs.

5.2 LMP7 in EnCs under disease conditions

Observations made on endothelial cells from naïve mice clearly showed a disturbance of cellular processes by the loss of LMP7. To further characterise the role of endothelial immunoproteasome expression, endothelial LMP7 was analysed under disease conditions. The upregulation of LMP7 in several tissues and cell types in disease has been described before (122, 156) and was further supported by the staining of human kidney biopsies during this project. Building on these findings, the role of LMP7 in two mouse models of kidney disease was analysed: in BTBR *ob/ob* mice as a model of diabetic nephropathy the regulation of LMP7 was assessed and in nephrotoxic nephritis (NTN) as a model of crescentic glomerulonephritis (cGN) the consequences of endothelial LMP7 deficiency were investigated.

5.2.1 LMP7 in BTBR *ob/ob* mice

During this project, BTBR *ob/ob* mice were used as a murine model of type 2 diabetes and especially diabetic nephropathy (DN). As such, mice developed albuminuria already at eight weeks of age, which was exacerbated at 20 weeks, confirming the mild impairment of kidney barrier function expected in this model. Importantly, protein levels of the immunoproteasomal subunit LMP7 were increased in isolated glomeruli of *ob/ob* mice compared to control littermates. However, while an increase in proteasomal activity caused by the increased level of immunoproteasomal subunits could have been expected (34), proteasomal activities were instead slightly reduced. Despite this reduced activity, polyubiquitylated proteins did not strongly accumulate in glomeruli of BTBR *ob/ob* mice. Furthermore, while K48-pUb was slightly accumulated only in 8-week-old BTBR *ob/ob* mice, but not in 20-week-old mice, the opposite trend was observed for K63-pUb. These different pUb accumulations over time indicate a more complex relationship between the proteasomal alterations and protein accumulation in the course of DN progression. Additionally, the proteostatic systems might be differentially affected by the diabetic condition in the different glomerular cell types. Since total isolated glomeruli were analysed, such differences could not be resolved in these experiments. Nevertheless, immunofluorescence microscopy images of both human and murine diabetic kidney tissue highlighted higher levels of LMP7 in EnCs, indicating an endothelial involvement in the progression of DN. While most research is done on the effect of the diabetic condition on podocytes, endothelial cells are also affected and possibly even mediate podocyte damage as highly damaged podocytes are often adjacent to damaged EnCs (91). In summary, these early findings indicated an involvement of the immunoproteasome in DN, and further experiments are required to more comprehensively dissect the proteostatic alterations in this mouse model of DN.

Since a specific modulation of LMP7 expression or function was not feasible in this model, a different kidney disease model was induced in the LMP7$^{\Delta EnC}$ mouse line to directly study the effect of endothelial LMP7 expression on kidney disease.

5.2.2 LMP7$^{\Delta EnC}$ mice and NTN

To this end, a mouse model of immune mediated kidney disease, nephrotoxic nephritis (NTN), was induced in LMP7$^{\Delta EnC}$ mice to assess the immunoproteasomal role under disease conditions. At least four weeks after inducing the LMP7 knockout by tamoxifen injections, NTN was induced by the injection of nephrotoxic antibodies. Indeed, mice showed a different disease course in this model depending on the genotype. LMP7$^{\Delta EnC}$ mice exhibited more severe disease compared to control littermates with increased uACR, exacerbated serum parameters and more crescentic glomeruli. Consistent with this overall worsened disease progression, both glomerular endothelial cells and podocytes were more susceptible to

damage when LMP7 was absent. Therefore, glomerular intercellular crosstalk seemed to be relevant also in NTN as already observed under homeostatic conditions. In summary, loss of endothelial LMP7 was detrimental in this disease model and led to a higher susceptibility to damage, especially in glomerular cells.

While the mechanism linking the lack of LMP7 and an exacerbated disease course in NTN could not be unravelled, some of the cellular alterations observed in naïve LMP7$^{\Delta EnC}$ mice could very well be part of the explanation. NTN is induced by the injection of sheep antibodies recognizing glomerular antigens into mice leading to glomerular damage and a subsequent immune reaction. Once bound, the fate of these antibodies could be different when endocytic pathways in resident kidney cells are altered through a lack of immunoproteasome in kidney EnCs. For example, if endocytosis is slowed, bound antibodies might reside at the cell surface longer than they would in a wildtype animal, potentially inducing a longer or stronger immune response. Considering the accumulation of msIgG on GEnCs in naïve animals, also the disease inducing shIgG might accumulate in LMP7$^{\Delta EnC}$ mice. Additionally, the following adaptive immune response against glomerular cells could also be altered. The extravasation of immune cells from the capillaries into the underlying tissue depends on proteins on the surface of EnCs (157). The changes in cell surface proteins, especially MHC class I and MHC class II on kidney EnCs probably alter the immune response against the EnCs themselves. Antibody turnover and especially the immune response are therefore interesting aspects of this kidney disease model that should be analysed next and, in part, were attempted to be addressed during this thesis.

The lack of reproducibility of the NTN experiments is most likely explained by a genetic drift of the LMP7$^{\Delta ENC}$ mouse line. A single nucleotide polymorphism (SNP) based background analysis revealed low accordance with the C57BL/6 background reference. It had already been described that different mouse strains are differentially susceptible to the NTN model of glomerular nephritis (158). Nevertheless, the initial reaction to the injury was still present as the mice developed high proteinuria on day two after injection of the nephrotoxic serum. The difference in disease progression is therefore most likely due to a difference in the immune reaction following antibody binding to glomerular antigens. Differences in T helper cell response between mouse strains have been extensively described (159, 160). This has also been shown to be the factor relevant for the mouse strain dependent differences in the NTN model (161). Therefore, backcrossing of the LMP7$^{\Delta EnC}$ mouse line onto the BL/6 background will most likely allow further experiments and a thorough analysis of the mechanism(s) behind the role of LMP7 in the NTN model. However, this backcrossing was still ongoing when this thesis was being written.

From these preliminary experiments on the NTN model in LMP7$^{\Delta EnC}$ mice, it can be concluded that the endothelial immunoproteasome does seem to play a protective role in NTN disease progression and that the crosstalk between resident and immune cells is likely to be relevant for this effect.

5.2.3 LMP7 in diseases beyond the kidney

While this project focused on LMP7 in kidney diseases, evidence regarding the immunoproteasome in e.g. different cancer settings has also been published (detailed below). While functional and mechanistic experiments regarding LMP7 are often not the focus of these studies, information regarding its expression still holds valuable clues for its general role in disease.

Whereas increased *Psmb8* expression has been shown to be favourable for the outcome in different tumour settings (162), the opposite has been described for *Psmb5* (163). While not analysed in those studies, the reciprocal relationship between β5i and β5c levels described in this thesis might at least partially explain those results. The higher expression of *Psmb5* (β5c) described to be detrimental possibly correlated with reduced levels of the corresponding LMP7 (β5i) subunit. If the immunoproteasomal impairment also leads to reduced MHC class I levels on tumour cells, this could lead to worse recognition of tumour cells by the immune system and poorer prognosis (reviewed in (164)). Therefore, the regulation of this reciprocal relationship might offer an exploitable pathway of proteasome regulation, a promising topic for further studies.

While IFNγ is usually considered the most potent inducer of (immuno)proteasomal gene expression, IFNα has been shown to induce the expression of antigen-presentation related genes in pancreatic cells (165). The dependence of immunoproteasomal gene expression on cytokines might also be cell-type specific, adding another layer of tissue and cell type specific immunoproteasome regulation. Importantly, this might also be relevant for the cell and disease contexts described in this thesis, namely diabetes and crescentic glomerulonephritis, as different cell types are involved in both contexts. The in-depth understanding of this regulation requires further studies but possibly offers new ways to modulate proteasomal activities in a cell type specific manner.

5.3 Limitations and outlook

This study has offered new insights into tissue specific roles of the immunoproteasomal subunit LMP7 in EnCs. At the same time, there are also certain limitations that must be kept in mind when interpreting its results.

Limitations

One aspect that was only superficially analysed during this thesis is the impact of the LMP7 loss on proteasomal composition. Potentially, both the proteasome subform and subtype distribution could be altered by the observed replacement of LMP7 by β5c. While the reduced levels determined via mass spectrometry indicate reduced total protein levels of 20S proteasomal subunits, this does not necessarily translate to lower levels in assembled proteasomes. Therefore, the presence of both β1i and β2i in assembled proteasomes in EnCs lacking LMP7 are unknown as are the distribution of different regulatory caps associated with the 20S core particle. The exact subtype composition of the proteasomal complexes would be very valuable to analyse, but these analyses are technically challenging in isolated murine EnCs due to the limited sample material. Whether effects observed in these experiments are a direct effect of LMP7 loss, of β1i/β2i loss or of a generally impaired (immuno)proteasomal function, is therefore uncertain and requires further study.

The LMP7$^{\Delta EnC}$ mouse line established during this study was endothelial specific, but a pan-endothelial knockout. As such, effects caused by loss of LMP7 in EnCs in certain tissues cannot be distinguished from one another. Development of organotypic endothelial specific Cre driver mice could help answer these questions, but Cre gene expression specificity at this level is currently hard to achieve. Nevertheless, especially GEnC or PtEnC specific knockout mouse lines would be a valuable research tool in the context of inflammatory kidney diseases. Additionally, since the mouse line employed an inducible Cre system, the LMP7 knockout was only present after tamoxifen injection in adult mice. A potential involvement of the immunoproteasome in vascular development can therefore not be evaluated with the presented data.

Finally, it must be noted that an off-target activity for the Cre driver used in the LMP7$^{\Delta EnC}$ mouse line has been described. Not immediately relevant for the basal characterisation of the LMP7 function in EnCs, it might become relevant when analysing the same under disease conditions. The *Cdh5* dependent expression of Cre recombinase has been shown to occur in CD11b^{+} dendritic cells in mice (166). In all situations with an involvement of dendritic cells, this effect must be carefully considered and excluded to play a role in the analysed effects. Bone marrow transplantation from non-induced animals should be performed to ultimately rule out that an observation is caused by this off-target effect.

Outlook

Numerous questions are still open about the role of the immunoproteasome in (glomerular) endothelial cells. While some are difficult to impossible to address with currently available techniques, others can, in principle, be addressed and are logical next steps in this project.

Considering the basal effects, the initial indications towards altered processing of MORF4L2 by the proteasome in LMP7$^{\Delta EnC}$ mice, are very promising results. Indeed, antibodies both for the detection of both the full-length protein and specifically the N-terminal IDR are available and would allow to support (or refute) the mass spectrometric data. Furthermore, elucidating the changes in endocytic vesicular trafficking via live cell imaging in the established EA.hy926 cell culture model can be done with established techniques.

Albeit requiring more preparation, dissecting which of the effects observed in LMP7$^{\Delta EnC}$ mice depend on LMP7 catalytic activity and which effects would still be observed with a catalytically inactive mutant protein, is also of high interest. While some effects on proteasome assembly have already been shown to only depend on the LMP7 propeptide, but not on catalytic activity, this has not been studied in an *in vivo* setting. A T1A LMP7 mutant was used in these studies, in which the catalytic threonine residues was mutated into an alanine (127). Such a mutant allows to discriminate between effects that are directly caused by the loss of LMP7 activity and potential secondary effects like the lower incorporation of β1i and β2i into proteasomal complexes upon loss of LMP7. Furthermore, it is well imaginable that proteasomal subunits even have functions completely independent from the proteasomal complex. Such a behaviour, called *moonlighting*, has been described for numerous proteins (reviewed in (167)), even some involved in proteostasis. As such, *Atg5* has been shown to target c-myc for proteasomal degradation, entirely independently of its role in the ALP (168). Generating a mouse line with a catalytically inactive mutant of LMP7 would allow such studies. Even more, in this system effects directly dependent on proteasomal incorporation of LMP7 could be discerned from those dependent on incorporation of β1i and β2i, which is not directly possible in an LMP7 knockout setting due to the cooperative incorporation mechanism of immunoproteasomal subunits (40).

Regarding the role of LMP7 in (kidney) disease, also some remaining questions can be answered in the near future. Firstly, more thoroughly analysing the regulation of the (immuno)proteasome in BTBR *ob/ob* mice could give hints towards its role in this complex setting of glomerular damage. Especially analysing cell type specific differences in this regulation would nicely complement the currently growing knowledge about the

immunoproteasome. Secondly, the role of LMP7 in the NTN model of cGN could well be analysed more deeply once the LMP7$^{\Delta EnC}$ mouse line is on a pure BL/6 background. The basic phenotype has been described in this thesis and first hints towards a functional link between immunoproteasomal loss and the exacerbated disease course have already been found. A flow cytometry-based characterisation of the immune cell infiltrations of the kidney during later stages of the disease would allow to analyse the implications of altered EnC immunoproteasomal activity for the immune response.

In the context of immunoproteasome in disease, the role of the antisense gene *PSMB8-AS1* is also intriguing. *PSMB8-AS1* has been described to be regulated in numerous diseases, potentially being a prognostic marker (169, 170). While some pathways responsible for this have been described both with and without the involvement of the proteasome (171), its precise mode of action remains unclear in most studies. It has recently been discovered that long non-coding RNAs (lncRNAs) can accelerate the translocation of their sense counterparts from the nucleus into the cytoplasm, where they are then translated into the corresponding protein (172). *PSMB8-AS1* might therefore ensure rapid translation of the immunoproteasomal subunit LMP7 from its mRNA in situations of stress. Otherwise, the cell's response might not be fast enough to adapt to certain external stressors. Therefore, it might be worthwhile to thoroughly examine the effect of *PSMB8-AS1* on proteasomal composition and function in these different disease settings.

In summary, this study provided new insights into the tissue specific role of the immunoproteasome. It highlighted the functional relevance of endothelial immunoproteasome expression and gained first insights into its exact role. Further studies can be based on these findings and more precisely pinpoint the involvement of endothelial LMP7 in both health and disease.

6 Literature

1. Hipp MS, Kasturi P, and Hartl FU. The proteostasis network and its decline in ageing. *Nat Rev Mol Cell Biol.* 2019;20(7):421-35.
2. Hershko A, and Ciechanover A. The ubiquitin system. *Annu Rev Biochem.* 1998;67:425-79.
3. Bedford L, Lowe J, Dick LR, Mayer RJ, and Brownell JE. Ubiquitin-like protein conjugation and the ubiquitin-proteasome system as drug targets. *Nat Rev Drug Discov.* 2011;10(1):29-46.
4. Benanti JA. Coordination of cell growth and division by the ubiquitin-proteasome system. *Semin Cell Dev Biol.* 2012;23(5):492-8.
5. Abbas R, and Larisch S. Killing by Degradation: Regulation of Apoptosis by the Ubiquitin-Proteasome-System. *Cells.* 2021;10(12).
6. Behrends C, and Harper JW. Constructing and decoding unconventional ubiquitin chains. *Nat Struct Mol Biol.* 2011;18(5):520-8.
7. Dikic I, and Schulman BA. An expanded lexicon for the ubiquitin code. *Nat Rev Mol Cell Biol.* 2023;24(4):273-87.
8. Kirisako T, Kamei K, Murata S, Kato M, Fukumoto H, Kanie M, et al. A ubiquitin ligase complex assembles linear polyubiquitin chains. *Embo j.* 2006;25(20):4877-87.
9. Komander D, and Rape M. The ubiquitin code. *Annu Rev Biochem.* 2012;81:203-29.
10. Lu K, den Brave F, and Jentsch S. Receptor oligomerization guides pathway choice between proteasomal and autophagic degradation. *Nat Cell Biol.* 2017;19(6):732-9.
11. Weeks SD, Grasty KC, Hernandez-Cuebas L, and Loll PJ. Crystal structures of Lys-63-linked tri- and di-ubiquitin reveal a highly extended chain architecture. *Proteins.* 2009;77(4):753-9.
12. Ciechanover A, and Stanhill A. The complexity of recognition of ubiquitinated substrates by the 26S proteasome. *Biochim Biophys Acta.* 2014;1843(1):86-96.
13. Kish-Trier E, and Hill CP. Structural biology of the proteasome. *Annu Rev Biophys.* 2013;42:29-49.
14. Saric T, Graef CI, and Goldberg AL. Pathway for degradation of peptides generated by proteasomes: a key role for thimet oligopeptidase and other metallopeptidases. *J Biol Chem.* 2004;279(45):46723-32.
15. Abi Habib J, De Plaen E, Stroobant V, Zivkovic D, Bousquet MP, Guillaume B, et al. Efficiency of the four proteasome subtypes to degrade ubiquitinated or oxidized proteins. *Sci Rep.* 2020;10(1):15765.
16. Murata S, Sasaki K, Kishimoto T, Niwa S, Hayashi H, Takahama Y, et al. Regulation of CD8+ T cell development by thymus-specific proteasomes. *Science.* 2007;316(5829):1349-53.
17. Zhang ZH, Jiang TX, Chen LB, Zhou W, Liu Y, Gao F, et al. Proteasome subunit α4s is essential for formation of spermatoproteasomes and histone degradation during meiotic DNA repair in spermatocytes. *J Biol Chem.* 2021;296:100130.
18. Xing Y, Jameson SC, and Hogquist KA. Thymoproteasome subunit-β5T generates peptide-MHC complexes specialized for positive selection. *Proc Natl Acad Sci U S A.* 2013;110(17):6979-84.
19. Uechi H, Hamazaki J, and Murata S. Characterization of the testis-specific proteasome subunit α4s in mammals. *J Biol Chem.* 2014;289(18):12365-74.
20. Sachs W, Blume L, Loreth D, Schebsdat L, Hatje F, Koehler S, et al. The proteasome modulates endocytosis specifically in glomerular cells to promote kidney filtration. *Nat Commun.* 2024;15(1):1897.
21. de la Visitación N, Chen W, Krishnan J, Van Beusecum JP, Amarnath V, Hennen EM, et al. Immunoproteasomal Processing of IsoLG-Adducted Proteins Is Essential for Hypertension. *Circ Res.* 2024;134(10):1276-91.

22. Krausgruber T, Fortelny N, Fife-Gernedl V, Senekowitsch M, Schuster LC, Lercher A, et al. Structural cells are key regulators of organ-specific immune responses. *Nature.* 2020;583(7815):296-302.
23. Gan J, Leestemaker Y, Sapmaz A, and Ovaa H. Highlighting the Proteasome: Using Fluorescence to Visualize Proteasome Activity and Distribution. *Front Mol Biosci.* 2019;6:14.
24. Kravtsova-Ivantsiv Y, Shomer I, Cohen-Kaplan V, Snijder B, Superti-Furga G, Gonen H, et al. KPC1-mediated ubiquitination and proteasomal processing of NF-κB1 p105 to p50 restricts tumor growth. *Cell.* 2015;161(2):333-47.
25. Solomon H, Bräuning B, Fainer I, Ben-Nissan G, Rabani S, Goldfinger N, et al. Post-translational regulation of p53 function through 20S proteasome-mediated cleavage. *Cell Death Differ.* 2017;24(12):2187-98.
26. Schubert U, Antón LC, Gibbs J, Norbury CC, Yewdell JW, and Bennink JR. Rapid degradation of a large fraction of newly synthesized proteins by proteasomes. *Nature.* 2000;404(6779):770-4.
27. Momburg F, Roelse J, Hämmerling GJ, and Neefjes JJ. Peptide size selection by the major histocompatibility complex-encoded peptide transporter. *J Exp Med.* 1994;179(5):1613-23.
28. Fehling HJ, Swat W, Laplace C, Kühn R, Rajewsky K, Müller U, et al. MHC class I expression in mice lacking the proteasome subunit LMP-7. *Science.* 1994;265(5176):1234-7.
29. Momburg F, Ortiz-Navarrete V, Neefjes J, Goulmy E, van de Wal Y, Spits H, et al. Proteasome subunits encoded by the major histocompatibility complex are not essential for antigen presentation. *Nature.* 1992;360(6400):174-7.
30. Aki M, Shimbara N, Takashina M, Akiyama K, Kagawa S, Tamura T, et al. Interferon-gamma induces different subunit organizations and functional diversity of proteasomes. *J Biochem.* 1994;115(2):257-69.
31. Shin EC, Seifert U, Kato T, Rice CM, Feinstone SM, Kloetzel PM, et al. Virus-induced type I IFN stimulates generation of immunoproteasomes at the site of infection. *J Clin Invest.* 2006;116(11):3006-14.
32. Hallermalm K, Seki K, Wei C, Castelli C, Rivoltini L, Kiessling R, et al. Tumor necrosis factor-alpha induces coordinated changes in major histocompatibility class I presentation pathway, resulting in increased stability of class I complexes at the cell surface. *Blood.* 2001;98(4):1108-15.
33. Murata S, Takahama Y, Kasahara M, and Tanaka K. The immunoproteasome and thymoproteasome: functions, evolution and human disease. *Nature Immunology.* 2018;19(9):923-31.
34. Huber EM, Basler M, Schwab R, Heinemeyer W, Kirk CJ, Groettrup M, et al. Immuno- and constitutive proteasome crystal structures reveal differences in substrate and inhibitor specificity. *Cell.* 2012;148(4):727-38.
35. Seifert U, Bialy LP, Ebstein F, Bech-Otschir D, Voigt A, Schröter F, et al. Immunoproteasomes preserve protein homeostasis upon interferon-induced oxidative stress. *Cell.* 2010;142(4):613-24.
36. Nathan JA, Spinnenhirn V, Schmidtke G, Basler M, Groettrup M, and Goldberg AL. Immuno- and constitutive proteasomes do not differ in their abilities to degrade ubiquitinated proteins. *Cell.* 2013;152(5):1184-94.
37. Winter MB, La Greca F, Arastu-Kapur S, Caiazza F, Cimermancic P, Buchholz TJ, et al. Immunoproteasome functions explained by divergence in cleavage specificity and regulation. *Elife.* 2017;6.
38. Mishto M, Liepe J, Textoris-Taube K, Keller C, Henklein P, Weberruß M, et al. Proteasome isoforms exhibit only quantitative differences in cleavage and epitope generation. *Eur J Immunol.* 2014;44(12):3508-21.
39. Kaur G, and Batra S. Emerging role of immunoproteasomes in pathophysiology. *Immunol Cell Biol.* 2016;94(9):812-20.

40. Griffin TA, Nandi D, Cruz M, Fehling HJ, Kaer LV, Monaco JJ, et al. Immunoproteasome assembly: cooperative incorporation of interferon gamma (IFN-gamma)-inducible subunits. *J Exp Med.* 1998;187(1):97-104.
41. Klare N, Seeger M, Janek K, Jungblut PR, and Dahlmann B. Intermediate-type 20 S proteasomes in HeLa cells: "asymmetric" subunit composition, diversity and adaptation. *J Mol Biol.* 2007;373(1):1-10.
42. Kingsbury DJ, Griffin TA, and Colbert RA. Novel propeptide function in 20 S proteasome assembly influences beta subunit composition. *J Biol Chem.* 2000;275(31):24156-62.
43. Joeris T, Schmidt N, Ermert D, Krienke P, Visekruna A, Kuckelkorn U, et al. The proteasome system in infection: impact of β5 and LMP7 on composition, maturation and quantity of active proteasome complexes. *PLoS One.* 2012;7(6):e39827.
44. De M, Jayarapu K, Elenich L, Monaco JJ, Colbert RA, and Griffin TA. Beta 2 subunit propeptides influence cooperative proteasome assembly. *J Biol Chem.* 2003;278(8):6153-9.
45. Gohlke S, Kloss A, Tsokos M, Textoris-Taube K, Keller C, Kloetzel PM, et al. Adult human liver contains intermediate-type proteasomes with different enzymatic properties. *Ann Hepatol.* 2014;13(4):429-38.
46. Guillaume B, Chapiro J, Stroobant V, Colau D, Van Holle B, Parvizi G, et al. Two abundant proteasome subtypes that uniquely process some antigens presented by HLA class I molecules. *Proc Natl Acad Sci U S A.* 2010;107(43):18599-604.
47. de Bruin G, Xin BT, Florea BI, and Overkleeft HS. Proteasome Subunit Selective Activity-Based Probes Report on Proteasome Core Particle Composition in a Native Polyacrylamide Gel Electrophoresis Fluorescence-Resonance Energy Transfer Assay. *J Am Chem Soc.* 2016;138(31):9874-80.
48. Allmeroth K, Horn M, Kroef V, Miethe S, Müller RU, and Denzel MS. Bortezomib resistance mutations in PSMB5 determine response to second-generation proteasome inhibitors in multiple myeloma. *Leukemia.* 2021;35(3):887-92.
49. Jenkins TW, Downey-Kopyscinski SL, Fields JL, Rahme GJ, Colley WC, Israel MA, et al. Activity of immunoproteasome inhibitor ONX-0914 in acute lymphoblastic leukemia expressing MLL-AF4 fusion protein. *Sci Rep.* 2021;11(1):10883.
50. Muchamuel T, Basler M, Aujay MA, Suzuki E, Kalim KW, Lauer C, et al. A selective inhibitor of the immunoproteasome subunit LMP7 blocks cytokine production and attenuates progression of experimental arthritis. *Nat Med.* 2009;15(7):781-7.
51. Türker F, Bharadwaj RA, Kleinman JE, Weinberger DR, Hyde TM, White CJ, et al. Orthogonal approaches required to measure proteasome composition and activity in mammalian brain tissue. *J Biol Chem.* 2023;299(6):104811.
52. Thomas T, Salcedo-Tacuma D, and Smith DM. Structure, Function, and Allosteric Regulation of the 20S Proteasome by the 11S/PA28 Family of Proteasome Activators. *Biomolecules.* 2023;13(9).
53. Fabre B, Lambour T, Garrigues L, Ducoux-Petit M, Amalric F, Monsarrat B, et al. Label-free quantitative proteomics reveals the dynamics of proteasome complexes composition and stoichiometry in a wide range of human cell lines. *J Proteome Res.* 2014;13(6):3027-37.
54. Baugh JM, Viktorova EG, and Pilipenko EV. Proteasomes can degrade a significant proportion of cellular proteins independent of ubiquitination. *J Mol Biol.* 2009;386(3):814-27.
55. Jariel-Encontre I, Bossis G, and Piechaczyk M. Ubiquitin-independent degradation of proteins by the proteasome. *Biochim Biophys Acta.* 2008;1786(2):153-77.
56. Reinheckel T, Sitte N, Ullrich O, Kuckelkorn U, Davies KJ, and Grune T. Comparative resistance of the 20S and 26S proteasome to oxidative stress. *Biochem J.* 1998;335 (Pt 3)(Pt 3):637-42.
57. Pepelnjak M, Rogawski R, Arkind G, Leushkin Y, Fainer I, Ben-Nissan G, et al. Systematic identification of 20S proteasome substrates. *Mol Syst Biol.* 2024;20(4):403-27.

58. Glickman MH, Rubin DM, Coux O, Wefes I, Pfeifer G, Cjeka Z, et al. A subcomplex of the proteasome regulatory particle required for ubiquitin-conjugate degradation and related to the COP9-signalosome and eIF3. *Cell.* 1998;94(5):615-23.
59. Martinez-Fonts K, Davis C, Tomita T, Elsasser S, Nager AR, Shi Y, et al. The proteasome 19S cap and its ubiquitin receptors provide a versatile recognition platform for substrates. *Nat Commun.* 2020;11(1):477.
60. Collins GA, and Goldberg AL. The Logic of the 26S Proteasome. *Cell.* 2017;169(5):792-806.
61. Huber EM, and Groll M. The Mammalian Proteasome Activator PA28 Forms an Asymmetric α(4)β(3) Complex. *Structure.* 2017;25(10):1473-80.e3.
62. Zhao J, Makhija S, Zhou C, Zhang H, Wang Y, Muralidharan M, et al. Structural insights into the human PA28-20S proteasome enabled by efficient tagging and purification of endogenous proteins. *Proc Natl Acad Sci U S A.* 2022;119(33):e2207200119.
63. Realini C, Dubiel W, Pratt G, Ferrell K, and Rechsteiner M. Molecular cloning and expression of a gamma-interferon-inducible activator of the multicatalytic protease. *J Biol Chem.* 1994;269(32):20727-32.
64. Raule M, Cerruti F, Benaroudj N, Migotti R, Kikuchi J, Bachi A, et al. PA28αβ reduces size and increases hydrophilicity of 20S immunoproteasome peptide products. *Chem Biol.* 2014;21(4):470-80.
65. Soza A, Knuehl C, Groettrup M, Henklein P, Tanaka K, and Kloetzel PM. Expression and subcellular localization of mouse 20S proteasome activator complex PA28. *FEBS Lett.* 1997;413(1):27-34.
66. Thomas TA, and Smith DM. Proteasome activator 28γ (PA28γ) allosterically activates trypsin-like proteolysis by binding to the α-ring of the 20S proteasome. *J Biol Chem.* 2022;298(8):102140.
67. Xu P, Duong DM, Seyfried NT, Cheng D, Xie Y, Robert J, et al. Quantitative proteomics reveals the function of unconventional ubiquitin chains in proteasomal degradation. *Cell.* 2009;137(1):133-45.
68. Saeki Y, Kudo T, Sone T, Kikuchi Y, Yokosawa H, Toh-e A, et al. Lysine 63-linked polyubiquitin chain may serve as a targeting signal for the 26S proteasome. *Embo j.* 2009;28(4):359-71.
69. Sachs W, Sachs M, Krüger E, Zielinski S, Kretz O, Huber TB, et al. Distinct Modes of Balancing Glomerular Cell Proteostasis in Mucolipidosis Type II and III Prevent Proteinuria. *J Am Soc Nephrol.* 2020;31(8):1796-814.
70. Choi WH, Yun Y, Park S, Jeon JH, Lee J, Lee JH, et al. Aggresomal sequestration and STUB1-mediated ubiquitylation during mammalian proteaphagy of inhibited proteasomes. *Proc Natl Acad Sci U S A.* 2020;117(32):19190-200.
71. Zhou J, Li C, Lu M, Jiang G, Chen S, Li H, et al. Pharmacological induction of autophagy reduces inflammation in macrophages by degrading immunoproteasome subunits. *PLoS Biol.* 2024;22(3):e3002537.
72. Babu JR, Geetha T, and Wooten MW. Sequestosome 1/p62 shuttles polyubiquitinated tau for proteasomal degradation. *J Neurochem.* 2005;94(1):192-203.
73. Liu WJ, Ye L, Huang WF, Guo LJ, Xu ZG, Wu HL, et al. p62 links the autophagy pathway and the ubiqutin-proteasome system upon ubiquitinated protein degradation. *Cell Mol Biol Lett.* 2016;21:29.
74. Myeku N, and Figueiredo-Pereira ME. Dynamics of the degradation of ubiquitinated proteins by proteasomes and autophagy: association with sequestosome 1/p62. *J Biol Chem.* 2011;286(25):22426-40.
75. Rocha SF, and Adams RH. Molecular differentiation and specialization of vascular beds. *Angiogenesis.* 2009;12(2):139-47.
76. Cleuren ACA, van der Ent MA, Jiang H, Hunker KL, Yee A, Siemieniak DR, et al. The in vivo endothelial cell translatome is highly heterogeneous across vascular beds. *Proc Natl Acad Sci U S A.* 2019;116(47):23618-24.
77. Jambusaria A, Hong Z, Zhang L, Srivastava S, Jana A, Toth PT, et al. Endothelial heterogeneity across distinct vascular beds during homeostasis and inflammation. *Elife.* 2020;9.

78. Amersfoort J, Eelen G, and Carmeliet P. Immunomodulation by endothelial cells - partnering up with the immune system? *Nat Rev Immunol.* 2022;22(9):576-88.
79. Finch NC, Neal CR, Welsh GI, Foster RR, and Satchell SC. The unique structural and functional characteristics of glomerular endothelial cell fenestrations and their potential as a therapeutic target in kidney disease. *Am J Physiol Renal Physiol.* 2023;325(4):F465-f78.
80. Alan S.L. Yu GMC, Valérie A. Luyckx, Philip A. Marsden, Karl Skorecki, Maarten W. Taal. *Brenner and Rector's The Kidney.* Philadelphia: Elsevier; 2020.
81. Birtasu AN, Wieland K, Ermel UH, Rahm JV, Scheffer MP, Flottmann B, et al. The molecular architecture of the kidney slit diaphragm. *bioRxiv.* 2023:2023.10.27.564405.
82. Lennon R, Randles MJ, and Humphries MJ. The importance of podocyte adhesion for a healthy glomerulus. *Front Endocrinol (Lausanne).* 2014;5:160.
83. Naylor RW, Morais M, and Lennon R. Complexities of the glomerular basement membrane. *Nat Rev Nephrol.* 2021;17(2):112-27.
84. Avraham S, Korin B, Chung JJ, Oxburgh L, and Shaw AS. The Mesangial cell - the glomerular stromal cell. *Nat Rev Nephrol.* 2021;17(12):855-64.
85. Ebefors K, Bergwall L, and Nyström J. The Glomerulus According to the Mesangium. *Front Med (Lausanne).* 2021;8:740527.
86. Lennon R, and Hosawi S. Glomerular cell crosstalk. *Curr Opin Nephrol Hypertens.* 2016;25(3):187-93.
87. Eremina V, Sood M, Haigh J, Nagy A, Lajoie G, Ferrara N, et al. Glomerular-specific alterations of VEGF-A expression lead to distinct congenital and acquired renal diseases. *J Clin Invest.* 2003;111(5):707-16.
88. Cohen C, Le Goff O, Soysouvanh F, Vasseur F, Tanou M, Nguyen C, et al. Glomerular endothelial cell senescence drives age-related kidney disease through PAI-1. *EMBO Mol Med.* 2021;13(11):e14146.
89. Bowen EE, Hurcombe JA, Barrington F, Keir LS, Farmer LK, Wherlock MD, et al. Shiga toxin targets the podocyte causing hemolytic uremic syndrome through endothelial complement activation. *Med.* 2023;4(11):761-77.e8.
90. Kovesdy CP. Epidemiology of chronic kidney disease: an update 2022. *Kidney Int Suppl (2011).* 2022;12(1):7-11.
91. Kriz W, Löwen J, and Gröne HJ. The complex pathology of diabetic nephropathy in humans. *Nephrol Dial Transplant.* 2023;38(10):2109-19.
92. Global, regional, and national burden of diabetes from 1990 to 2021, with projections of prevalence to 2050: a systematic analysis for the Global Burden of Disease Study 2021. *Lancet.* 2023;402(10397):203-34.
93. Sethi S, De Vriese AS, and Fervenza FC. Acute glomerulonephritis. *Lancet.* 2022;399(10335):1646-63.
94. Mueller A, Zhao Y, Cicek H, Paust HJ, Sivayoganathan A, Linke A, et al. Transcriptional and Clonal Characterization of Cytotoxic T Cells in Crescentic Glomerulonephritis. *J Am Soc Nephrol.* 2023;34(6):1003-18.
95. Pober JS, Merola J, Liu R, and Manes TD. Antigen Presentation by Vascular Cells. *Front Immunol.* 2017;8:1907.
96. Hudkins KL, Pichaiwong W, Wietecha T, Kowalewska J, Banas MC, Spencer MW, et al. BTBR Ob/Ob mutant mice model progressive diabetic nephropathy. *J Am Soc Nephrol.* 2010;21(9):1533-42.
97. Frederich RC, Hamann A, Anderson S, Löllmann B, Lowell BB, and Flier JS. Leptin levels reflect body lipid content in mice: evidence for diet-induced resistance to leptin action. *Nat Med.* 1995;1(12):1311-4.
98. Azushima K, Gurley SB, and Coffman TM. Modelling diabetic nephropathy in mice. *Nat Rev Nephrol.* 2018;14(1):48-56.
99. Saad R, Tadmor H, Ertracht O, Nakhoul N, Nakhoul F, Evgeny F, et al. The Molecular Effects of SGLT2i Empagliflozin on the Autophagy Pathway in Diabetes Mellitus Type 2 and Its Complications. *J Diabetes Res.* 2022;2022:8337823.

100. Quigg RJ, He C, Lim A, Berthiaume D, Alexander JJ, Kraus D, et al. Transgenic mice overexpressing the complement inhibitor crry as a soluble protein are protected from antibody-induced glomerular injury. *J Exp Med.* 1998;188(7):1321-31.
101. Odobasic D, Ghali JR, O'Sullivan KM, Holdsworth SR, and Kitching AR. Glomerulonephritis Induced by Heterologous Anti-GBM Globulin as a Planted Foreign Antigen. *Curr Protoc Immunol.* 2014;106:15.26.1-15.26.0.
102. Kaneko Y, Nimmerjahn F, Madaio MP, and Ravetch JV. Pathology and protection in nephrotoxic nephritis is determined by selective engagement of specific Fc receptors. *J Exp Med.* 2006;203(3):789-97.
103. Schmidt T, Luebbe J, Kilian C, Riedel JH, Hiekmann S, Asada N, et al. IL-17 Receptor C Signaling Controls CD4(+) T(H)17 Immune Responses and Tissue Injury in Immune-Mediated Kidney Diseases. *J Am Soc Nephrol.* 2021;32(12):3081-98.
104. Sörensen I, Adams RH, and Gossler A. DLL1-mediated Notch activation regulates endothelial identity in mouse fetal arteries. *Blood.* 2009;113(22):5680-8.
105. Wang Y, Nakayama M, Pitulescu ME, Schmidt TS, Bochenek ML, Sakakibara A, et al. Ephrin-B2 controls VEGF-induced angiogenesis and lymphangiogenesis. *Nature.* 2010;465(7297):483-6.
106. Nancy L. Wayne SD-V, Stacey Kraemer, Joseph D. Rager. Exposure assessment of laboratory workers to hazardous waste from mice treated with tamoxifen and bromodeoxyuridine. *Journal of Chemical Health and Safety.* 2019;26(1):2-8.
107. Krebs CF, Reimers D, Zhao Y, Paust HJ, Bartsch P, Nuñez S, et al. Pathogen-induced tissue-resident memory T(H)17 (T(RM)17) cells amplify autoimmune kidney disease. *Sci Immunol.* 2020;5(50).
108. Hatje FA, Wedekind U, Sachs W, Loreth D, Reichelt J, Demir F, et al. Tripartite Separation of Glomerular Cell Types and Proteomes from Reporter-Free Mice. *J Am Soc Nephrol.* 2021;32(9):2175-93.
109. Hewings DS, Flygare JA, Wertz IE, and Bogyo M. Activity-based probes for the multicatalytic proteasome. *Febs j.* 2017;284(10):1540-54.
110. Shen YF, Liu MJ, Long Z, Shi X, and Liu ML. A simple, flexible, and high-efficiency western blot analysis for age-related human induced neurons. *Biotechnol J.* 2023;18(10):e2300089.
111. Feng Z, Jensen SM, Messenheimer DJ, Farhad M, Neuberger M, Bifulco CB, et al. Multispectral Imaging of T and B Cells in Murine Spleen and Tumor. *J Immunol.* 2016;196(9):3943-50.
112. Hughes CS, Moggridge S, Müller T, Sorensen PH, Morin GB, and Krijgsveld J. Single-pot, solid-phase-enhanced sample preparation for proteomics experiments. *Nat Protoc.* 2019;14(1):68-85.
113. Demichev V, Messner CB, Vernardis SI, Lilley KS, and Ralser M. DIA-NN: neural networks and interference correction enable deep proteome coverage in high throughput. *Nat Methods.* 2020;17(1):41-4.
114. Tyanova S, Temu T, Sinitcyn P, Carlson A, Hein MY, Geiger T, et al. The Perseus computational platform for comprehensive analysis of (prote)omics data. *Nat Methods.* 2016;13(9):731-40.
115. Schmidt C, Berger T, Groettrup M, and Basler M. Immunoproteasome Inhibition Impairs T and B Cell Activation by Restraining ERK Signaling and Proteostasis. *Front Immunol.* 2018;9:2386.
116. Moebius J, van den Broek M, Groettrup M, and Basler M. Immunoproteasomes are essential for survival and expansion of T cells in virus-infected mice. *Eur J Immunol.* 2010;40(12):3439-49.
117. . Kidney Precision Medicine Project. https://www.kpmp.org. Accessed 04.12.2023.
118. He B, Chen P, Zambrano S, Dabaghie D, Hu Y, Möller-Hackbarth K, et al. Single-cell RNA sequencing reveals the mesangial identity and species diversity of glomerular cell transcriptomes. *Nat Commun.* 2021;12(1):2141.
119. Inholz K, Anderl JL, Klawitter M, Goebel H, Maurits E, Kirk CJ, et al. Proteasome composition in immune cells implies special immune-cell-specific immunoproteasome function. *Eur J Immunol.* 2024;54(4):e2350613.

120. Crozier L, Foy R, Adib R, Kar A, Holt JA, Pareri AU, et al. CDK4/6 inhibitor-mediated cell overgrowth triggers osmotic and replication stress to promote senescence. *Mol Cell.* 2023;83(22):4062-77.e5.
121. Devoucoux M, Roques C, Lachance C, Lashgari A, Joly-Beauparlant C, Jacquet K, et al. MRG Proteins Are Shared by Multiple Protein Complexes With Distinct Functions. *Mol Cell Proteomics.* 2022;21(7):100253.
122. Beeken M, Lindenmeyer MT, Blattner SM, Radón V, Oh J, Meyer TN, et al. Alterations in the ubiquitin proteasome system in persistent but not reversible proteinuric diseases. *J Am Soc Nephrol.* 2014;25(11):2511-25.
123. Hudkins KL, Li X, Holland AL, Swaminathan S, and Alpers CE. Regression of diabetic nephropathy by treatment with empagliflozin in BTBR ob/ob mice. *Nephrol Dial Transplant.* 2021.
124. Papendorf JJ, Ebstein F, Alehashemi S, Piotto DGP, Kozlova A, Terreri MT, et al. Identification of eight novel proteasome variants in five unrelated cases of proteasome-associated autoinflammatory syndromes (PRAAS). *Front Immunol.* 2023;14:1190104.
125. Kincaid EZ, Che JW, York I, Escobar H, Reyes-Vargas E, Delgado JC, et al. Mice completely lacking immunoproteasomes show major changes in antigen presentation. *Nat Immunol.* 2011;13(2):129-35.
126. Rana PS, Ignatz-Hoover JJ, Guo C, Mosley AL, Malek E, Federov Y, et al. Immunoproteasome Activation Expands the MHC Class I Immunopeptidome, Unmasks Neoantigens, and Enhances T-cell Anti-Myeloma Activity. *Mol Cancer Ther.* 2024;23(12):1743-60.
127. Toes RE, Nussbaum AK, Degermann S, Schirle M, Emmerich NP, Kraft M, et al. Discrete cleavage motifs of constitutive and immunoproteasomes revealed by quantitative analysis of cleavage products. *J Exp Med.* 2001;194(1):1-12.
128. Uchihara Y, Permata TBM, Sato H, Kawabata-Iwakawa R, Katada S, Gu W, et al. DNA damage promotes HLA class I presentation by stimulating a pioneer round of translation-associated antigen production. *Mol Cell.* 2022;82(14):2557-70.e7.
129. Grandea AG, 3rd, Golovina TN, Hamilton SE, Sriram V, Spies T, Brutkiewicz RR, et al. Impaired assembly yet normal trafficking of MHC class I molecules in Tapasin mutant mice. *Immunity.* 2000;13(2):213-22.
130. Bloodworth N, Chen W, Hunter K, Patrick D, Palubinsky A, Phillips E, et al. Posttranslationally modified self-peptides promote hypertension in mouse models. *J Clin Invest.* 2024;134(16).
131. Pang KC, Sanders MT, Monaco JJ, Doherty PC, Turner SJ, and Chen W. Immunoproteasome subunit deficiencies impact differentially on two immunodominant influenza virus-specific CD8+ T cell responses. *J Immunol.* 2006;177(11):7680-8.
132. Tewari MK, Sinnathamby G, Rajagopal D, and Eisenlohr LC. A cytosolic pathway for MHC class II-restricted antigen processing that is proteasome and TAP dependent. *Nat Immunol.* 2005;6(3):287-94.
133. Ichimura K, Stan RV, Kurihara H, and Sakai T. Glomerular endothelial cells form diaphragms during development and pathologic conditions. *J Am Soc Nephrol.* 2008;19(8):1463-71.
134. Auvinen K, Lokka E, Mokkala E, Jäppinen N, Tyystjärvi S, Saine H, et al. Fenestral diaphragms and PLVAP associations in liver sinusoidal endothelial cells are developmentally regulated. *Sci Rep.* 2019;9(1):15698.
135. Pyzik M, Kozicky LK, Gandhi AK, and Blumberg RS. The therapeutic age of the neonatal Fc receptor. *Nat Rev Immunol.* 2023;23(7):415-32.
136. Yu A, and Malek TR. The proteasome regulates receptor-mediated endocytosis of interleukin-2. *J Biol Chem.* 2001;276(1):381-5.
137. Basler M, Youhnovski N, Van Den Broek M, Przybylski M, and Groettrup M. Immunoproteasomes down-regulate presentation of a subdominant T cell epitope from lymphocytic choriomeningitis virus. *J Immunol.* 2004;173(6):3925-34.
138. Ito Y, Kondo E, Demachi-Okamura A, Akatsuka Y, Tsujimura K, Tanimoto M, et al. Three immunoproteasome-associated subunits cooperatively generate a cytotoxic T-

lymphocyte epitope of Epstein-Barr virus LMP2A by overcoming specific structures resistant to epitope liberation. *J Virol.* 2006;80(2):883-90.
139. Neurohr GE, Terry RL, Lengefeld J, Bonney M, Brittingham GP, Moretto F, et al. Excessive Cell Growth Causes Cytoplasm Dilution And Contributes to Senescence. *Cell.* 2019;176(5):1083-97.e18.
140. Biran A, Zada L, Abou Karam P, Vadai E, Roitman L, Ovadya Y, et al. Quantitative identification of senescent cells in aging and disease. *Aging Cell.* 2017;16(4):661-71.
141. Joung J, Heo Y, Kim Y, Kim J, Choi H, Jeon T, et al. Cell enlargement modulated by GATA4 and YAP instructs the senescence-associated secretory phenotype. *Nat Commun.* 2025;16(1):1696.
142. Ogrodnik M, Carlos Acosta J, Adams PD, d'Adda di Fagagna F, Baker DJ, Bishop CL, et al. Guidelines for minimal information on cellular senescence experimentation in vivo. *Cell.* 2024;187(16):4150-75.
143. Benzing T, and Salant D. Insights into Glomerular Filtration and Albuminuria. *N Engl J Med.* 2021;384(15):1437-46.
144. van den Berg JG, van den Bergh Weerman MA, Assmann KJ, Weening JJ, and Florquin S. Podocyte foot process effacement is not correlated with the level of proteinuria in human glomerulopathies. *Kidney Int.* 2004;66(5):1901-6.
145. Basgen JM, Wong JS, Ray J, Nicholas SB, and Campbell KN. Podocyte Foot Process Effacement Precedes Albuminuria and Glomerular Hypertrophy in CD2-Associated Protein Deficient Mice. *Front Med (Lausanne).* 2021;8:745319.
146. Dijkman HB, Gerlofs-Nijland ME, van der Laak JA, Wetzels JF, Groenen PJ, and Assmann KJ. Podocyte changes after induction of acute albuminuria in mice by anti-aminopeptidase A mAb. *Nephron Exp Nephrol.* 2003;94(3):e85-93.
147. Birn H, Nielsen R, and Weyer K. Tubular albumin uptake: is there evidence for a quantitatively important, receptor-independent mechanism? *Kidney Int.* 2023;104(6):1069-73.
148. He HY, Ahsan A, Bera R, McLain N, Faulkner R, Ramachandran KV, et al. Neuronal membrane proteasomes regulate neuronal circuit activity in vivo and are required for learning-induced behavioral plasticity. *Proc Natl Acad Sci U S A.* 2023;120(3):e2216537120.
149. Türker F, Brennan A, and Margolis SS. Neuronal membrane proteasome-derived peptides modulate NMDAR-dependent neuronal signaling to promote changes in gene expression. *Mol Biol Cell.* 2024;35(1):ar6.
150. Ramachandran KV, and Margolis SS. A mammalian nervous-system-specific plasma membrane proteasome complex that modulates neuronal function. *Nat Struct Mol Biol.* 2017;24(4):419-30.
151. Soh WT, Roetschke HP, Cormican JA, Teo BF, Chiam NC, Raabe M, et al. Protein degradation by human 20S proteasomes elucidates the interplay between peptide hydrolysis and splicing. *Nat Commun.* 2024;15(1):1147.
152. Dalet A, Vigneron N, Stroobant V, Hanada K, and Van den Eynde BJ. Splicing of distant peptide fragments occurs in the proteasome by transpeptidation and produces the spliced antigenic peptide derived from fibroblast growth factor-5. *J Immunol.* 2010;184(6):3016-24.
153. Mishto M, and Liepe J. Post-Translational Peptide Splicing and T Cell Responses. *Trends Immunol.* 2017;38(12):904-15.
154. Admon A. Are There Indeed Spliced Peptides in the Immunopeptidome? *Mol Cell Proteomics.* 2021;20:100099.
155. Ferrari V, Stroobant V, Abi Habib J, Naulaerts S, Van den Eynde BJ, and Vigneron N. New Insights into the Mechanisms of Proteasome-Mediated Peptide Splicing Learned from Comparing Splicing Efficiency by Different Proteasome Subtypes. *J Immunol.* 2022;208(12):2817-28.
156. Ugras S, Daniels MJ, Fazelinia H, Gould NS, Yocum AK, Luk KC, et al. Induction of the Immunoproteasome Subunit Lmp7 Links Proteostasis and Immunity in α-Synuclein Aggregation Disorders. *EBioMedicine.* 2018;31:307-19.

157. Engelhardt B, and Wolburg H. Mini-review: Transendothelial migration of leukocytes: through the front door or around the side of the house? *Eur J Immunol.* 2004;34(11):2955-63.
158. Nagai H, Yamada H, Nishigaki T, Nakazawa M, and Koda A. The susceptibility of experimental glomerulonephritis in six different strains of mice. *J Pharmacobiodyn.* 1985;8(7):586-9.
159. Heinzel FP, Sadick MD, Holaday BJ, Coffman RL, and Locksley RM. Reciprocal expression of interferon gamma or interleukin 4 during the resolution or progression of murine leishmaniasis. Evidence for expansion of distinct helper T cell subsets. *J Exp Med.* 1989;169(1):59-72.
160. Stewart D, Fulton WB, Wilson C, Monitto CL, Paidas CN, Reeves RH, et al. Genetic contribution to the septic response in a mouse model. *Shock.* 2002;18(4):342-7.
161. Holdsworth SR, Kitching AR, and Tipping PG. Th1 and Th2 T helper cell subsets affect patterns of injury and outcomes in glomerulonephritis. *Kidney Int.* 1999;55(4):1198-216.
162. Geoffroy K, Araripe Saraiva B, Viens M, Béland D, and Bourgeois-Daigneault MC. Increased expression of the immunoproteasome subunits PSMB8 and PSMB9 by cancer cells correlate with better outcomes for triple-negative breast cancers. *Sci Rep.* 2023;13(1):2129.
163. Liu J, Mi J, Liu S, Chen H, and Jiang L. PSMB5 overexpression is correlated with tumor proliferation and poor prognosis in hepatocellular carcinoma. *FEBS Open Bio.* 2022;12(11):2025-41.
164. Dhatchinamoorthy K, Colbert JD, and Rock KL. Cancer Immune Evasion Through Loss of MHC Class I Antigen Presentation. *Front Immunol.* 2021;12:636568.
165. Jiang H, Li Y, Shen M, Liang Y, Qian Y, Dai H, et al. Interferon-α promotes MHC I antigen presentation of islet β cells through STAT1-IRF7 pathway in type 1 diabetes. *Immunology.* 2022;166(2):210-21.
166. He Q, Li X, Singh K, Luo Z, Meija-Cordova M, Jamalpour M, et al. The Cdh5-CreERT2 transgene causes conditional Shb gene deletion in hematopoietic cells with consequences for immune cell responses to tumors. *Sci Rep.* 2019;9(1):7548.
167. Jeffery CJ. Protein moonlighting: what is it, and why is it important? *Philos Trans R Soc Lond B Biol Sci.* 2018;373(1738).
168. Li S, Zhang L, Zhang G, Shangguan G, Hou X, Duan W, et al. A nonautophagic role of ATG5 in regulating cell growth by targeting c-Myc for proteasome-mediated degradation. *iScience.* 2021;24(11):103296.
169. Feng J, Yu Y, Yin W, and Qian S. Development and verification of a 7-lncRNA prognostic model based on tumor immunity for patients with ovarian cancer. *J Ovarian Res.* 2023;16(1):31.
170. Mo X, Hu D, Li Y, Nai A, Ma F, Bashir S, et al. A novel pyroptosis-related prognostic lncRNAs signature, tumor immune microenvironment and the associated regulation axes in bladder cancer. *Front Genet.* 2022;13:936305.
171. Li S, He RC, Wu SG, Song Y, Zhang KL, Tang ML, et al. LncRNA PSMB8-AS1 Instigates Vascular Inflammation to Aggravate Atherosclerosis. *Circ Res.* 2024;134(1):60-80.
172. Coban I, Lamping JP, Hirsch AG, Wasilewski S, Shomroni O, Giesbrecht O, et al. dsRNA formation leads to preferential nuclear export and gene expression. *Nature.* 2024;631(8020):432-8.

7 Appendix

7.1 GO enrichment analysis on proteomic data

Table 7-1: The top 10 most significantly enriched GO terms for each ontology within the less abundant proteins in glomerular endothelial cells from LMP7$^{\Delta EnC}$ mice. For detailed explanation, refer to section 4.2.2.

Description	P value	p.adjust	Ontology
proteasome-mediated ubiquitin-dependent protein catabolic process	6.11E-08	1.00E-04	BP
proteasomal protein catabolic process	3.81E-06	3.13E-03	BP
ubiquitin-dependent protein catabolic process	9.46E-06	5.19E-03	BP
modification-dependent protein catabolic process	1.36E-05	5.59E-03	BP
modification-dependent macromolecule catabolic process	1.72E-05	5.66E-03	BP
regulation of inflammatory response to antigenic stimulus	2.27E-05	6.21E-03	BP
antigen processing and presentation	7.87E-05	1.85E-02	BP
inflammatory response to antigenic stimulus	1.84E-04	3.77E-02	BP
proteolysis involved in protein catabolic process	2.24E-04	4.09E-02	BP
protein catabolic process	3.68E-04	6.05E-02	BP
proteasome core complex	7.72E-18	1.64E-15	CC
proteasome complex	3.26E-12	3.46E-10	CC
endopeptidase complex	5.14E-11	3.63E-09	CC
peptidase complex	1.04E-09	5.49E-08	CC
intracellular protein-containing complex	1.26E-05	5.34E-04	CC
Golgi membrane	8.82E-04	3.12E-02	CC
P-body	3.06E-03	9.27E-02	CC
cytoplasmic ribonucleoprotein granule	7.85E-03	1.91E-01	CC
MHC class I peptide loading complex	8.12E-03	1.91E-01	CC
ribonucleoprotein granule	1.06E-02	2.24E-01	CC
MHC class I protein binding	1.27E-02	5.82E-01	MF
MHC protein binding	1.44E-02	5.82E-01	MF
14-3-3 protein binding	3.37E-02	6.85E-01	MF
endopeptidase activity	3.64E-02	6.85E-01	MF
antigen binding	4.71E-02	6.85E-01	MF
transmembrane transporter binding	6.18E-02	6.85E-01	MF
cytoskeletal protein binding	6.21E-02	6.85E-01	MF
PDZ domain binding	6.84E-02	6.85E-01	MF
peptidase activity	7.83E-02	6.85E-01	MF
antiporter activity	8.88E-02	6.85E-01	MF

Table 7-2: The top 10 most significantly enriched GO terms for each ontology within the more abundant proteins in glomerular endothelial cells from LMP7$^{\Delta EnC}$ mice. For detailed explanation, refer to section 4.2.2.

Description	P value	p.adjust	Ontology
maturation of SSU-rRNA	1.38E-04	1.53E-01	BP
ribosomal small subunit biogenesis	3.86E-04	2.13E-01	BP
maturation of SSU-rRNA from tricistronic rRNA transcript (SSU-rRNA, 5.8S rRNA, LSU-rRNA)	9.35E-04	3.44E-01	BP
regulation of calcium ion transmembrane transport	2.48E-03	5.37E-01	BP
positive regulation of release of sequestered calcium ion into cytosol	2.85E-03	5.37E-01	BP
regulation of monoatomic cation transmembrane transport	3.18E-03	5.37E-01	BP
chaperone-mediated protein complex assembly	4.14E-03	5.37E-01	BP
regulation of monoatomic ion transmembrane transport	4.45E-03	5.37E-01	BP
negative regulation of cation transmembrane transport	4.46E-03	5.37E-01	BP
proteasome assembly	4.87E-03	5.37E-01	BP
intracellular protein-containing complex	8.37E-03	4.40E-01	CC
cortical actin cytoskeleton	8.83E-03	4.40E-01	CC
postsynaptic density, intracellular component	1.25E-02	4.40E-01	CC
90S preribosome	1.48E-02	4.40E-01	CC
postsynaptic specialization, intracellular component	1.98E-02	4.40E-01	CC
cortical cytoskeleton	2.04E-02	4.40E-01	CC
protein folding chaperone complex	2.12E-02	4.40E-01	CC
H4 histone acetyltransferase complex	2.12E-02	4.40E-01	CC
nucleolus	3.04E-02	5.43E-01	CC
preribosome	3.27E-02	5.43E-01	CC
hexosyltransferase activity	1.53E-02	5.86E-01	MF
phosphatidylinositol binding	3.02E-02	5.86E-01	MF
aminoacyltransferase activity	3.94E-02	5.86E-01	MF
glycosyltransferase activity	4.06E-02	5.86E-01	MF
UDP-glycosyltransferase activity	4.77E-02	5.86E-01	MF
ubiquitin protein ligase activity	6.06E-02	5.86E-01	MF
phosphatidylinositol bisphosphate binding	6.42E-02	5.86E-01	MF
acyltransferase activity	6.73E-02	5.86E-01	MF
catalytic activity, acting on a tRNA	7.31E-02	5.86E-01	MF
ubiquitin-like protein ligase activity	7.42E-02	5.86E-01	MF

Table 7-3: The top 10 most significantly enriched GO terms for each ontology within the less abundant proteins in peritubular endothelial cells from LMP7$^{\Delta EnC}$ mice. For detailed explanation, refer to section 4.2.2.

Description	P value	p.adjust	Ontology
proteasome-mediated ubiquitin-dependent protein catabolic process	2.12E-11	2.17E-08	BP
proteasomal protein catabolic process	1.47E-10	7.51E-08	BP
proteolysis involved in protein catabolic process	2.50E-09	8.52E-07	BP
ubiquitin-dependent protein catabolic process	4.94E-09	1.27E-06	BP
modification-dependent protein catabolic process	7.52E-09	1.54E-06	BP
modification-dependent macromolecule catabolic process	9.85E-09	1.68E-06	BP

protein catabolic process	1.21E-07	1.77E-05	BP
regulation of inflammatory response to antigenic stimulus	2.52E-06	3.23E-04	BP
inflammatory response to antigenic stimulus	1.45E-05	1.65E-03	BP
natural killer cell activation	5.52E-05	5.65E-03	BP
proteasome core complex	4.4E-26	5.7E-24	CC
proteasome complex	2.2E-17	1.4E-15	CC
peptidase complex	3.6E-16	1.2E-14	CC
endopeptidase complex	3.7E-16	1.2E-14	CC
intracellular protein-containing complex	1.1E-05	0.00028	CC
MHC protein complex	0.0022	0.04757	CC
MHC class I peptide loading complex	0.00267	0.04961	CC
Golgi medial cisterna	0.00436	0.05875	CC
lumenal side of membrane	0.00436	0.05875	CC
P-body	0.00452	0.05875	CC
peptide antigen binding	0.0001	0.01498	MF
endopeptidase activity	0.00065	0.03369	MF
antigen binding	0.00069	0.03369	MF
T cell receptor binding	0.00199	0.07245	MF
lipopolysaccharide binding	0.00289	0.08428	MF
MHC class I protein binding	0.00453	0.11029	MF
MHC protein binding	0.00582	0.1214	MF
peptidase activity	0.00899	0.16412	MF
14-3-3 protein binding	0.01146	0.18592	MF
peptide binding	0.06521	0.45669	MF

Table 7-4: The top 10 most significantly enriched GO terms for each ontology within the more abundant proteins in peritubular endothelial cells from LMP7$^{\Delta EnC}$ mice. For detailed explanation, refer to section 4.2.2.

Description	P value	p.adjust	Ontology
glutathione metabolic process	2.59E-05	4.44E-02	BP
sulfur compound catabolic process	4.45E-04	3.58E-01	BP
sulfur compound metabolic process	6.27E-04	3.58E-01	BP
alpha-amino acid metabolic process	1.05E-03	4.48E-01	BP
cellular modified amino acid metabolic process	1.42E-03	4.85E-01	BP
L-amino acid catabolic process	1.92E-03	5.49E-01	BP
peptide catabolic process	3.18E-03	7.10E-01	BP
retrograde protein transport, ER to cytosol	3.73E-03	7.10E-01	BP
endoplasmic reticulum to cytosol transport	3.73E-03	7.10E-01	BP
regulation of cytoplasmic translation	4.34E-03	7.12E-01	BP
centriole	2.60E-03	5.61E-01	CC
protein folding chaperone complex	1.10E-02	9.69E-01	CC
intracellular protein-containing complex	1.86E-02	9.69E-01	CC
lysosomal lumen	1.92E-02	9.69E-01	CC
sno(s)RNA-containing ribonucleoprotein complex	2.53E-02	9.69E-01	CC
vacuolar lumen	2.86E-02	9.69E-01	CC
microtubule organizing center	3.33E-02	9.69E-01	CC
P-body	4.34E-02	9.69E-01	CC
mitochondrial outer membrane	4.44E-02	9.69E-01	CC

outer membrane	6.11E-02	9.69E-01	CC
polyubiquitin modification-dependent protein binding	2.16E-04	4.94E-02	MF
glutathione binding	4.89E-04	4.94E-02	MF
oligopeptide binding	4.89E-04	4.94E-02	MF
modification-dependent protein binding	1.78E-03	1.35E-01	MF
transferase activity, transferring alkyl or aryl (other than methyl) groups	2.26E-03	1.37E-01	MF
glutathione transferase activity	3.54E-03	1.79E-01	MF
modified amino acid binding	9.16E-03	3.96E-01	MF
ubiquitin-dependent protein binding	1.12E-02	4.26E-01	MF
carbon-carbon lyase activity	1.42E-02	4.45E-01	MF
NADP binding	1.55E-02	4.45E-01	MF

Table 7-5: The top 10 most significantly enriched GO terms for each ontology within the less abundant proteins in heart endothelial cells from LMP7$^{\Delta EnC}$ mice. For detailed explanation, refer to section 4.2.2.

Description	**P value**	**p.adjust**	**Ontology**
acute inflammatory response	4.04E-03	2.49E-01	BP
regulation of proteolysis	4.57E-03	2.49E-01	BP
regulation of peptidase activity	6.59E-03	2.49E-01	BP
proteasome-mediated ubiquitin-dependent protein catabolic process	7.26E-03	2.49E-01	BP
antigen processing and presentation	7.69E-03	2.49E-01	BP
T cell activation	1.02E-02	2.49E-01	BP
positive regulation of protein secretion	1.66E-02	2.49E-01	BP
T cell proliferation	1.81E-02	2.49E-01	BP
proteasomal protein catabolic process	1.89E-02	2.49E-01	BP
positive regulation of T cell activation	2.04E-02	2.49E-01	BP
proteasome core complex	7.78E-04	5.76E-02	CC
Golgi cisterna	3.70E-03	1.28E-01	CC
cell surface	5.42E-03	1.28E-01	CC
Golgi stack	7.22E-03	1.28E-01	CC
proteasome complex	8.62E-03	1.28E-01	CC
endopeptidase complex	1.28E-02	1.58E-01	CC
peptidase complex	1.98E-02	2.09E-01	CC
MHC protein complex	2.48E-02	2.10E-01	CC
MHC class I peptide loading complex	2.72E-02	2.10E-01	CC
cytoplasmic dynein complex	3.21E-02	2.10E-01	CC
14-3-3 protein binding	1.77E-03	1.09E-01	MF
methylated histone binding	4.29E-03	1.09E-01	MF
methylation-dependent protein binding	4.74E-03	1.09E-01	MF
peptidase regulator activity	1.98E-02	1.64E-01	MF
T cell receptor binding	2.53E-02	1.64E-01	MF
protein kinase B binding	2.78E-02	1.64E-01	MF
endopeptidase activity	2.92E-02	1.64E-01	MF
modification-dependent protein binding	3.02E-02	1.64E-01	MF
cysteine-type endopeptidase activator activity involved in apoptotic process	3.03E-02	1.64E-01	MF
chromatin-protein adaptor activity	3.03E-02	1.64E-01	MF

Table 7-6: The top 10 most significantly enriched GO terms for each ontology within the more abundant proteins in heart endothelial cells from LMP7$^{\Delta EnC}$ mice. For detailed explanation, refer to section 4.2.2.

Description	P value	p.adjust	Ontology
protein hydroxylation	9.33E-05	2.44E-01	BP
cell morphogenesis	3.51E-04	3.19E-01	BP
regulation of cellular component biogenesis	4.94E-04	3.19E-01	BP
gastrulation	1.20E-03	3.19E-01	BP
negative regulation of catalytic activity	1.30E-03	3.19E-01	BP
epithelial cell development	1.84E-03	3.19E-01	BP
cellular response to hexose stimulus	1.85E-03	3.19E-01	BP
cellular response to glucose stimulus	1.85E-03	3.19E-01	BP
cellular response to monosaccharide stimulus	2.04E-03	3.19E-01	BP
extracellular matrix organization	2.12E-03	3.19E-01	BP
actin cytoskeleton	2.27E-03	4.17E-01	CC
cortical actin cytoskeleton	4.60E-03	4.17E-01	CC
cortical cytoskeleton	5.17E-03	4.17E-01	CC
actin filament	5.20E-03	4.17E-01	CC
cell cortex	6.57E-03	4.22E-01	CC
cluster of actin-based cell projections	9.69E-03	4.75E-01	CC
aggresome	1.04E-02	4.75E-01	CC
brush border	1.21E-02	4.87E-01	CC
RNA polymerase II, holoenzyme	1.47E-02	5.24E-01	CC
focal adhesion	1.71E-02	5.29E-01	CC
L-ascorbic acid binding	1.84E-04	6.37E-02	MF
actin filament binding	7.15E-04	1.24E-01	MF
actin binding	2.30E-03	2.65E-01	MF
DNA helicase activity	8.86E-03	4.62E-01	MF
2-oxoglutarate-dependent dioxygenase activity	8.86E-03	4.62E-01	MF
protein tyrosine kinase activity	9.69E-03	4.62E-01	MF
ribonucleoside triphosphate phosphatase activity	1.01E-02	4.62E-01	MF
hydrolase activity, acting on acid anhydrides, in phosphorus-containing anhydrides	1.33E-02	4.62E-01	MF
hydrolase activity, acting on acid anhydrides	1.36E-02	4.62E-01	MF
glycosyltransferase activity	1.43E-02	4.62E-01	MF

Table 7-7: The top 10 most significantly enriched GO terms for each ontology within the less abundant proteins in liver endothelial cells from LMP7$^{\Delta EnC}$ mice. For detailed explanation, refer to section 4.2.2.

Description	P value	p.adjust	Ontology
actin cytoskeleton organization	1.38E-07	3.91E-04	BP
cell junction organization	2.88E-07	4.08E-04	BP
actin filament-based process	5.82E-07	5.49E-04	BP
cell morphogenesis	1.25E-06	8.84E-04	BP
cell junction assembly	1.74E-06	9.85E-04	BP
regulation of actin cytoskeleton organization	2.59E-06	1.22E-03	BP
protein localization to cell junction	3.21E-06	1.30E-03	BP
actin filament organization	8.10E-06	2.87E-03	BP
regulation of actin filament organization	1.43E-05	4.50E-03	BP
regulation of actin filament-based process	1.62E-05	4.60E-03	BP

proteasome core complex	1.12E-15	3.81E-13	CC
proteasome complex	3.36E-08	5.74E-06	CC
anchoring junction	1.07E-07	1.22E-05	CC
peptidase complex	4.41E-07	3.76E-05	CC
endopeptidase complex	7.60E-07	5.18E-05	CC
cell leading edge	5.94E-06	3.38E-04	CC
cell-substrate junction	1.93E-05	9.42E-04	CC
actin cytoskeleton	2.52E-05	1.08E-03	CC
lamellipodium	3.26E-05	1.23E-03	CC
cell-cell junction	7.13E-05	2.43E-03	CC
cytoskeletal protein binding	8.43E-07	3.99E-04	MF
actin filament binding	1.05E-05	2.49E-03	MF
cell adhesion molecule binding	1.39E-04	2.20E-02	MF
modified amino acid binding	2.72E-04	2.75E-02	MF
endopeptidase activity	2.90E-04	2.75E-02	MF
actin binding	3.58E-04	2.83E-02	MF
integrin binding	4.66E-04	3.16E-02	MF
G protein activity	7.04E-04	4.17E-02	MF
phosphatidylserine binding	8.98E-04	4.73E-02	MF
protein homodimerization activity	1.28E-03	6.02E-02	MF

Table 7-8: The top 10 most significantly enriched GO terms for each ontology within the more abundant proteins in liver endothelial cells from LMP7$^{\Delta EnC}$ mice. For detailed explanation, refer to section 4.2.2.

Description	P value	p.adjust	Ontology
chaperone-mediated protein complex assembly	9.50E-04	2.41E-01	BP
proteasome assembly	1.12E-03	2.41E-01	BP
negative regulation of osteoblast differentiation	1.30E-03	2.41E-01	BP
regulation of transcription by RNA polymerase I	4.87E-03	4.82E-01	BP
chromatin organization	5.85E-03	4.82E-01	BP
transcription by RNA polymerase I	8.56E-03	4.82E-01	BP
protein-DNA complex organization	9.43E-03	4.82E-01	BP
regulation of osteoblast differentiation	1.05E-02	4.82E-01	BP
hindbrain development	1.86E-02	4.82E-01	BP
osteoblast differentiation	2.34E-02	4.82E-01	BP
histone acetyltransferase complex	8.95E-04	3.68E-02	CC
intracellular protein-containing complex	1.19E-03	3.68E-02	CC
protein acetyltransferase complex	1.31E-03	3.68E-02	CC
acetyltransferase complex	1.60E-03	3.68E-02	CC
NuA4 histone acetyltransferase complex	2.37E-03	3.68E-02	CC
H4/H2A histone acetyltransferase complex	2.37E-03	3.68E-02	CC
protein folding chaperone complex	5.14E-03	5.97E-02	CC
H4 histone acetyltransferase complex	5.14E-03	5.97E-02	CC
chromatin	8.01E-03	8.28E-02	CC
protein-DNA complex	1.22E-02	1.14E-01	CC
histone acetyltransferase activity	2.79E-03	1.31E-01	MF
peptide-lysine-N-acetyltransferase activity	2.79E-03	1.31E-01	MF
peptide N-acetyltransferase activity	3.32E-03	1.31E-01	MF

histone modifying activity	4.79E-03	1.41E-01	MF
N-acetyltransferase activity	6.22E-03	1.47E-01	MF
N-acyltransferase activity	1.19E-02	2.33E-01	MF
acetyltransferase activity	1.44E-02	2.44E-01	MF
insulin-like growth factor I binding	3.58E-02	2.78E-01	MF
bHLH transcription factor binding	3.58E-02	2.78E-01	MF
histone H4 acetyltransferase activity	3.93E-02	2.78E-01	MF

Table 7-9: The top 10 most significantly enriched GO terms for each ontology within the less abundant proteins in lung endothelial cells from LMP7$^{\Delta EnC}$ mice. For detailed explanation, refer to section 4.2.2.

Description	P value	p.adjust	Ontology
proteasome-mediated ubiquitin-dependent protein catabolic process	3.15E-08	3.41E-05	BP
proteasomal protein catabolic process	5.46E-08	3.41E-05	BP
proteolysis involved in protein catabolic process	3.16E-07	1.32E-04	BP
ubiquitin-dependent protein catabolic process	1.00E-06	3.14E-04	BP
modification-dependent protein catabolic process	1.50E-06	3.74E-04	BP
modification-dependent macromolecule catabolic process	1.93E-06	4.03E-04	BP
protein catabolic process	4.10E-06	7.33E-04	BP
regulation of inflammatory response to antigenic stimulus	9.15E-06	1.43E-03	BP
inflammatory response to antigenic stimulus	1.23E-04	1.71E-02	BP
proton-transporting two-sector ATPase complex assembly	1.93E-04	2.41E-02	BP
proteasome core complex	8.18E-23	1.64E-20	CC
proteasome complex	5.80E-14	5.83E-12	CC
endopeptidase complex	1.46E-12	9.79E-11	CC
peptidase complex	3.82E-11	1.92E-09	CC
intracellular protein-containing complex	1.67E-06	6.73E-05	CC
myosin filament	5.48E-04	1.84E-02	CC
sarcomere	1.46E-03	4.18E-02	CC
myofibril	2.77E-03	6.96E-02	CC
Golgi membrane	3.55E-03	7.93E-02	CC
contractile fiber	3.99E-03	8.03E-02	CC
transcription coregulator activity	5.84E-03	2.39E-01	MF
mannose binding	7.47E-03	2.39E-01	MF
histone H3 demethylase activity	7.47E-03	2.39E-01	MF
endopeptidase activity	8.41E-03	2.39E-01	MF
histone demethylase activity	8.76E-03	2.39E-01	MF
protein demethylase activity	8.76E-03	2.39E-01	MF
myosin binding	9.66E-03	2.39E-01	MF
lipopolysaccharide binding	1.02E-02	2.39E-01	MF
methylation-dependent protein binding	1.10E-02	2.39E-01	MF
MHC protein binding	1.32E-02	2.57E-01	MF

Table 7-10: The top 10 most significantly enriched GO terms for each ontology within the more abundant proteins in lung endothelial cells from LMP7$^{\Delta EnC}$ mice. For detailed explanation, refer to section 4.2.2.

Description	P value	p.adjust	Ontology
proteasome assembly	4.56E-05	1.85E-02	BP
chaperone-mediated protein complex assembly	4.56E-05	1.85E-02	BP
positive regulation of fat cell differentiation	6.68E-03	5.38E-01	BP
stress granule assembly	9.98E-03	5.38E-01	BP
epithelial cell apoptotic process	1.12E-02	5.38E-01	BP
negative regulation of peptidase activity	1.35E-02	5.38E-01	BP
regulation of alternative mRNA splicing, via spliceosome	1.47E-02	5.38E-01	BP
regulation of mRNA processing	1.61E-02	5.38E-01	BP
fat cell differentiation	1.70E-02	5.38E-01	BP
regulation of mRNA metabolic process	1.73E-02	5.38E-01	BP
centriolar satellite	1.53E-02	4.63E-01	CC
P-body	2.77E-02	4.63E-01	CC
extracellular space	2.84E-02	4.63E-01	CC
centrosome	3.98E-02	4.63E-01	CC
cytoplasmic ribonucleoprotein granule	4.04E-02	4.63E-01	CC
cytoplasmic stress granule	4.17E-02	4.63E-01	CC
ribonucleoprotein granule	4.71E-02	4.63E-01	CC
collagen-containing extracellular matrix	5.35E-02	4.63E-01	CC
microtubule organizing center	5.90E-02	4.63E-01	CC
extracellular matrix	6.12E-02	4.63E-01	CC
serine-type endopeptidase inhibitor activity	6.33E-04	4.81E-02	MF
endopeptidase inhibitor activity	2.86E-03	6.12E-02	MF
peptidase inhibitor activity	3.01E-03	6.12E-02	MF
mRNA 3'-UTR AU-rich region binding	3.22E-03	6.12E-02	MF
endopeptidase regulator activity	4.34E-03	6.59E-02	MF
peptidase regulator activity	1.03E-02	1.30E-01	MF
enzyme inhibitor activity	3.48E-02	2.79E-01	MF
mRNA 3'-UTR binding	4.72E-02	2.79E-01	MF
profilin binding	4.95E-02	2.79E-01	MF
oxidoreductase activity, acting on other nitrogenous compounds as donors	4.95E-02	2.79E-01	MF

7.2 Genes altered on both mRNA and protein level

Table 7-11: Genes detected to be significantly altered on both mRNA and protein level in GEnCs isolated from LMP7$^{\Delta EnC}$ mice. Refer to chapter 4.2.3 for detailed description.

Gene	Fold change mRNA	Fold change protein
Psmb8	- 0.75	- 3.08
Psmb5	- 0.20	+ 1.94
Uqcc2	- 0.30	- 0.63
Smim12	- 0.23	- 0.87
Rflnb	+ 0.25	- 1.26

Table 7-12: Genes detected to be significantly altered on both mRNA and protein level in PtEnCs isolated from LMP7$^{\Delta EnC}$ mice. Refer to chapter 4.2.3 for detailed description.

Gene	Fold change mRNA	Fold change protein
Psmb8	- 2.01	- 3.60
Psma4	+ 0.41	- 0.70
Psma7	+ 0.49	- 0.67
Psmb3	+ 0.42	- 0.84
Psma1	+ 0.36	- 0.75
Psmb4	+ 0.38	- 1.03
Psmb1	+ 0.32	- 1.01
Psma2	+ 0.32	- 0.79
Psma3	+ 0.32	- 0.76
Psmb2	+ 0.31	- 0.88
Psma6	+ 0.33	- 0.71
Psmb5	+ 0.25	+ 2.4
Me1	+ 1.52	+ 1.68
Mgst1	+ 0.70	+ 0.58
Isg20	+ 0.90	+ 0.68
Dhcr24	- 0.70	- 1.47
Acyp2	+ 0.68	+ 0.74
Vcp	+ 0.33	+ 0.56
Syngr3	+ 0.81	+ 0.72
Impact	+ 0.32	+ 0.42
Ctla2a	+ 0.45	- 0.64
Cyth3	- 0.30	- 0.42
Sgk3	- 0.39	+ 0.59
Mvp	+ 0.29	+ 0.21
Plaa	+ 0.25	+ 0.42
Coasy	+ 0.32	+ 0.40
Chid1	+ 0.36	- 1.14
Pkm	+ 0.22	+ 0.29
Ufd1	+ 0.23	+ 0.47
Vat1	+ 0.21	+ 0.30
Zbtb14	- 0.22	- 0.61
Hmbs	+ 0.30	+ 0.45
Tuba4a	+ 0.46	+ 0.37
Rasa4	+ 0.29	+ 0.29
Bag3	+ 0.18	+ 0.93
Mlkl	+ 0.21	+ 0.40
Il16	+ 0.31	+ 0.30
Kdm2b	- 0.24	+ 0.80

Sgk1	- 0.30	- 0.60
Gfod1	- 0.40	- 0.60
Rpl22l1	+ 0.28	+ 0.63
Ccdc9b	+ 0.30	+ 1.08
Fam117b	- 0.13	+ 0.34
Dtd1	+ 0.20	+ 0.25
Fbxo6	+ 0.16	+ 0.38

7.3 Hazard Statements

Table 7-13: Hazard statements relevant for the chemicals used during this thesis.

H224	Extremely flammable liquid and vapour
H225	Highly flammable liquid and vapour
H226	Flammable liquid and vapour
H228	Flammable solid
H271	May cause fire or explosion; strong oxidiser
H290	May be corrosive to metals
H301	Toxic if swallowed
H301+H311+H331	Toxic if swallowed, in contact with skin or if inhaled
H302	Harmful if swallowed
H302+H312+H332	Harmful if swallowed, in contact with skin or inhaled.
H302+H332	Harmful if swallowed or if inhaled
H304	May be fatal if swallowed and enters airways
H311	Toxic in contact with skin
H312	Harmful in contact with skin
H312+H332	Harmful in contact with skin or if inhaled
H314	Causes severe skin burns and eye damage
H315	Causes skin irritation
H317	May cause an allergic skin reaction
H318	Causes serious eye damage
H319	Causes serious eye irritation
H331	Toxic if inhaled
H332	Harmful if inhaled
H334	May cause allergy or asthma symptoms or breathing difficulties if inhaled
H335	May cause respiratory irritation
H336	May cause drowsiness or dizziness
H341	Suspected of causing genetic defects
H350	May cause cancer
H351	Suspected of causing cancer
H360	May damage fertility or the unborn child
H361	Suspected of damaging fertility or the unborn child
H361d	Suspected of damaging the unborn child
H361fd	Suspected of damaging fertility. Suspected of damaging the unborn child
H370	Causes damage to organs
H372	Causes damage to organs through prolonged or repeated exposure
H373	May cause damage to organs through prolonged or repeated exposure

H400	Very toxic to aquatic life
H402	Harmful to aquatic life
H410	Very toxic to aquatic life with long lasting effects
H411	Toxic to aquatic life with long lasting effects
H412	Harmful to aquatic life with long lasting effects

7.4 Precautionary statements

Table 7-14: Precautionary statements relevant for the chemicals used during this thesis.

P201	Obtain special instructions before use
P202	Do not handle until all safety precautions have been read and understood
P210	Keep away from heat
P220	Keep away from clothing and other combustible materials
P233	Keep container tightly closed
P234	Keep only in original packaging
P240	Ground and bond container and receiving equipment
P241	Use explosion-proof [electrical/ventilating/lighting/…] equipment
P243	Take action to prevent static discharges.
P260	Do not breathe dusts or mists
P261	Avoid breathing dust/fume/gas/mist/vapours/spray
P264	Wash thoroughly after handling
P271	Use only outdoors or in a well-ventilated area
P272	Contaminated work clothing should not be allowed out of the workplace
P273	Avoid release to the environment
P280	Wear eye protection/face protection
P284	Wear respiratory protection
P301+P310	IF SWALLOWED: Immediately call a POISON CENTER or doctor/physician
P301+P312	IF SWALLOWED: Call a POISON CENTER/doctor/… if you feel unwell.
P301+P312+P330	IF SWALLOWED: Call a POISON CENTER/doctor if you feel unwell. Rinse mouth
P301+P330	IF SWALLOWED: Rinse mouth.
P301+P330+P331	IF SWALLOWED: Rinse mouth. Do NOT induce vomiting
P302+P352	IF ON SKIN: Wash with plenty of soap and water
P302 + P352 + P312	IF ON SKIN: Wash with plenty of soap and water. Call a POISON CENTER or doctor/physician if you feel unwell.
P303+P361+P353	IF ON SKIN (or hair): Remove/Take off immediately all contaminated clothing. Rinse skin with water/shower

P304+P340	IF INHALED: Remove person to fresh air and keep comfortable for breathing
P304+P340+P310	IF INHALED: Remove person to fresh air and keep comfortable for breathing. Immediately call a POISON CENTER/doctor/…
P304+P340+P311	IF INHALED: Remove person to fresh air and keep comfortable for breathing. Call a POISON CENTER/doctor/…
P304+P340+P312	IF INHALED: Remove person to fresh air and keep comfortable for breathing. Call a POISON CENTER or doctor/physician if you feel unwell
P305+P351+P338	IF IN EYES: Rinse cautiously with water for several minutes. Remove contact lenses, if present and easy to do. Continue rinsing
P308+P310	IF exposed or concerned: immediately call a POISON CENTER or doctor/ physician
P308+P313	IF exposed or concerned: Get medical advice/ attention
P310	Immediately call a POISON CENTER or doctor
P311	Call a POISON CENTER/doctor/…
P312	Call a POISON CENTER or doctor/physician if you feel unwell
P314	Get medical advice/attention if you feel unwell.
P331	Do NOT induce vomiting
P332 + P313	If skin irritation occurs: Get medical advice/attention.
P333 + P313	If skin irritation or rash occurs: Get medical advice/attention.
P337 + P313	If eye irritation persists: Get medical advice/attention
P342 + P311	If experiencing respiratory symptoms: Call a POISON CENTER/doctor/…
P361	Remove/take off immediately all contaminated clothing
P362 + P364	Take off contaminated clothing and was it before reuse
P391	Collect spillage
P403 + P233	Store in a well-ventilated place. Keep container tightly closed
P403 + P235	Store in a well-ventilated place. Keep cool
P405	Store locked up.
P501	Dispose of contents/container to industrial combustion plant

List of abbreviations

Abp(s):	activity based probe(s)
AF:	AlexaFluor
ALP:	autophagosomal-lysosomal pathway
Amc:	amino methyl cumarine
ANCA:	anti neutrophile cytoplasmic antigen
APC:	allophycocyanine
ATP:	adenosine triphosphate
bp(s):	base pair(s)
BSA:	bovine serum albumin
BUN:	blood urea nitrogen
BV:	brilliant violet
°C:	degrees Celsius
C:	clone
CANDLE:	chronic atypical neutrophilic dermatosis with lipodystrophy and elevated temperature
Cas9:	CRISPR associated 9
CD:	Cluster of differentiation
cGN:	crescentic glomerulonephritis
CI:	confidence interval
cP:	constitutive proteasome (= standard proteasome)
CP:	core particle
CTL:	chymotrypsin like
Ctrl:	control
CRISPR:	clustered regularly interspaced short palindromic repeats
DEG(s)	Differentially expressed genes
DIA:	data independent acquisition
DMSO:	dimethyl sulfoxide
DN:	diabetic nephropathy
DNA:	desoxyribonucleic acid
dNTPs:	desoxyribonucleosidtriphosphates
DRiPs:	defective ribosomal products
DTT:	dithiothreitol
DUB(s):	deubiquitinating enzyme(s)
ECL:	enzymatic chemoluminescence
EDTA:	ethylene diamine tetra acetic acid
ELISA:	Enzyme linked immunosorbent assay
e.g.:	example given
EM:	electron microscopy
EnC(s):	Endothelial cell(s)
ER:	endoplasmic reticulum
ERAD:	ER associated degradation
EtOH:	ethanol
FA:	formic acid
FACS™:	fluorescence activated cell sorting
FBS:	fetal bovine serum
FcRn	neonatal Fc receptor (encoded by *Fcgrt*)

FDR:	false discovery rate
FFPE:	Formalin fixed paraffin embedded tissue
FPE:	Foot process effacement
FSC-A:	forward scatter area
FPKM:	fragments per kilobases per million mapped reads
GBM:	glomerular basement membrane
GEnC(s):	Glomerular endothelial cell(s)
GFB:	glomerular filtration barrier
GFR:	glomerular filtration rate
GO:	gene ontology
GT(s)	genotype(s)
HBSS:	Hanks balanced salt solution
HRP:	horseradish peroxidase
IDP:	Intrinsically disordered protein
IDR:	Intrinsically disordered region
IFNγ:	interferon γ
IgG:	Immunoglobulin G
IMDM:	Iscove's modified Dulbecco's medium
iP:	immuno proteasome
intP:	intermediate proteasome
K(48/63):	lysine(48/63)
kDa:	kilo-Dalton
Kim1:	kidney injury molecule 1
KO:	knockout
(UHP)LC:	(ultra-high performance) liquid chromatography
lncRNA:	long non-coding RNA
MACS:	magnetically assisted cell sorting
MAE:	murine albumin ELISA
MC(s):	mesangial cells
MHC:	major histocompatibility complex
MFI:	mean fluorescent intensity
(m)M:	(milli) mole per liter
MORF4L2:	mortality factor 4 like protein 2
MPC:	magnetic particle collector
Mrgx:	Morf related protein on the x chromosome
MS:	mass spectrometry
mRNA(seq):	messenger ribonucleic acid sequencing
msIgG:	mouse Immunoglobulin G
NFDM:	non-fat dry milk
NTN:	Nephrotoxic nephritis
NTS:	Nephrotoxic serum
PA:	proteasome activator
PAS:	periodic acid Schiff staining
PC(s):	Podocyte(s)
PCA:	principal component analysis
(q)PCR:	(quantitative) Polymerase chain reaction
PE:	R-phycoerythrin

PFA:	para formaldehyde
PI:	propidium iodide
PAI-1:	plasminogen activator inhibitor 1
PRAAS:	proteasome associated autoinflammatory syndromes
PtEnC(s):	Peritubular endothelial cell(s)
PTSA:	para toluene sulfonic acid
(p)Ub:	(poly) ubiquitin
PB(S):	phosphate buffer(ed saline)
PI:	propidium iodide
PVDF:	polyvinylidene fluoride
r:	relative
RNA:	ribonucleic acid
RPGN:	rapidly progressive glomerulonephritis
S:	Svedberg (sedimentation constant)
SASP:	senescence associated secretory phenotype
sc:	single cell
(SDS-) PAGE:	(sodium dodecysulfate) polyacrylamide gel electrophoresis
shIgG:	sheep Immunoglobulin G
αSMA	α smooth muscle actin
SNP(s):	single nucleotide polymorphism(s)
SSC-A:	sideward scatter area
T2D:	type 2 diabetes
TBS(-T)	Tris buffered saline (with Tween-20)
TIC:	total ion chromatogramm
tP:	thymoproteasome
TPER™:	tissue protein extraction reagent
uACR:	urinary albumin creatinine ratio
UPR:	unfolded protein response
UPS:	ubiquitin proteasome system
V:	Volt
WT:	wild type

No generative artificial intelligence-based services were used during the writing of this thesis.

Parts of the data presented in this thesis have been published in the following manuscript:

Sachs W, **Blume L**, Loreth D, Schebsdat L, Hatje F, Koehler S, Wedekind U, Sachs M, Zieliniski S, Brand J, Conze C, Florea BI, Heppner F, Krüger E, Rinschen MM, Kretz O, Thünauer R, Meyer-Schwesinger C. The proteasome modulates endocytosis specifically in glomerular cells to promote kidney filtration. *Nat Commun.* 2024 Mar 1;15(1):1897.

As part of this project, a review article and an editorial were published:

Heintz L, Meyer-Schwesinger C. The Intertwining of Autophagy and the Ubiquitin Proteasome System in Podocyte (Patho)Physiology. *Cell Physiol Biochem*. 2021 Sep 15;55(S4):68-95.

Blume L, Meyer-Schwesinger C. Autoantibodies in the Pathogenesis of Podocytopathies. J Am Soc Nephrol. 2025 Jan 30. doi: 10.1681/ASN.0000000624. Epub ahead of print. PMID: 39883526.

While not yet published, (raw) data and program code used for analyses can be made available upon reasonable request to Catherine Meyer-Schwesinger.

Acknowledgements

This work would not have been possible without the help of numerous people. First of all, I would like to thank Prof. Catherine Meyer-Schwesinger for introducing me to the world of the proteasome and letting me conduct this work under her supervision. None of the work described here would have been possible without her expertise, vision and perseverance. Secondly, I would like to thank Prof. Hartmut Schlüter for accepting the role as second reviewer of my thesis and for his help with the proteomic analyses of isolated endothelial cells.

I owe a lot of gratitude to Dr. Wiebke Sachs for introducing me to the lab, all the techniques involved and her help throughout this project over the years. Her earlier work on and experience with the (immuno)proteasome made this project possible. Sorting days were long and exhausting enough as they were but would certainly have been worse without her help and the tubuli song. Everyone else in the Meyer-Schwesinger lab and the IZIP also greatly contributed to this work: Dr. Desirée Loreth, Dr. Julia Reichelt and Dr. Helga Vitzthum I would like to thank for their help, guidance and fruitful discussions over the years. Karen Lahme, Sarah Frömbling and Man Wang were amazing colleagues, struggling just like me with all the hurdles of basic medical science during our journey. Johannes Brand, Stephanie Zielinski and Elena Tassika provided excellent help over the years – be it with proteasomal activity measurements, histological stainings or mouse work. Dr. Katrin Neuman I would like to thank for her immunological expertise and her help with the cytometry-based characterisation of immune cell infiltrations. Dr. Oliver Kretz and Dr. Desirée Loreth deserve an extra thank you for performing the electron microscopic analyses of LMP7$^{\Delta EnC}$ kidney tissue.

Members of the III. Medical clinic provided valuable input and reagents. Prof. Dr. Ulf Panzer, Anna Kaffke and Annett Peters helped with the NTN experiments and Dr. Hajo Paust was a great help setting up flow cytometry experiments and workflows. Dr. Shuya Liu was an especially valued colleague during the project employing BTBR *ob*/*ob* mice. I thank Thomas Mair und Ali Biabani from the mass spectrometry core unit for the mass spectrometric analysis of the isolated mouse endothelial cells and the subsequent (discussion on) data analysis. I also enjoyed working with all members of the FACS-Core Unit, especially Dr. Regine Thiele, Melanie Lachmann-Schwemm and Dr. Anne Rissiek, who were an invaluable help getting to grips with all practical aspects and pitfalls of cell sorting.

Last but most certainly not least I would like to thank those who might not have been directly involved in my doctoral project but got me there to begin with: My family, my colleagues during my biochemistry studies in Kiel and my wife Christina. Especially Christina also endured and helped me get through the difficult times of a doctoral thesis. Thank you!

Eidesstattliche Versicherung

Hiermit versichere ich an Eides statt, die vorliegende Dissertationsschrift selbst verfasst und keine anderen als die angegebenen Quellen und Hilfsmittel benutzt zu haben. Sofern im Zuge der Erstellung der vorliegenden Dissertationsschrift generative Künstliche Intelligenz (gKI) basierte elektronische Hilfsmittel verwendet wurden, versichere ich, dass meine eigene Leistung im Vordergrund stand und dass eine vollständige Dokumentation aller verwendeten Hilfsmittel gemäß der Guten wissenschaftlichen Praxis vorliegt. Ich trage die Verantwortung für eventuell durch die gKI generierte fehlerhafte oder verzerrte Inhalte, fehlerhafte Referenzen, Verstöße gegen das Datenschutz- und Urheberrecht oder Plagiate.

Hamburg, 08.07.2025

Lukas Blume